CONSTANT VOLTAGE, CONSTANT FREQUENCY OPERATION OF A
SELF-EXCITED INDUCTION GENERATOR

A THESIS SUBMITTED TO
THE GRADUATE SCHOOL OF NATURAL AND APPLIED SCIENCES
OF
MIDDLE EAST TECHNICAL UNIVERSITY

BY

AHMET ÇALIŞKAN

IN PARTIAL FULFILLMENT OF THE REQUIREMENTS
FOR
THE DEGREE OF MASTER OF SCIENCE
IN
ELECTRICAL AND ELECTRONICS ENGINEERING

SEPTEMBER 2005

Approval of the Graduate School of Natural and Applied Sciences

_____

Prof. Dr. Canan ÖZGEN
Director

I certify that this thesis satisfies all the requirements as a thesis for the degree of Master of Science.

_____

Prof. Dr. İsmet ERKMEN
Head of Department

This is to certify that we have read this thesis and that in our opinion it is fully adequate, in scope and quality, as a thesis for the degree of Master of Science.

_____

Prof. Dr. Yıldırım ÜÇTUĞ
Supervisor

Examining Committee Members

Prof. Dr. Muammer ERMİŞ   (METU, EE)   _____

Prof. Dr. Yıldırım ÜÇTUĞ   (METU, EE)   _____

Prof. Dr. Işık ÇADIRCI   (Hacettepe Univ.)   _____

Asst. Prof. Dr. Ahmet HAVA   (METU, EE)   _____

Asst. Prof. Dr. İres İSKENDER   (Gazi Univ.)   _____

I hereby declare that all information in this document has been obtained and presented in accordance with academic rules and ethical conduct. I also declare that, as required by these rules and conduct, I have fully cited and referenced all material and results that are not original to this work.

Name, Last name: Ahmet ÇALIŞKAN

Signature   :

ABSTRACT

CONSTANT VOLTAGE, CONSTANT FREQUENCY OPERATION OF A
SELF-EXCITED INDUCTION GENERATOR

Çalışkan, Ahmet

M.Sc., Department of Electrical and Electronics Engineering

Supervisor: Prof. Dr. Yıldırım Üçtuğ

September 2005, 130 pages

In this thesis, control schemes for the self-excited induction generator are developed
with Matlab/Simulink. Self-excited induction generator is considered as a constant
voltage-constant frequency supply for an isolated load. A wind turbine is assumed to
be the variable-speed drive of the induction generator. Control schemes aim to ensure
a constant voltage-constant frequency operation of the induction generator in case of
the variations in the wind speed and/or the load.

From the general model of the self-excited induction generator, the characteristics of
the system and the dynamic responses of the system in case of any disturbance are
examined. Next, the control strategies are developed both for the squirrel-cage rotor
induction generator and for the wound-rotor induction generator. Two control loops
are necessary for constant voltage-constant frequency operation of a variable speed
induction generator, one for the voltage regulation and the other for the frequency
regulation. After developing the control loops, constant voltage-constant frequency
operation of the self-excited induction generator is simulated with a cage type

saturation adaptive induction generator, a fixed capacitor with thyristor controlled reactor (TCR) used for frequency regulation and switched external resistors connected to the stator terminals used for voltage regulation.

ÖZ

KENDİNDEN UYARTIMLI ASENKRON GENERATÖRÜN SABİT GERİLİM, SABİT FREKANS ALTINDA ÇALIŞMASI

Çalışkan, Ahmet

Yüksek Lisans, Elektrik Elektronik Mühendisliği Bölümü

Tez Yöneticisi: Prof. Dr. Yıldırım Üçtuğ

Eylül 2005, 130 sayfa

Bu tezde, kendinden uyartımlı asenkron generatörü için Matlab/Simulink ile denetim şemaları geliştirilmiştir. Kendinden Uyartımlı Asenkron generatörü, sabit gerilim-sabit frekansta çalışan ve şebekeden bağımsız bir yükü besleyen bir güç kaynağı olarak düşünülmüştür. Asenkron generatörün bir rüzgar türbini tarafından sürüldüğü varsayılmıştır. Denetim şemalarının amacı, rüzgar hızı ve/veya yükteki değişimlere karşın asenkron generatörün sabit gerilim-sabit frekansta çalışmasını sağlamaktır.

Kendinden uyartımlı asenkron generatörün genel modelinden, sistemin çalışma prensipleri ve rüzgar/yük değişimlere olan dinamik tepkileri incelenmiştir. Hem sincap kafesli asenkron generatör hem de bilezikli asenkron generatör için farklı tiplerde denetim yöntemleri geliştirilmiştir. Değişken hızlı asenkron generatörün sabit gerilim-sabit frekansta çalışması için iki adet denetim döngüsü gerekmektedir, biri gerilim regülasyonu için, diğeri frekans regülasyonu için. Elde edilen denetim döngüleri ile, kendinden uyartımlı asenkron generatörün sabit gerilim-sabit frekansta çalışmasının benzetimi yapılmıştır. Benzetimde; a) sincap kafesli doyumlu asenkron

makine, b) frekans kontrolü için kullanılan sabit kondansatör ile tristör kontrollü reaktör ve c) gerilim kontrolü için kullanılan statora bağlı anahtarlanabilen harici dirençler kullanılmıştır.

Anahtar Kelimeler: Asenkron generatörü, kendinden uyartım, değişken hız, sabit gerilim, sabit frekans, rüzgar türbini, tristör kontrollü reaktör, matlab

ACKNOWLEDGMENTS

I would like to express my deepest gratitude to my supervisor Prof. Dr. Yıldırım Üçtuğ for his invaluable guidance and advice throughout the study.

I would like to thank to Prof. Dr. Muammer Ermiş and Dr. Ahmet Hava for their encouragements.

Special thanks to Halil İbrahim Çetin for his encouragements and continuous support during the study, without his support this work could not be completed.

TABLE OF CONTENTS

LIST OF TABLES

LIST OF FIGURES

xvii

LIST OF SYMBOLS

C   Excitation capacitance

E   Air-gap voltage

f   Frequency

F   Magnetomotive force

G   Load conductance

I   Current, unit matrix

j   Imaginary number

J   Moment of inertia

ℓ Leakage inductance

L   Self-inductance

M   Mutual inductance

n_t Transmission ratio

N   Number of turns

p   Differential operator, d/dt

(pp)   Number of pole pairs

r_r, r_r' Rotor (rotor referred) resistances

R   Resistance

s   Slip

t   Time

T   Torque

v   Wind speed

w   Angular frequency

V   Voltage

X   Reactance

B   Susceptance

θ   Angle between the phases of the stator and the rotor

θ_s Phase angle of the synchronously rotating reference frarne

Γ   Reciprocal inductance

λ   Flux linkage

ψ   Phase angle of the rotor flux phasor

Subscripts

1,2	Stator, rotor
a, b, c	a, b and c phases of the rotor
A, B, C	A, B and C phases of the stator
al, be	Fictitious al and be phases of the rotor
AL, BE	Fictitious AL and BE phases of the stator
d, q	Fictitious d and q phases of the rotor
D, Q	Fictitious D and Q phases of the stator
e	Electrical
ext	External
m	Magnetising, mechanical
o	Steady-state
rms	Root mean square
R	Resultant
s	Synchronous, stator
t	Turbine

LIST OF ABBREVIATIONS

CVCF   Constant voltage - constant frequency

HAWT   Horizontal axis wind turbine

IG   Induction generator

IM   Induction machine

MMF   Magnetomotive force

PSB   Power system blockset

SEIG   Self-excited induction generator

TCR   Thyristor controlled reactor

VAR   Volt ampere reactive

VAWT   Vertical axis wind turbine

WECS   Wind energy conversion systems

CHAPTER 1

INTRODUCTION

1.1. SELF-EXCITED INDUCTION GENERATOR

An induction machine (IM) can be operated as a stand-alone generator. Capacitive self-excitation of IM has been known for over 70 years [1], [2]. Self-excitation of IM is initiated by means of the residual magnetism existing in the core of the machine [3], [4]. These types of generators are then called as self-excited induction generators (SEIG) in literature [3], [5], [6], [7].

The fundamental superiority of an IG is its ability to generate power at constant voltage constant frequency (CVCF) when driven by a variable speed source. Therefore, in the wind power applications, most of the generators are IGs, which are grid connected [8]. However, there have been few examples for stand-alone (not grid connected) applications of IG due to some important drawbacks of this method. The main drawback of an induction generator is its reactive power demand for excitation. Therefore, capacitors should be connected across the generator terminals. Another drawback is that they have poor voltage and frequency regulations under varying load and wind speeds. This type of operation requires active and reactive power balances every time [7]. Reactive power balance requires variable capacitance, which can be supplied with power semi-conductors circuits. Active power balance, on the other hand requires external elements to divert the excessive power from the system, when the source power exceeds the amount required by the load. Excessive power can be absorbed by the resistors connected to the rotor terminals or by the resistors connected to the stator terminals. Another drawback is that, the machine

demagnetizes and stops generating voltage either when the wind speed falls below or the load rises beyond certain values. After that, even with the wind speed and the load returning to the rated values, the IG cannot start working again without the help of an auxiliary energy source and a controller [6]. Therefore these drawbacks should be considered during the design phase.

The reactive volt-ampere (VAR) requirements of the IG and the load are supplied by means of VAR Generator connected to the stator terminals. There are various possibilities to generate reactive power;

    i.   Synchronous Condenser

   ii.   The combination of capacitors and saturated reactors

  iii.   Static exciters

Static Exciters are classified in [3] as;

   a.   Inverter based schemes

   b.   Force-commutated cycloconverters

   c.   Naturally-commutated cycloconverters with an auxiliary high frequency bank to facilitate commutation

   d.   A full- or half-wave controlled rectifier loaded with a single dc inductor and connected in parallel to a fixed capacitors

   e.   Two controlled rectifiers one is naturally-commutated and the other force-commutated, connected in parallel and loaded by a single dc inductor

   f.   Thyristor-controlled inductor connected in parallel to a fixed capacitor

   g.   Thyristor-switched capacitors

   h.   The combination of thyristor-switched capacitor and a thyristor-controlled inductor.

The active power balance is also a major problem of a variable speed IG when there is no control on its speed [7]. If the source power exceeds the amount required by the load, then, the excessive power should be absorbed from the system by resistors connected;

a. to rotor terminals (when using wound-rotor IM)

b. to stator terminals [9]

The effective value of the rotor or stator external resistances should also be modified according to the variations in the supply power or the load demand.

In recent years, SEIGs have been identified as a possible source of energy to be used with the modern power electronics applications [6]. There are some practical examples of applications [9].

The operating principles and the potential applications of a SEIG are discussed in various studies in METU [3], [5], [7], [10]. It has been shown that, by means of a static exciter and a static rotor resistance controller, the IG can satisfactorily be operated as a variable speed, CVCF supply for isolated loads. Reduced order model of the system was obtained and the control strategies were developed which permit the successful utilization of SEIG's in wind power applications [7].

SEIG can be used with different variable speed drives like water turbine and wind turbine. In this study, the SEIG is considered to be driven by a wind turbine. A brief survey of the wind energy with the new advances is given below.

1.2. WIND ENERGY

Energy demand of the world is increasing year by year. With the increasing demand of energy, besides of the exploitation of the traditional sources, new energy sources are searched and used throughout the world depending upon their availability and their relative benefits [7]. Within the new energy sources wind energy can play a significant role in solving the world energy problem [11].

Wind energy is a form of solar energy, created by circulation patterns in the Earth's atmosphere that are driven by heat from the sun [12]. Although people have made

use of wind energy for thousands of years, in sailing and in mills to grind grain, extracting electrical energy from the wind appears to be a new application which gains increasing interest with the advances in the turbine and control technologies. Today the wind energy is the world's fastest growing energy source. Cumulative global wind energy generating capacity reached 40,300 MW and installed wind turbines reached 67,950 units at the end of 2003 [11]. 8,344 MW new capacity was installed worldwide during the year 2003, an increase of 26%, according to estimates by the American Wind Energy Association (AWEA) and the European Wind Energy Association (EWEA). The global wind energy capacity and consumption are shown in Table 1.1 [12]. However, the upper limit for the utilization of the earth's wind supply is estimated 130,000 GW [5]. A number of assessments confirm that the world's wind resources are extremely large and well distributed all regions. The total available resource that is technically recoverable is estimated to be 53,000 TWh/year [11].

Table 1.1 The global wind power capacity and wind energy consumption

Year	Global GW	Global TWh	% Increase	Wind GW	Wind TWh	% Increase	% of Wind TWh in Total
1997	3,221	13,949	2.8	7.64	15.39	25.8	0.11
1998	3,298	14,340	2.8	10.15	21.25	38.1	0.15
1999	3,377	14,741	2.8	13.93	28.18	32.6	0.19
2000	3,458	15,153	2.8	18.45	37.30	32.0	0.25
2001	3,540	15,577	2.8	24.93	50.27	34.8	0.32
2002	3,625	15,951	2.8	32.04	62.77	28	0.39
2003	3,715	16,666	2.8	40.30	84.70	28	0.51

Wind energy conversion systems (WECS) consist of a wind turbine, which transforms the energy in the wind into mechanical energy and an electric generator coupled to the shaft of the turbine end, which converts the mechanical energy at the shaft into electrical energy. The types of the turbine and the generator used depend on different factors such as the wind characteristic, the size of the power plant and the nature of the application [7].

The wind turbines can be classified according to the position of their axes as horizontal axis wind turbines (HAWT) and vertical axis wind turbines (VAWT).
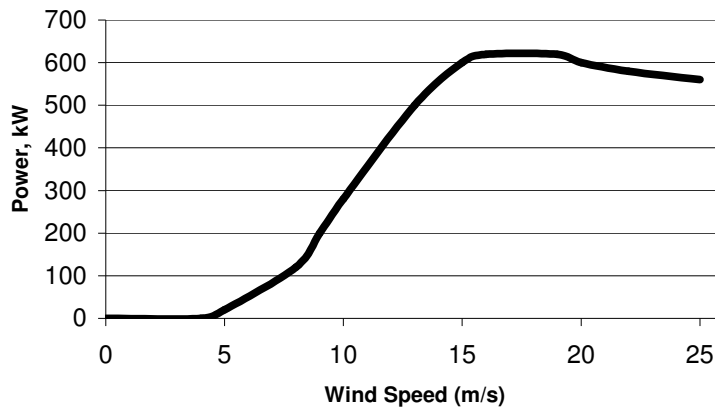
Figure 1.1 Power curve for a typical Danish 600 kW wind turbine

All grid-connected commercial wind turbines today are built with a propeller-type rotor on a horizontal axis [8]. Power curve of such a curve is shown in Fig.1.1.

The second unit in WECS is the electric generator. Similar to the case of turbines, different alternatives exist for the generator types. Most wind turbines in the world use induction generator to generate alternating current [8].

According to the nature of the application, the electrical power generating systems can also be classified as grid-connected and stand-alone systems.

1.3. SCOPE OF THE THESIS

This study aims simulation of a wind turbine driven SEIG supplying power to an isolated load. An IG can satisfy constant voltage-constant frequency (CVCF) operation, if an appropriate control is applied to the control variables.

The system can be thought of consisting of a VAWT-SEIG combination with two output variables - stator voltage V_s and frequency f - to be kept at pre-specified values, two control variables - excitation capacitance C and external load connected to the stator, G_{ext} (1/ohm) or external resistance connected to the rotor, R_{ext} (ohm) - and two disturbances - wind speed v and load conductance G (1/ohm). Block diagram of the system is shown in Figure 1.2.
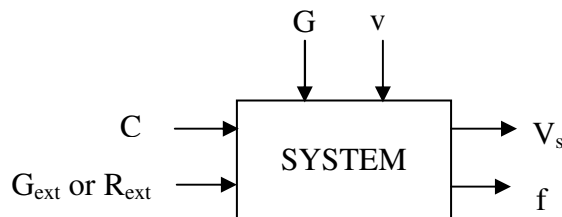
Figure 1.2 System Block Diagram.

In the second chapter, the dynamical model of the system is derived with a set of seven non-linear differential equations. Steady-state operation of the SEIG is obtained by deriving the equilibrium conditions.

In the third chapter, SEIG is modeled in Matlab/Simulink. Control Strategies are developed for constant frequency and constant voltage operations separately. Final simulation is done by a saturation adaptive cage-type IG driven by a wind turbine and supplying power to a variable load with two controllers;

i) Voltage Controller, which controls the external loads (eight three-phase resistors), connected to the stator terminals.

ii) Frequency Controller, which controls the value of the excitation-capacitance by controlling the conduction angle of the thyristor controlled reactor connected parallel to a fixed capacitor.

It is seen that the desired terminal conditions (CVCF) is satisfied with this control scheme.

Chapter 4 is the conclusion chapter. A brief conclusion is given in this chapter.

CHAPTER 2

DYNAMIC MODEL OF THE INDUCTION GENERATOR

2.1.   INTRODUCTION

In this chapter, the dynamic model of the VAWT-SEIG-resistive load combination is derived and, based on this model; its steady-state operating conditions are obtained.

The dynamic model of an IM considers the instantaneous effects of varying voltages, currents, frequency, and torque disturbances [13]. The dynamic model of the three-phase IM is very complex, because the three-phase rotor windings move with respect to the three-phase stator windings [14]. Coupling coefficients between the stator and the rotor phases change continuously with the change of the angle between the corresponding phases of the stator and the rotor, θ.

First, the transformation techniques are applied to eliminate the presence of θ in the equations. Resulting model is obtained in a synchronously rotating reference frame.

Second, the current variables are replaced by equivalent flux linkage variables and the terminal equations corresponding to the excitation capacitors and the load, together with the torque-balance equation, are included to obtain the complete mathematical model of the system.

Finally, the equilibrium conditions of the state variables are derived to determine the steady-state operating conditions of the model with the varying wind speed and load disturbances.

2.2. THE DYNAMIC MODEL OF THE SYSTEM

2.2.1. The Induction Machine Model

The voltage-current relationship of the three-phase IM shown in Figure 2.1 can be written as follows [15];
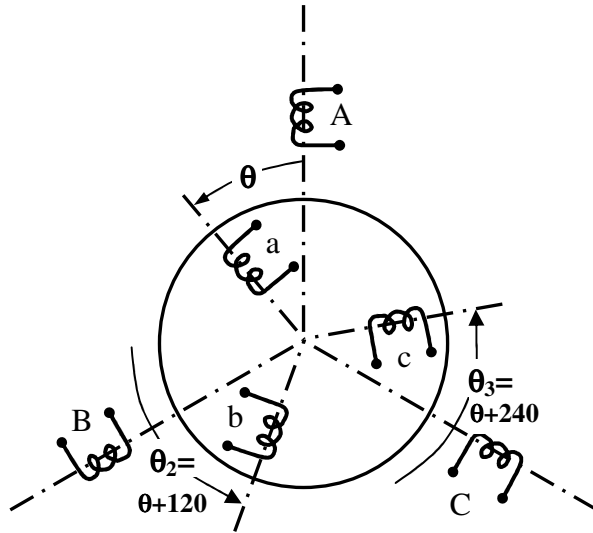
Figure 2.1 The Idealized Three-Phase Induction Machine

Stator voltage equations:

$$V_A = R_s I_A + \frac{d\lambda_A}{dt}$$

$$V_B = R_s I_B + \frac{d\lambda_B}{dt} \tag{2.1}$$

$$V_C = R_s I_C + \frac{d\lambda_C}{dt}$$

Rotor voltage equations:

$$V_a = r_r I_a + \frac{d\lambda_a}{dt}$$

$$V_b = r_r I_b + \frac{d\lambda_b}{dt} \tag{2.2}$$

$$V_c = r_r I_c + \frac{d\lambda_c}{dt}$$

where λ's are flux linkages, R_s and r_r are stator and rotor phase resistances, A, B and C represent stator windings while a, b and c represent rotor windings.

Flux linkages of the stator and the rotor windings can be written in terms of the winding inductances and the currents [15]. After writing the flux linkages in terms of the winding inductances and the currents, the voltage-current equations of the three-phase IM can be written in the matrix form given in [7] and shown in Eq. 2.3. The equations in Eq.2.3 are obtained with some simplifying assumptions. First, the effects of hysteresis and eddy-currents are ignored and teeth and slot effects are neglected. Next, it is assumed that the IM is balanced and the saturation reduces all the component fluxes in a particular region of the machine and related with each winding by the same proportion. Also, the fundamental and third harmonic components of the mutual inductances are assumed to be the general characteristics for IM's [7].

In Eq. 2.3, L_{11} is the stator self-inductance, L_{22} is the rotor self-inductance, M_{11} is the mutual inductance between stator phases, M_{22} is the mutual inductance between rotor phases, M_{121} and M_{123} are the fundamental and third harmonic components of the mutual inductance between stator and corresponding rotor phase windings at $\theta = 0$. θ, θ_2 and θ_3 are the angles between the stator phase A and rotor phases a, b, and c. The differential equations obtained are non-linear due to the presence of cosinusoidal functions of θ. A further non-linearity is introduced by the fact that the inductance parameters are affected by the saturation due to the variations in the currents.

To eliminate the non-linearity present due to the rotor angle θ, the well-known phase, commutator and turns ratio transformations can be applied to the model. The difficulty related with the application of these transformations arises from the fact that inductance coefficients depend both on the rotor angle and the currents. Hence, to carry out mathematical expressions on terms of the form $\frac{d}{dt}(L\cos\theta(t).i(t))$, where L is a non-linear function of i, becomes difficult. This difficulty can be overcome by using separation principle stated as follows [7] : The variation of L, with θ on the one

$$
\begin{bmatrix}
V_A \\
V_B \\
V_C \\
V_a \\
V_b \\
V_c
\end{bmatrix}
=
\begin{bmatrix}
R_s + pL_{11} & pM_{11} & pM_{11} & pM_{121}\cos\theta + pM_{123}\cos3\theta & pM_{121}\cos\theta_2 + pM_{123}\cos3\theta & pM_{121}\cos\theta_3 + pM_{123}\cos3\theta \\
pM_{11} & R_s + pL_{11} & pM_{11} & pM_{121}\cos\theta_3 + pM_{123}\cos3\theta & pM_{121}\cos\theta + pM_{123}\cos3\theta & pM_{121}\cos\theta_2 + pM_{123}\cos3\theta \\
pM_{11} & pM_{11} & R_s + pL_{11} & pM_{121}\cos\theta_2 + pM_{123}\cos3\theta & pM_{121}\cos\theta_3 + pM_{123}\cos3\theta & pM_{121}\cos\theta + pM_{123}\cos3\theta \\
pM_{121}\cos\theta + pM_{123}\cos3\theta & pM_{121}\cos\theta_3 + pM_{123}\cos3\theta & pM_{121}\cos\theta_2 + pM_{123}\cos3\theta & r_r + pL_{22} & pM_{22} & pM_{22} \\
pM_{121}\cos\theta_2 + pM_{123}\cos3\theta & pM_{121}\cos\theta + pM_{123}\cos3\theta & pM_{121}\cos\theta_3 + pM_{123}\cos3\theta & pM_{22} & r_r + pL_{22} & pM_{22} \\
pM_{121}\cos\theta_3 + pM_{123}\cos3\theta & pM_{121}\cos\theta_2 + pM_{123}\cos3\theta & pM_{121}\cos\theta + pM_{123}\cos3\theta & pM_{22} & pM_{22} & r_r + pL_{22}
\end{bmatrix}
\begin{bmatrix}
I_A \\
I_B \\
I_C \\
I_a \\
I_b \\
I_c
\end{bmatrix}
$$

(2.3)

hand and with i(saturation) on the other, are deemed to be separable, in the sense that it is legitimate to carry out certain mathematical operations on the quantity $\frac{d}{dt}(Li)$ while considering only the variation of L with θ, then when this series of operations is completed, to consider the variation of L with i.

Hence, based on the separation principle, during the application of the transformation techniques, the dependence of the inductance parameters on the currents (saturation) is ignored.

2.2.2. General Mathematical Model In A Synchronously Rotating Reference Frame

Since the current-voltage relations of the three-phase IM given in Eq.2.3 are quite complex and involve non-linearities due to the presence of cosinusoidal functions of the rotor angle θ, the variable transformation techniques are applied to obtain a new model of the IM in a different reference frame.
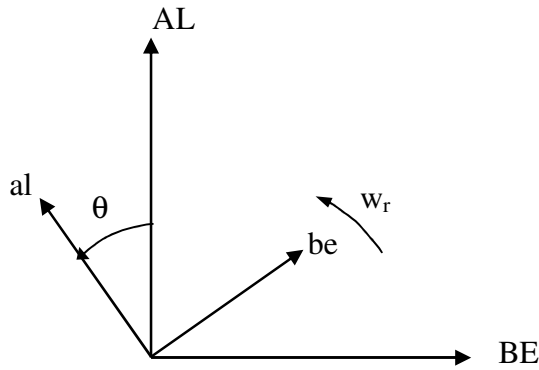
Figure 2.2 Representation of the Two-Phase Equivalent of the Induction Machine

where, w_r is the rotor speed in electrical radians per second and $w_r = \frac{d\theta}{dt}$

First, two-phase equivalent IM model with time variance inductances is obtained. It is usual to align the stator AL-axis with the stator phase A-winding. (For rotor align al-axis with the rotor a-winding). Representation of the two-phase IM is shown in

Fig.2.2. The transformation matrix from ABC to AL,BE variables is given as

$$
T_{ABC\text{-}ALBE} = \frac{2}{3}
\begin{bmatrix}
1 & -\dfrac{1}{2} & -\dfrac{1}{2} \\[2mm]
0 & -\dfrac{\sqrt{3}}{2} & \dfrac{\sqrt{3}}{2} \\[2mm]
\dfrac{1}{2} & \dfrac{1}{2} & \dfrac{1}{2}
\end{bmatrix}
\tag{2.4}
$$

$$
I_{AL,BE,0} = [T_{ABC\text{-}ALBE}]\, I_{ABC} \tag{2.5}
$$

The current I_0 represents the imbalances in the A, B, and C phase currents and it is called as the zero-sequence component of the current. The same transformation can be applied to the voltages and the fluxes both for the stator and for the rotor variables.

This transformation is called the constant phase and turns-ratio transformation. The differential equations corresponding to this representation are given as

V_{AL}		$R_s + p\,L_s$		$pM\cos\theta$	$pM\sin\theta$		I_{AL}
V_{BE}			$R_s + p\,L_s$	$-pM\sin\theta$	$pM\cos\theta$		I_{BE}
V_{al}	$=$	$pM\cos\theta$	$-pM\sin\theta$	$r_r{}' + p\,L_r$			I_{al}
V_{be}		$pM\sin\theta$	$pM\cos\theta$		$r_r{}' + p\,L_r$		I_{be}

$$\tag{2.6.a}$$

where

p=d/dt, $\tag{2.6.b}$

$L_s = L_{11} - M_{11}$ $\tag{2.6.c}$

$L_r = (N_1/N_2)^2\,(L_{22} - M_{22})$ $\tag{2.6.d}$

$r_r{}' = (N_1/N_2)^2\, r_r$ $\tag{2.6.e}$

$$M = (N_1/N_2)\ (3/2)\ M_{121} \tag{2.6.f}$$

N_1 is the stator effective turns per phase

N_2 is the rotor effective turns per phase

Next, the commutator transformation is applied to eliminate the rotor angle θ in Eq.2.6. For this purpose, different reference frames can be selected such as stationary axes fixed at the stator, rotating axes fixed at the rotor, synchronously rotating axes, etc. The basic advantage of preferring a synchronously rotating reference frame is that, for balanced stator voltages, all the state variables will assume constant values at steady-state. The axes of the synchronously rotating reference frame relative to the two-phase axes AL, BE, al and be are represented in Fig. 2.3.
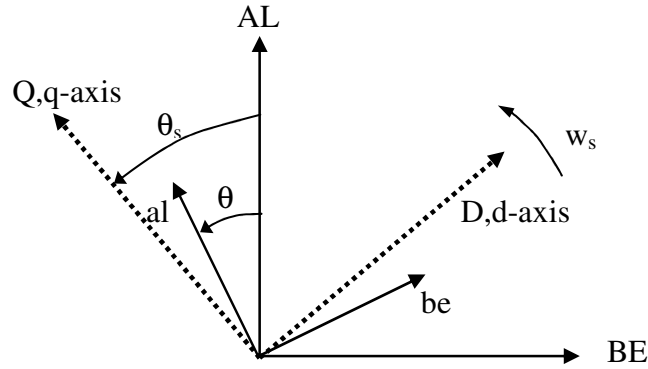
Figure 2.3 Schematic Representations of Stationary and Rotating Axes

where θ_s is the instantaneous angular position of the reference frame. In that case, the transformation matrix for the stator AL,BE to D,Q variables is given as $T_{ALBE\text{-}DQ}$ and the transformation matrix for the rotor al,be to d,q variables is given as $T_{albe\text{-}dq}$:

$$T_{ALBE\text{-}DQ} = \begin{bmatrix} \sin\theta_s & \cos\theta_s \\ \cos\theta_s & -\sin\theta_s \end{bmatrix} \tag{2.7}$$

$$I_{DQ} = [T_{ALBE\text{-}DQ}]\ I_{AL,BE} \tag{2.8}$$

$$T_{albe-dq} = \begin{bmatrix} \sin(\theta_s - \theta) & \cos(\theta_s - \theta) \\ \cos(\theta_s - \theta) & -\sin(\theta_s - \theta) \end{bmatrix} \quad (2.9)$$

$$I_{dq} = [T_{albe-dq}]\, I_{al,be} \quad (2.10)$$

Applying the commutator transformation, the commutator equivalent of the IM obtained as follows:

$$\begin{bmatrix} V_D \\ V_Q \\ V_d \\ V_q \end{bmatrix} = \begin{bmatrix} R_s + p\,L_s & -w_s\,L_s & pM & -w_s\,M \\ w_s\,L_s & R_s + p\,L_s & w_s\,M & pM \\ pM & -s\,w_s\,M & r_r{'} + p\,L_r & -s\,w_s\,L_r \\ w_s\,M & pM & s\,w_s\,L_r & r_r{'} + p\,L_r \end{bmatrix} \begin{bmatrix} I_D \\ I_Q \\ I_d \\ I_q \end{bmatrix} \quad (2.11)$$

where;

$$w_s = \frac{d\theta_s}{dt}$$ is a constant and is defined as the synchronous speed of rotation of the reference frame, and

$$-sw_s = \frac{d(\theta - \theta_s)}{dt} \quad (2.12)$$

where

$$s = \frac{(w_s - w_r)}{w_s}$$ is defined as the slip and is a function of the rotor speed w_r.

Eq.2.11 is a generalized model in the sense that different values of w_s correspond to different reference frames. For example, setting w_s equal to zero would result in a stationary reference frame fixed at the stator whereas taking w_s equal to w_r would give a reference frame fixed at the rotor. For any other choice of w_s, the steady-state variables appear as balanced sinusoids at a frequency equal to the difference between the speed of the reference frame and the system frequency.

The complete transformation matrix from ABC to DQ for the stator windings can be written as:

$$T_{ABC-DQ0} = \frac{2}{3} \begin{bmatrix} \sin\theta_s & \sin(\theta_s - \frac{2\pi}{3}) & \sin(\theta_s + \frac{2\pi}{3}) \\ \cos\theta_s & \cos(\theta_s - \frac{2\pi}{3}) & \cos(\theta_s + \frac{2\pi}{3}) \\ \frac{1}{2} & \frac{1}{2} & \frac{1}{2} \end{bmatrix} \qquad (2.13)$$

$$I_{DQ0} = [T_{ABC-DQ0}] \, I_{ABC} \qquad (2.14)$$

The inverse transformation matrix $[T_{ABC-DQ0}]^{-1}$ can be written as

$$[T_{ABC-DQ0}]^{-1} = \begin{bmatrix} \sin\theta_s & \cos\theta_s & 1 \\ \sin(\theta_s - \frac{2\pi}{3}) & \cos(\theta_s - \frac{2\pi}{3}) & 1 \\ \sin(\theta_s + \frac{2\pi}{3}) & \cos(\theta_s + \frac{2\pi}{3}) & 1 \end{bmatrix} \qquad (2.15)$$

$$I_{ABC} = [T_{ABC-DQ0}]^{-1} \, I_{DQ0} \qquad (2.16)$$

The transformation matrices for the rotor variables can be written by putting $(\theta_s - \theta)$ instead of θ_s in the transformation matrices given for the stator variables.

Figure 2.4 Three-Phase Induction Machine with D-Q axes

2.2.3. The Model of the Excitation Capacitors and the Load

Eq.2.11 represents the general model of an IM at a synchronously rotating reference frame. The system considered in this work is a SEIG supplying voltage to a load and controlled by external resistors inserted in the rotor circuit or by an external resistors connected to stator terminals, the external equations representing the self-excitation capacitors, the load and the rotor resistors should also be added to the system model.

The per-phase equivalent circuit of the SEIG referred to the stator side is shown in Figure 2.5. In Figure 2.5, $L_s - M = \ell_{11}$ and $L_r - M = \ell_{22}$. ℓ_{11} and ℓ_{22} are stator and rotor leakage inductances referred to the stator side, respectively. M is the mutual inductance between a stator and a rotor winding.

Figure 2.5 Per-Phase Equivalent Circuit of the SEIG system

If we use wound rotor IM, a three-phase resistor bank is connected to the rotor circuit whose voltage equations are as follows:

$$\begin{bmatrix} V_d \\ V_q \end{bmatrix} = \begin{bmatrix} R_{ext} & \\ & R_{ext} \end{bmatrix} \begin{bmatrix} -I_d \\ -I_q \end{bmatrix}$$

2.17

where R_{ext} is the variable resistor inserted in the rotor circuit.

Similarly, a matrix equation can be derived for the self-excitation capacitors in the synchronously rotating reference frame:

$$\begin{bmatrix} I_A \\ I_B \\ I_C \end{bmatrix} = \begin{bmatrix} pC & & \\ & pC & \\ & & pC \end{bmatrix} \begin{bmatrix} V_A \\ V_B \\ V_C \end{bmatrix}$$

2.18

Using the transformation matrices, the resultant matrix equation in the synchronously rotating reference frame:

$$
\begin{bmatrix} I_D{}^C \\ I_Q{}^C \end{bmatrix} = \begin{bmatrix} Cp & -C\,w_s \\ C\,w_s & Cp \end{bmatrix} \begin{bmatrix} V_D \\ V_Q \end{bmatrix}
$$

2.19

The load of the SEIG is assumed to be purely resistive. From Figure 2.5, load model can be written as

$$
\begin{bmatrix} I_D{}^L \\ I_Q{}^L \end{bmatrix} = \begin{bmatrix} -G & \\ & -G \end{bmatrix} \begin{bmatrix} V_D \\ V_Q \end{bmatrix}
$$

2.20

The external load connected to the stator terminals also can be added to the main load. From Figure 2.5, the current equations of the stator terminals can be written as:

$$
I_D + I_D{}^C + I_D{}^L = 0 \tag{2.21.a}
$$
$$
I_Q + I_Q{}^C + I_Q{}^L = 0 \tag{2.21.b}
$$

Then, combining Eqs. 2.19, 2.20, 2.21, we can obtain the differential equations of the stator voltages as

$$
p\begin{bmatrix} V_D \\ V_Q \end{bmatrix} = \begin{bmatrix} -1/C & & -G/C & w_s \\ & -1/C & -w_s & -G/C \end{bmatrix} \begin{bmatrix} I_D \\ I_Q \\ V_D \\ V_Q \end{bmatrix} \tag{2.22}
$$

18

Substituting external rotor resistors Eq.2.11 can be rewritten as:

$$
\begin{bmatrix} V_D \\ V_Q \\ 0 \\ 0 \end{bmatrix} = \begin{bmatrix} R_s + p\,L_s & -w_s\,L_s & pM & -w_s\,M \\ w_s\,L_s & R_s + p\,L_s & w_s\,M & pM \\ pM & -s\,w_s\,M & R_r + p\,L_r & -s\,w_s\,L_r \\ w_s\,M & pM & s\,w_s\,L_r & R_r + p\,L_r \end{bmatrix} \begin{bmatrix} I_D \\ I_Q \\ I_d \\ I_q \end{bmatrix}
$$

(2.23)

where; $R_r = r_r{}' + R_{ext}$

solving for the derivatives of the current variables, Eq.2.23 result in a set of differential equations in the form given in Eq.2.24.

$$
p\begin{bmatrix} I_D \\ I_Q \\ I_d \\ I_q \end{bmatrix} = \frac{1}{L_s L_r - M^2} \begin{bmatrix} -L_r R_s & w_s(L_s L_r - sM^2) & MR_r & w_s ML_r(1-s) & L_r & \\ -w_s(L_s L_r - sM^2) & -L_r R_s & -w_s ML_r(1-s) & MR_r & & L_r \\ MR_s & -w_s ML_s(1-s) & -L_s R_r & -w_s(M^2 - sL_s L_r) & -M & \\ w_s ML_s(1-s) & MR_s & w_s(M^2 - sL_s L_r) & -L_s R_r & & -M \end{bmatrix} \begin{bmatrix} I_D \\ I_Q \\ I_d \\ I_q \\ V_D \\ V_Q \end{bmatrix}
$$

(2.24)

19

At this stage, the currents are replaced by flux linkages, due to the fact that flux linkages in coupled circuits tend to change more slowly than currents; therefore, the use of flux linkages provides more computational stability.

$$
\begin{bmatrix} \lambda_D \\ \lambda_Q \\ \lambda_d \\ \lambda_q \end{bmatrix} =
\begin{bmatrix}
L_s & & M & \\
& L_s & & M \\
M & & L_r & \\
& M & & L_r
\end{bmatrix}
\begin{bmatrix} I_D \\ I_Q \\ I_d \\ I_q \end{bmatrix}
\tag{2.25}
$$

Defining the reciprocal inductances Γ_s , Γ_r and Γ_m as:

$$
\Gamma_s = \frac{L_r}{L_s L_r - M^2} \quad , \quad
\Gamma_r = \frac{L_s}{L_s L_r - M^2} \quad , \quad
\Gamma_m = \frac{-M}{L_s L_r - M^2}
\tag{2.26}
$$

The differential equations corresponding to the state variables V_D , V_Q , λ_D , λ_Q , λ_d and λ_q can be obtained as:

$$
p \begin{bmatrix} V_D \\ V_Q \\ \lambda_D \\ \lambda_Q \\ \lambda_d \\ \lambda_q \end{bmatrix} =
\begin{bmatrix}
-G/C & w_s & -\Gamma_s/C & & -\Gamma_m/C & \\
-w_s & -G/C & & -\Gamma_s/C & & -\Gamma_m/C \\
1 & & -R_s\Gamma_s & w_s & -R_s\Gamma_m & \\
& 1 & -w_s & -R_s\Gamma_s & & -R_s\Gamma_m \\
& & -R_r\Gamma_m & & -R_r\Gamma_r & sw_s \\
& & & -R_r\Gamma_m & -sw_s & -R_r\Gamma_r
\end{bmatrix}
\begin{bmatrix} V_D \\ V_Q \\ \lambda_D \\ \lambda_Q \\ \lambda_d \\ \lambda_q \end{bmatrix}
\tag{2.27}
$$

Eq. 2.27 can be transformed in a set of third order complex differential equations, defining the following variables:

$$V_s = V_D + jV_Q \tag{2.28.a}$$

$$\lambda_s = \lambda_D + j\lambda_Q \tag{2.28.b}$$

$$\lambda_r = \lambda_d + j\lambda_q \tag{2.28.c}$$

$$p\begin{vmatrix} V_s \\ \lambda_s \\ \lambda_r \end{vmatrix} = \begin{vmatrix} -G/C - jw_s & -\Gamma_s/C & -\Gamma_m/C \\ 1 & -R_s\Gamma_s - jw_s & -R_s\Gamma_m \\ & -R_r\Gamma_m & -R_r\Gamma_r - jw_s \end{vmatrix} \begin{vmatrix} V_s \\ \lambda_s \\ \lambda_r \end{vmatrix} \tag{2.29}$$

2.2.4. The Torque-Balance Equation

The torque-balance equation for a rotating system can be written as:

$$Jpw_r = T_e + T_m \tag{2.30}$$

where, w_r is the rotor speed in mechanical radians per second, J is the total inertia including machine and drive, T_m is the mechanical torque output, which is negative in motoring condition, and T_e is the electrical torque input. The above equation is written on a motor convention basis.

For the electrical torque, the torque expression derived from the generalized machine theory can be used [7] :

$$T_e = \bar{\imath}^T G \bar{\imath} \tag{2.31.a}$$

where, $\bar{\imath}$ is the current vector and G can be expressed as:

$$G = \frac{1}{1-s} \begin{bmatrix} & -L_s & & -M \\ L_s & & M & \\ & -sM & & -sL_r \\ sM & & sL_r & \end{bmatrix} \qquad (2.31.b)$$

Then, the expression for the electrical torque is obtained as:

$$T_e = -M(I_D I_q - I_Q I_d) \qquad (2.32)$$

where the effect of the saturation on the inductance coefficients is ignored. T_e can be expressed in terms of flux linkages as:

$$T_e = \Gamma_m(\lambda_D \lambda_q - \lambda_d \lambda_Q) \qquad (2.33)$$

To express Eq.2.22 in terms of the slip variables, s, pw_r can be written as:

$$pw_r = -\frac{1}{(pp)} w_s ps \qquad (2.34)$$

where, (pp), the number of pole pairs of the IM, is included to account for the transformation between electrical and mechanical radians per second.

Assuming that the mechanical input torque expression can also be written as a function of the shaft speed or, equivalently, of the slip, and combining Eqs.2.30, 2.33 and 2.34, generator convention the torque-balance equation takes the form given by:

$$-\frac{Jw_s}{(pp)} ps = -\Gamma_m (\lambda_D \lambda_q - \lambda_d \lambda_Q) + T_m(s) \qquad (2.35)$$

The above expression can be used as a general torque balance equation of an IM driven by a variable speed source. Since, in this work, a wind turbine is considered as

the variable speed drive for the IG, the torque-shaft speed characteristic of the wind turbine should be included in Eq.2.35 instead of $T_m(s)$. Although such characteristics for wind turbines are given in the forms of family of curves with the wind speed as a parameter for each, for the purpose of analysis, an analytical expression given in [7] is used:

$$T_m(w_t, v) = c_1 R_m^2 w_t v + c_2 R_m v^2 + c_3 \frac{v^3}{w_t} \tag{2.36}$$

where, c1 c2 and c3 are constants for the given turbine,

R_m is the maximum radius of the rotor,

v is the wind speed perpendicular to the swept area of the turbine, and

w_t is the shaft speed of the turbine.

Since the turbine has a low rotational speed a simple gear box of transmission ratio nt is used. Hence, the relationship between rotational speeds of IG and VAWT is given by:

$$w_r = n_t . w_t \tag{2.37}$$

Then, the torque component of the VAWT referred to the shaft of the IG is expressed as:

$$T_m (w_r , v) = T_m (w_t , v) / n_t \tag{2.38}$$

Finally, combining Eqs.2.35, 2.36, 2.37 and 2.38, substituting s for w_r, the torque-balance equation of the VAWT driven SEIG becomes:

$$\frac{Jw_s}{(pp)}ps = (pp)\Gamma_m (-\lambda_D\lambda_q + \lambda_d\lambda_Q) - \left[\frac{c_1 R_m^2 vw_s(1-s)}{(pp)n_t^2} + \frac{c_2 R_m v^2}{n_t} + \frac{c_3(pp)v^3}{w_s(1-s)}\right] \tag{2.39}$$

$$ps = \frac{(pp)}{Jw_s}\left[(pp)\Gamma_m (\lambda_d\lambda_Q - \lambda_D\lambda_q) - \frac{c_1 R_m^2 vw_s(1-s)}{(pp)n_t^2} - \frac{c_2 R_m v^2}{n_t} - \frac{c_3(pp)v^3}{w_s(1-s)}\right] \tag{2.40}$$

Thus, combining Eqs.2.27 and 2.40, the general mathematical model of the turbine IG-load combination is obtained as a set of seventh order non-linear real algebraic

differential equations or as a set of fourth order non-linear complex differential equations given in Eqs.2.29 and 2.40.

Since the excitation capacitors and the external resistors (connected to the stator or to the rotor terminals) are the variables to be controlled in order to keep the stator voltage and frequency constant at their prescribed values with the changing load and/or wind speed conditions, the capacitance value C and the external resistance value R_{ext} are considered as the inputs, and the stator voltage and frequency as the outputs of the system.

Since the magnitude of the complex stator voltage V_s is a function of the real rms phase voltage of the IG, the first output variable is expressed as:

$$\left|V_s\right|^2 = V_D^2 + V_Q^2 = 3.V_{rms}^2 \tag{2.41}$$

An expression for the stator frequency can be derived as the rate of change of the angle between the rotor flux phasor and the synchronously rotating reference frame D-axis and is given by:

$$f = f_s + \frac{1}{2\pi}\frac{d}{dt}\left(\tan^{-1}\frac{\lambda_q}{\lambda_d}\right) = f_s + \frac{1}{2\pi}\left(\frac{\lambda_d p\lambda_q}{\lambda_d^2 + \lambda_q^2} + \frac{\lambda_q p\lambda_d}{\lambda_d^2 + \lambda_q^2}\right) \tag{2.42}$$

where, f_s is the frequency corresponding to the speed of rotation of the synchronously rotating reference frame. The detailed information about obtaining the expression for the stator frequency is given in Chapter 3 part 5. However, it should be reminded that the above choice is arbitrary, as the frequency could as well be expressed in terms of the stator voltage or the stator flux phasor.

2.3. MODELING OF THE SATURATION

The evaluations of the saturation level and the mutual inductance term at a particular operating point require the representation of the magnetization curve of the IM under consideration. For this purpose, the magnetization characteristic of the IG used as a test machine in [7] is obtained in terms of the peak air-gap volts per synchronous speed versus peak resultant MMF per stator turns. The magnetizing characteristic is plotted in Fig.2.6 with the help of the measurements done in [7].
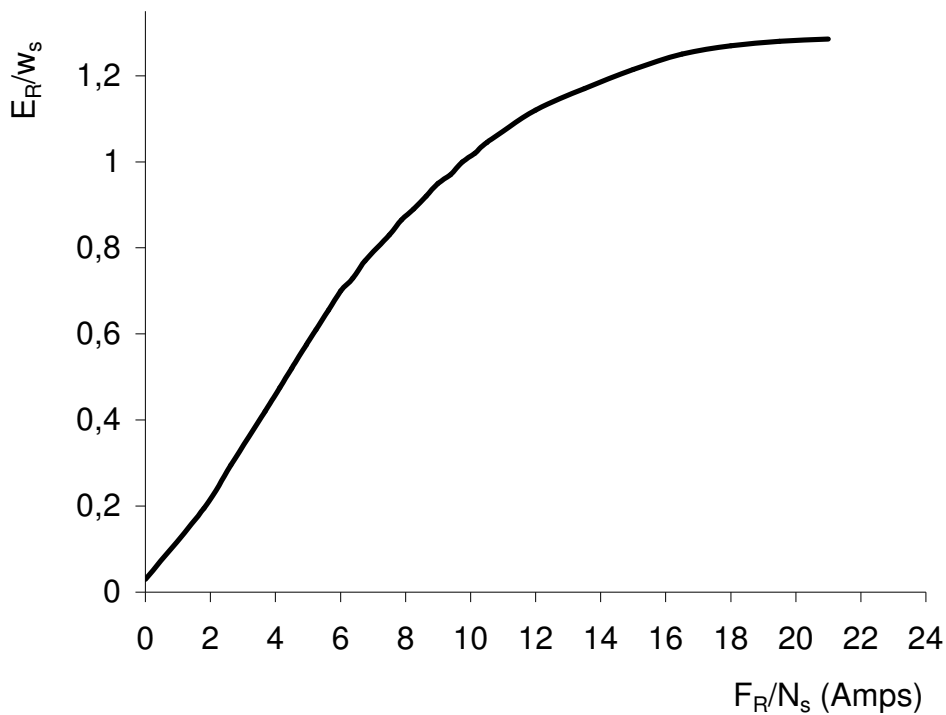
Figure 2.6 The Magnetization Characteristic of the IM

In Fig.2.6 E_R/w_s is the peak air-gap volts per synchronous speed and
F_R/N_s is the peak resultant MMF per stator turns.

The evaluation of the saturation level requires the determination of the resultant MMF in the air-gap by using the instantaneous values of the flux linkages. Figure 2.7 shows the mmf components in the air-gap of the machine, where F_s, F_r and F_R are space phasors, which represent the stator, rotor and resultant mmf, respectively.
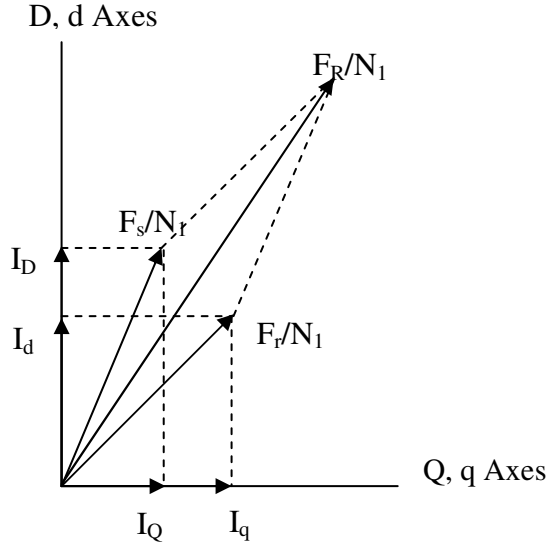
Figure 2.7 MMF Components in the Air-Gap of the IM

From Fig.2.7, an expression for the resultant mmf can be written as:

$$F_R = N_1 \, [\, (I_D + I_d)^2 + (I_Q + I_q)^2 \,]^{1/2} \tag{2.43}$$

and, Eq.2.43 can be expressed in terms of the flux linkages as:

$$F_R = N_1 \, [\, (\Gamma_s + \Gamma_m)^2 \, |\lambda_s|^2 + (\Gamma_r + \Gamma_m)^2 \, |\lambda_r|^2 + 2(\Gamma_s + \Gamma_m) \, (\Gamma_r + \Gamma_m) \, (\lambda_D \lambda_d + \lambda_Q \lambda_q)]^{1/2} \tag{2.44}$$

The relationship between the magnitudes of MMF's per turn of the actual machine and its two-phase equivalent as given by:

$$F_R / N_S = \sqrt{3/2} \; F_R / N_1 \tag{2.45}$$

The effect of the saturation can then be taken into account by evaluating the saturated value of the mutual inductance M using the magnetization curve as:

$$M_{(sat)} = \frac{E_R / w_s}{F_R / N_S} \cdot \frac{3}{2} \tag{2.46}$$

26
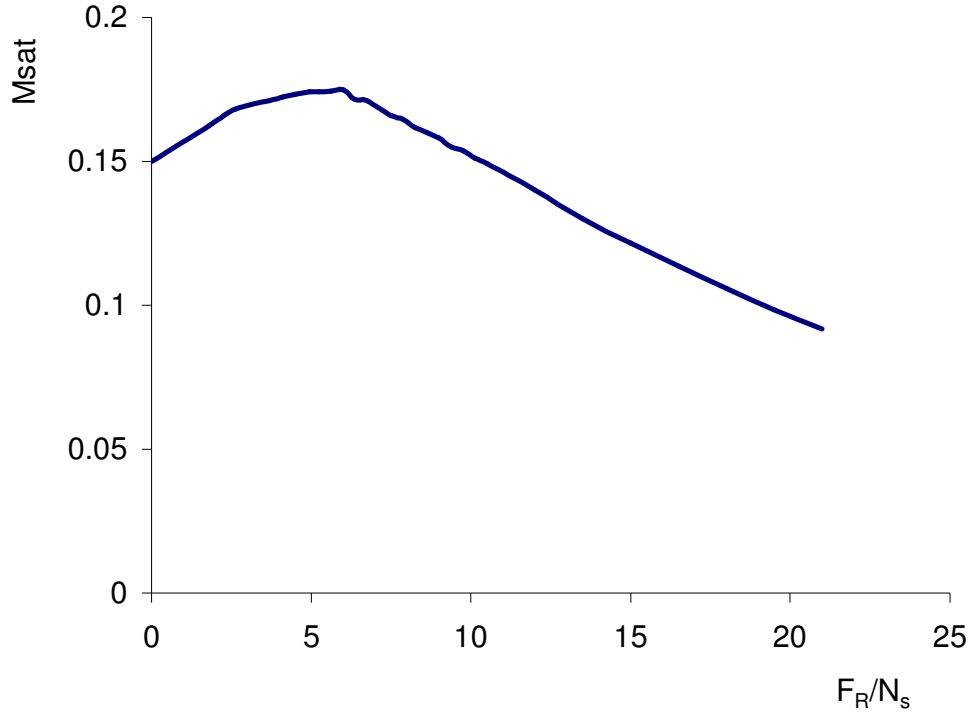
Figure 2.8 The experimental curve of the mutual inductance of the IM

The solution of the equations 2.44, 2.45 and 2.46 by a numerical method requires a complete representation of the magnetization curve. For this purpose, magnetizing characteristic should be approximated using methods such as curve fitting and straight-line approximation. The saturation curve is represented by a double-exponential function of the form [7] :

$$\frac{E_R}{w_s} = k1[1 - \exp(-k2\frac{F_R}{N_S})] + k3[1 - \exp(-k4\frac{F_R}{N_S})] + k5\frac{F_R}{N_S} \qquad (2.47)$$

The constants k1, k2, k3, k4 and k5 of the approximating function are determined by curve-fitting method and are found to be [7]:

k1=1.528544, k2=0.164617, k3=-0.291987, k4=21.888520, k5=0.005858

The corresponding double exponential function curve is shown in Figure 2.9.
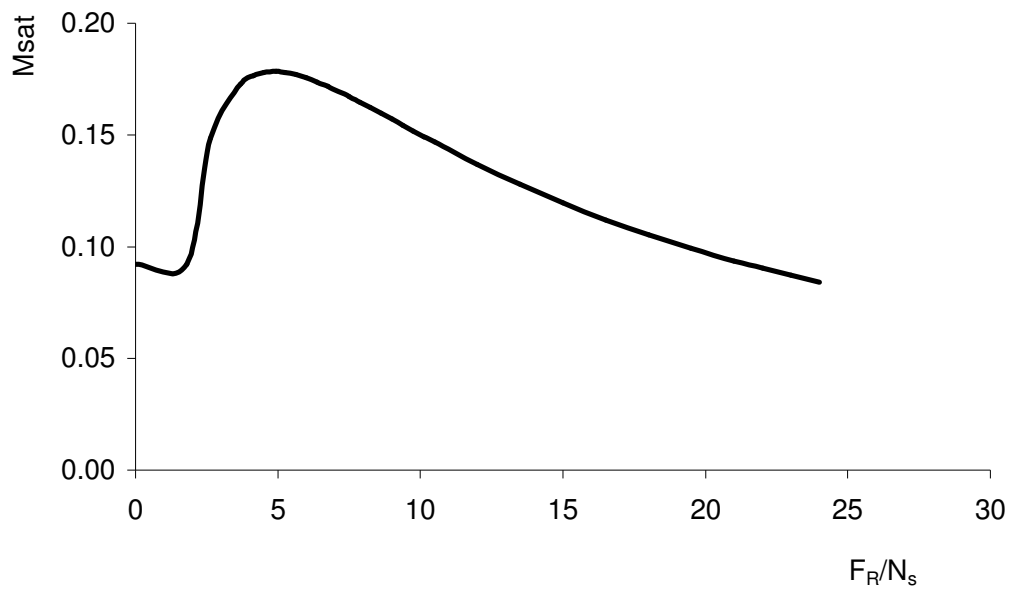
Figure 2.9 Representation of the Mutual Inductance by double-exponential function

2.4. STEADY-STATE OPERATION

2.4.1. Derivation of the Equilibrium Conditions

The conditions corresponding to the steady-state operation of the system described in the previous section can be derived as the equilibrium points of the non-linear model given in Eq.2.29 and Eq.2.40. To determine the steady-state operating conditions of the VAWT-IG-load combination, the derivative terms in Eq.2.29 and Eq.2.40 are equated to zero, i.e.:

$$p \left[\begin{array}{c|c|c|c} V_{so} & \lambda_{so} & \lambda_{ro} & s_o \end{array} \right]^T = 0 \tag{2.48}$$

where V_{so}, λ_{so}, λ_{ro} and s_o represent the steady-state values of the corresponding state variables.

For this purpose, the matrix A the vector β are defined as follows:

$$A = \left[\begin{array}{c|c} -G/C & -\Gamma_s/C \\ \hline 1 & -R_s\Gamma_s \end{array} \right] \qquad \beta = \left[\begin{array}{c} 1/C \\ \hline R_s \end{array} \right] \tag{2.49}$$

Then, Eq.2.29 is rearranged as:

$$p \left[\begin{array}{c} V_s \\ \hline \lambda_s \\ \hline \lambda_r \end{array} \right] = \left\{ \left[\begin{array}{c|c} A & -\Gamma_m\beta \\ \hline 0 \quad -R_r\Gamma_m & -R_r\Gamma_r \end{array} \right] - jw \left[\begin{array}{c|c} 1 & \\ \hline & s \end{array} \right] \left[\begin{array}{c} V_s \\ \hline \lambda_s \\ \hline \lambda_r \end{array} \right] \right\} \tag{2.50}$$

where, w is the resonance frequency of the system. It is the frequency of the state variables and its value is determined by the disturbances (G and v) and the control variables (C and R_r or G_{ext})

Equating the first two rows of Eq.2.50 to zero gives:

$$(A - jwI) \begin{bmatrix} V_{so} \\ \lambda_{so} \end{bmatrix} - \Gamma_m \beta \lambda_{ro} = 0 \tag{2.51}$$

which then yields:

$$\begin{bmatrix} V_{so} \\ \lambda_{so} \end{bmatrix} = \Gamma_m (A - jwI)^{-1} \beta \lambda_{ro} \tag{2.52}$$

But, since

$$(A - jwI)^{-1} = A(A^2 + w^2 I)^{-1} + jwI (A^2 + w^2 I)^{-1} \tag{2.53}$$

Eq.2.52 can be rewritten as:

$$\begin{bmatrix} V_{so} \\ \lambda_{so} \end{bmatrix} = \Gamma_m \{ A (A^2 + w^2 I)^{-1} \beta + jw (A^2 + w^2 I)^{-1} \beta \} \lambda_{ro} \tag{2.54}$$

Then, the third row of Eq.2.50 is equated to zero and the following expression is obtained:

$$R_r \Gamma_m \lambda_{so} + (R_r \Gamma_r + jws_o) \lambda_{ro} = 0 \tag{2.55}$$

Substituting Eq.2.54 in Eq.2.55, and defining the new variables γ, δ, ξ and η as:

$$\gamma = e_2^T \ A \ (A^2 + w^2 I)^{-1} \beta \tag{2.56.a}$$

$$\delta = e_2^T \ (A^2 + w^2 I)^{-1} \beta \tag{2.56.b}$$

$$\xi = e_1^T \ A \ (A^2 + w^2 I)^{-1} \beta \tag{2.56.c}$$

$$\eta = e_1^T \ (A^2 + w^2 I)^{-1} \beta \tag{2.56.d}$$

where, e1 and e2 are the canonical basis vectors of dimension two, Eq.2.55 takes the form of:

$$[\, R_r\, (\, \Gamma_r + \Gamma_m^{\,2}\, \gamma\,) + jw\, (\, s_o + R_r\, \Gamma_m^{\,2}\, \delta)\,]\, \lambda_{ro}\ =\ 0 \tag{2.57}$$

From Eq.2.57, for the existence of a non-zero solution for the steady-state rotor flux linkage, two conditions are obtained as:

$$\mathbf{\Gamma_r + \Gamma_m^{\,2}\, \gamma\ =\ 0} \tag{2.58}$$

$$\mathbf{s_o\ =\ -\, R_r\, \Gamma_m^{\,2}\, \delta} \tag{2.59}$$

Similarly, equating the right-hand side of the torque-balance equation to zero and substituting λ_{so} from Eq.2.54, an equilibrium condition corresponding to the rotor flux linkage is derived as:

$$\left|\lambda_{ro}\right|^2 = \frac{T_m(s_o, v)}{(pp)w\Gamma_m^2\delta} \tag{2.60}$$

Finally, the equilibrium values corresponding to the stator voltage V_s and the stator flux linkage λ_s can be derived using Eq.2.54 in terms of the steady-state value of the rotor flux linkage as:

$$\left|\lambda_{so}\right|^2 = \Gamma_m^2\, (\gamma^2 + w\delta^2)\, \left|\lambda_{ro}\right|^2 \tag{2.61}$$

$$\left|V_{so}\right|^2 = \Gamma_m^2\, (\xi^2 + w^2\eta^2)\, \left|\lambda_{ro}\right|^2 \tag{2.62}$$

The equations 2.58-2.62 form together the equilibrium conditions of the system described in Eq.2.29 and 2.40.

Using the equilibrium equations obtained, some fundamental results can be deduced concerning the conditions for the existence of the equilibrium points for the system, the effects of various system parameters on the steady-state operation of the SEIG, the steady-state performance characteristics of the system, etc.

2.4.2. Steady-State Performance of the System

The steady-state operating conditions of the system have been derived by solving the equilibrium points of the non-liner model of the system. From the classical per-phase equivalent circuit of the IM, the equations 2.58-2.62 correspond to the basic active and reactive power balance expressions. The active power supplied by the IM is to be absorbed by the load and the reactive power balance between the capacitor C and the IM should be present for the IM to generate sinusoidal voltages at constant frequency.

It is important to note that, with the effect of the saturation neglected, the equation 2.58 is totally independent of the state variables and thus is termed as the "**resonance condition**" to be satisfied for the occurrence of steady-state oscillations at machine terminals. Eq.2.58 can be written in an open form by replacing γ variable with the original parameters as:

$$\Gamma_r C^2 w^4 + [\ C\ (\Gamma_m{}^2 - 2\Gamma_s\Gamma_r) + C^2 R_s{}^2\Gamma_s\ (\Gamma_s\Gamma_r - \Gamma_m{}^2) + \Gamma_r G^2\ ]\ w^2 +$$
$$\Gamma_s\ [\ \Gamma_r\ (\Gamma_s G^2 + 2R_s\Gamma_s G + \Gamma_s) - \Gamma_m{}^2\ (2R_s G + R_s{}^2 G - 1)] = 0 \qquad (2.63)$$

Equation 2.63 is the solution of the resonance frequency w of the system. If, then, the resonance condition is satisfied at steady state for a specific w, this value will correspond to the constant frequency of oscillations, which, for the capacitive self-excited case, depends on the internal properties of the machine (Rs, Ls, Lr, M), the value of the capacitor C and the load G.

Simulation studies in the next chapter show that, there is no unique equilibrium state due to the fact that the phase of the resulting oscillation is determined by initial conditions. There are, therefore, an infinity of equilibrium states, each of which has the same voltage and current amplitude, but a different absolute phase.

The operation of a SEIG is highly effected by the magnetic saturation. However, it is concluded in [7] that, it is possible for the generator to self-excite and rotate at a constant speed while producing constant voltage and frequency by appropriate adjustments of the two control variables, R_{ext} and C.

The steady-state equilibrium conditions of the SEIG are summarized in tables below for two different representations of the magnetization characteristic given in Fig.2.6;

  a) The operating line passing through the point corresponding to rated voltage and flux is used as an approximation to the magnetization characteristic. The results are in Table 2.1.
  b) The saturation curve is represented by a double exponential function given in Eq.2.47. The results are in Table 2.2.

The parameters of the IM and the VAWT used in computations are given as:

$R_s = 0.9$ Ω

$l_s = 0.011$ H

$l_r = 0.0017$ H

$r_r = 0.2$ Ω

$N_1/N_2 = 2.5$

$n_t = 7.2$

$h1 = c_1 R_m{}^2 = -3.2281,$ $h2 = c_2 R_m = 12.9094,$ $h3 = c3 = -8.80384$

$(pp) = 2$

$J = 1$ kg-m^2

$v =$ wind speed in m/sec

M = Mutual inductance in Henry

f_o, s_o, λ_{ro}, λ_{so} and V_{so} are the steady-state values of the frequency, slip, rotor flux linkage, stator flux linkage and Stator phase voltage in rms, respectively.

Table 2.1 Equilibrium States Obtained for M=0.157832 H Constant (Rr=1.25Ω, C=78.518 μF)

M, H	G, mho	v, m/s	f_o, Hz	s_o	λ_{ro}	λ_{so}	V_{so}, V
0.1578	0.015	10	46.039	-0.02205	1.647	1.772	291.91
0.1578	0.017	10	46.646	-0.02497	1.523	1.641	273.46
0.1578	0.019	10	47.347	-0.02791	1.412	1.525	257.54
0.1578	0.021	10	48.156	-0.03090	1.311	1.420	243.38
0.1578	0.023	10	49.092	-0.03395	1.216	1.321	230.42
0.1578	0.02469	10	50.000	-0.03658	1.139	1.240	220.00
0.1578	0.027	10	51.455	-0.04030	1.033	1.130	205.95
0.1578	0.029	10	52.969	-0.04367	0.938	1.032	193.29
0.1578	0.031	10	54.805	-0.04726	0.836	0.927	179.16
0.1578	0.033	10	57.105	-0.05119	0.719	0.804	161.76
0.1578	0.02469	7.25	50.000	-0.03658	0.084	0.091	16.18
0.1578	0.02469	7.5	50.000	-0.03658	0.330	0.359	63.73
0.1578	0.02469	8	50.000	-0.03658	0.569	0.620	109.94
0.1578	0.02469	8.5	50.000	-0.03658	0.743	0.809	143.59
0.1578	0.02469	9	50.000	-0.03658	0.890	0.969	171.95
0.1578	0.02469	9.5	50.000	-0.03658	1.020	1.111	197.12
0.1578	0.02469	10	50.000	-0.03658	1.139	1.240	220.00
0.1578	0.02469	10.5	50.000	-0.03658	1.248	1.359	241.08
0.1578	0.02469	11	50.000	-0.03658	1.349	1.469	260.63
0.1578	0.02469	11.5	50.000	-0.03658	1.443	1.572	278.83
0.1578	0.02469	12	50.000	-0.03658	1.531	1.667	295.78
0.1578	0.02469	13	50.000	-0.03658	1.688	1.839	326.23

Table 2.2 Equilibrium States Obtained for Double-Exponential Representation of the Magnetization Characteristic (Rr=1.25Ω, C=78.518 μF)

M, H	G, mho	v, m/s	f_o, Hz	s_o	λ_{ro}	λ_{so}	V_{so}, V
0.1270	0.015	10	51.009	-0.02299	1.412	1.546	282.18
0.1344	0.017	10	50.343	-0.02574	1.358	1.482	266.55
0.1412	0.019	10	49.935	-0.02850	1.302	1.419	252.67
0.1475	0.021	10	49.753	-0.03130	1.246	1.357	240.24
0.1532	0.023	10	49.802	-0.03414	1.188	1.294	228.90
0.1578	0.02469	10	50.000	-0.03658	1.139	1.240	220.00
0.1636	0.027	10	50.541	-0.04000	1.067	1.165	208.41
0.16822	0.029	10	51.277	-0.04306	1.002	1.096	198.56
0.17232	0.031	10	52.340	-0.04628	0.929	1.019	188.27
0.1759	0.033	10	53.818	-0.04971	0.844	0.932	176.69
0.17845	0.02469	7.9	47.074	-0.03576	0.696	0.751	125.42
0.17838	0.02469	8	47.083	-0.03576	0.729	0.787	131.39
0.17528	0.02469	8.5	47.491	-0.03587	0.863	0.932	157.02
0.17014	0.02469	9	48.19	-0.03607	0.969	1.049	179.33
0.16414	0.02469	9.5	49.047	-0.03631	1.059	1.150	200.09
0.1578	0.02469	10	50.000	-0.03658	1.139	1.240	220.00
0.1514	0.02469	10.5	51.032	-0.03689	1.209	1.322	239.39
0.14472	0.02469	11	52.176	-0.03725	1.271	1.396	258.39
0.13805	0.02469	11.5	53.400	-0.03764	1.326	1.463	277.23
0.1315	0.02469	12	54.691	-0.03807	1.376	1.526	296.01
0.1188	0.02469	13	57.496	-0.03908	1.458	1.636	333.72

The steady-state solution of the system and the evaluation of the mutual inductance term with the double exponential representation of the saturation curve are given as a matlab file in the Appendix A.

The results in Table 2.1 and Table 2.2 are shown below in graphical representations;
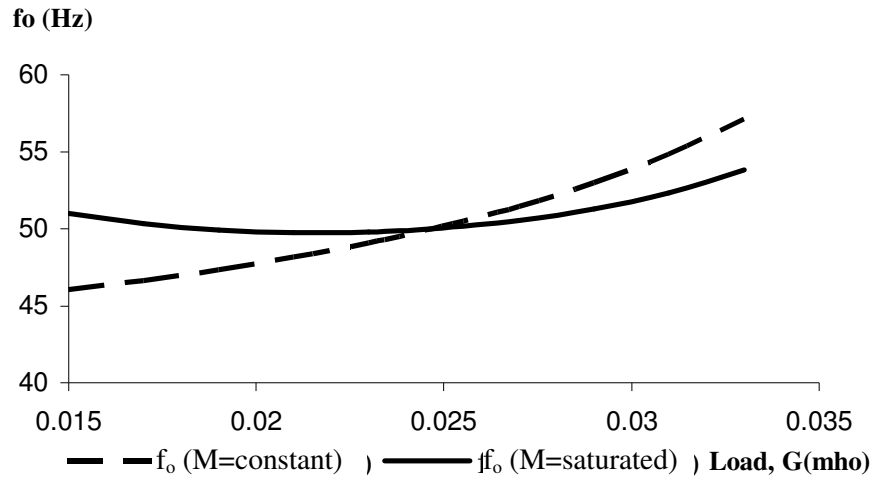
Figure 2.10 Steady-state equilibrium points of the frequency for different loads (R_r=1.25Ω, C=78.518 μF).
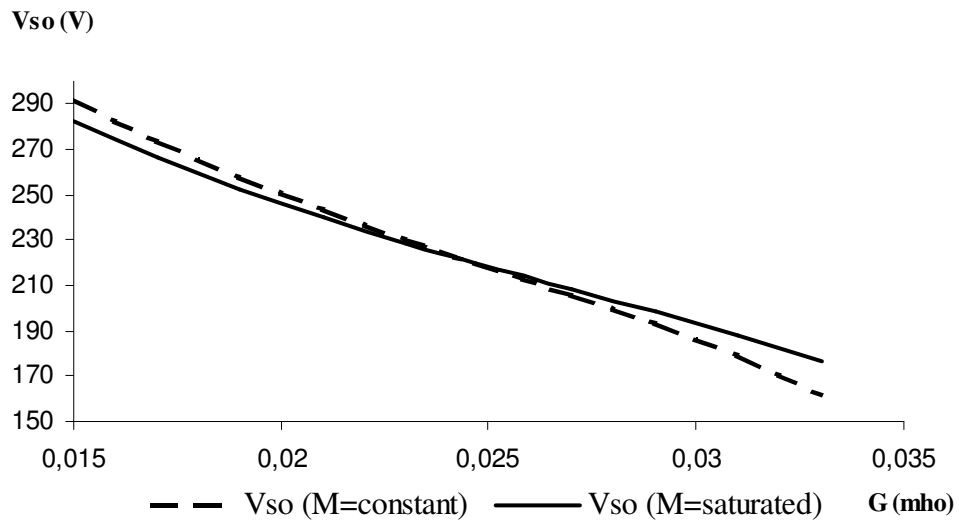
Figure 2.11 Steady-state equilibrium points of the Stator Voltage for different loads (R_r=1.25Ω, C=78.518 μF).
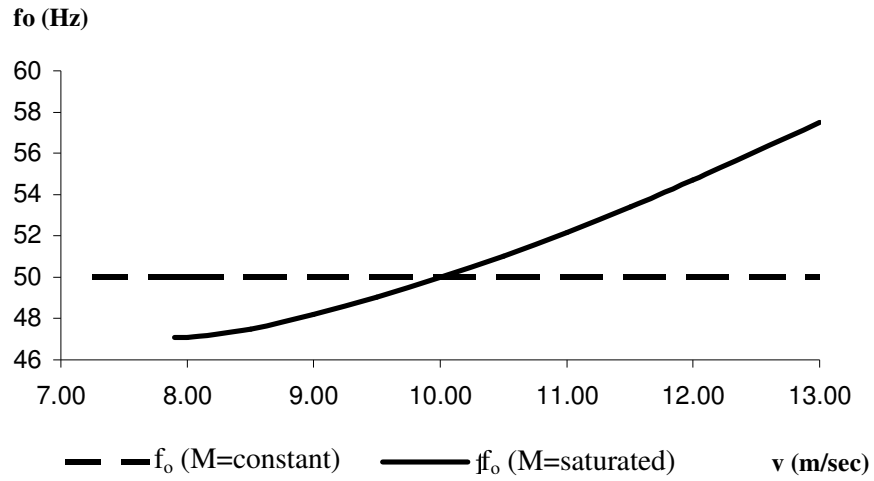
Figure 2.12 Steady-state equilibrium points of the frequency for different wind speeds (R_r=1.25Ω, C=78.518 μF).
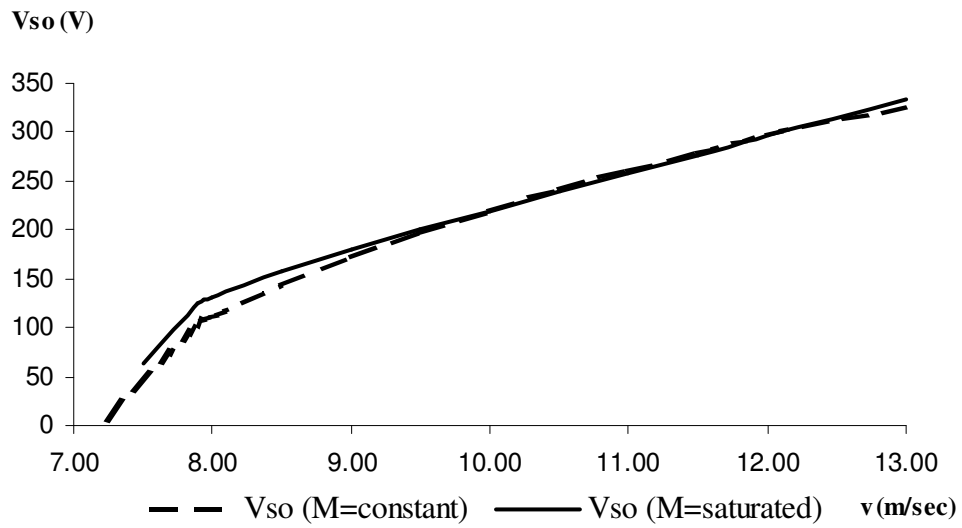
Figure 2.13 Steady-state equilibrium points of the Stator Voltage for different wind speeds (R_r=1.25Ω, C=78.518 μF).

The results show that approximation of the magnetizing curve gives acceptable results for the steady-state conditions especially near the rated voltage and flux values. However, for the constant mutual inductance, wind speed has no effect on frequency and slip so on rotor shaft speed. Therefore, for variable wind speed applications, saturation effect should be taken into account.

Below the steady-state effects of the control variables, C and R_r (Rotor total resistor $r_r^{'} + R_{ext}$), on the steady-state values of the output variables, V_{so} and f_o, are shown for the wound rotor IM. For the squirrel-cage IM, since the control variables are C and G_{ext}(External load connected to the stator), effect of the G_{ext} is the same as the normal load effect given in Fig. 2.10 and Fig. 2.11.
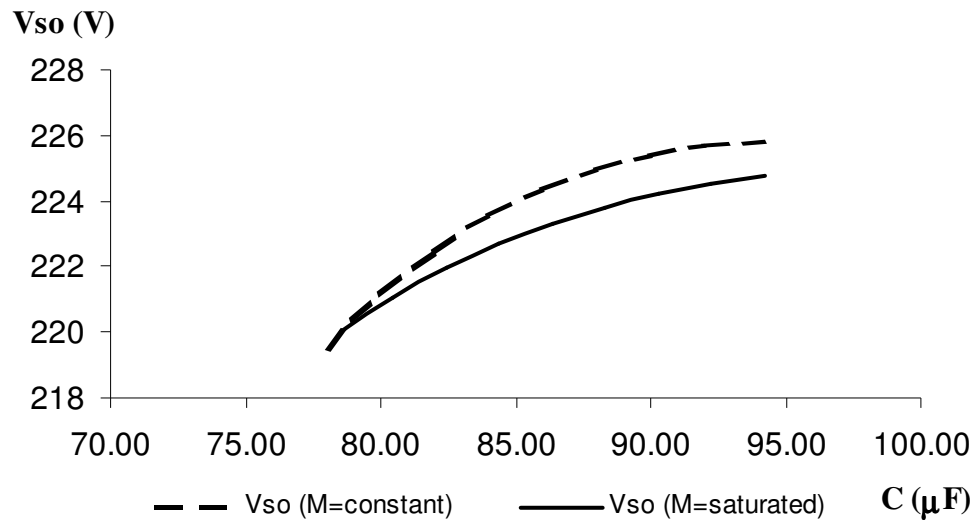
Figure 2.14 C versus V_{so} in steady-state (R_r=1.25Ω, G=0.0247 mho).

38
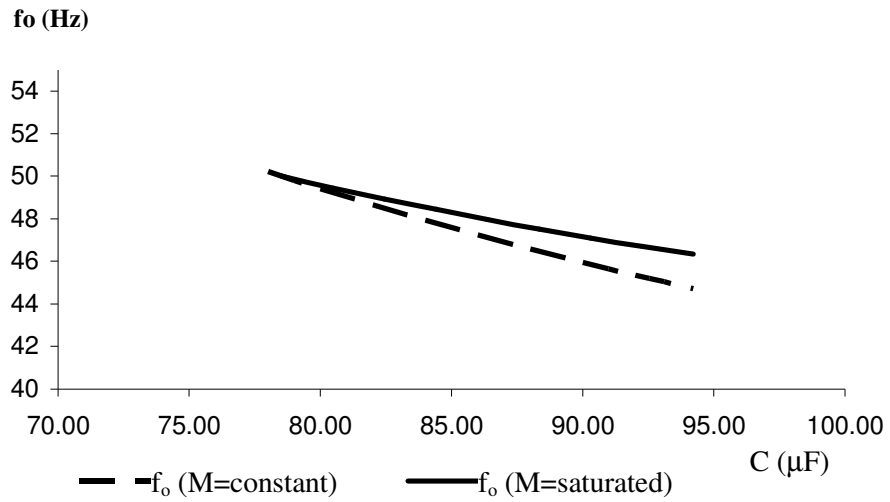
Figure 2.15 C versus f_o in steady-state (R_r=1.25Ω, G=0.0247 mho).
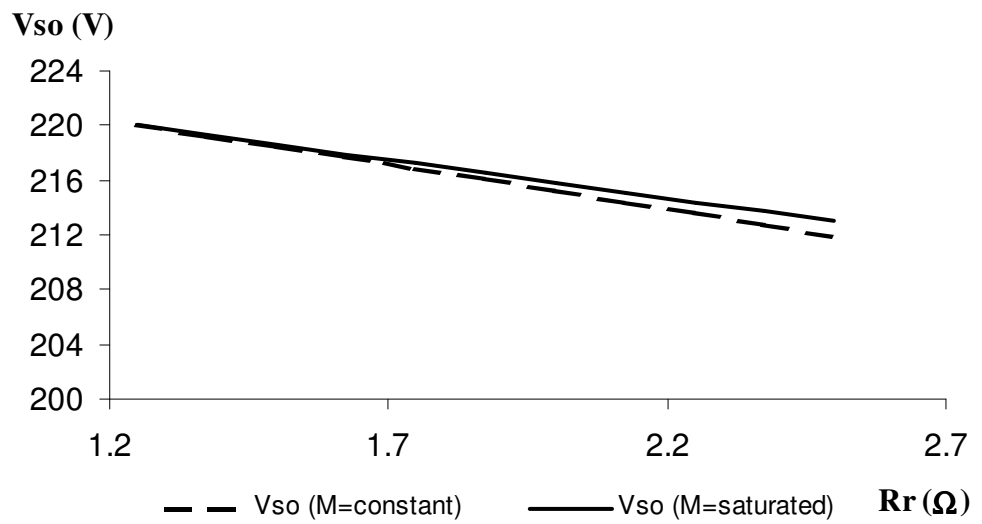
Figure 2.16 R_r versus V_{so} in steady-state (C=78.518 µF, G=0.0247 mho).
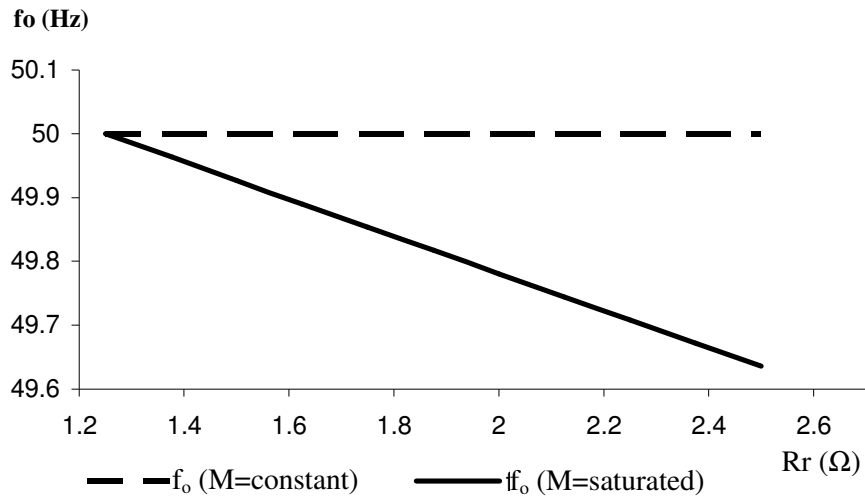
Figure 2.17 R_r versus f_o in steady-state (C=78.518 μF, G=0.0247 mho).

The self-excitation phenomenon depends on whether the equations 2.58 to 2.62 are satisfied for different load and wind speeds. C versus G plane should be obtained for the existence of the self-excitation defined in Eq.2.63. C versus G plane is shown in Fig 2.18, as long as the excitation capacitance value is adjusted above the curve, the self-excitation can occur at a constant frequency determined from the resonance conditions.
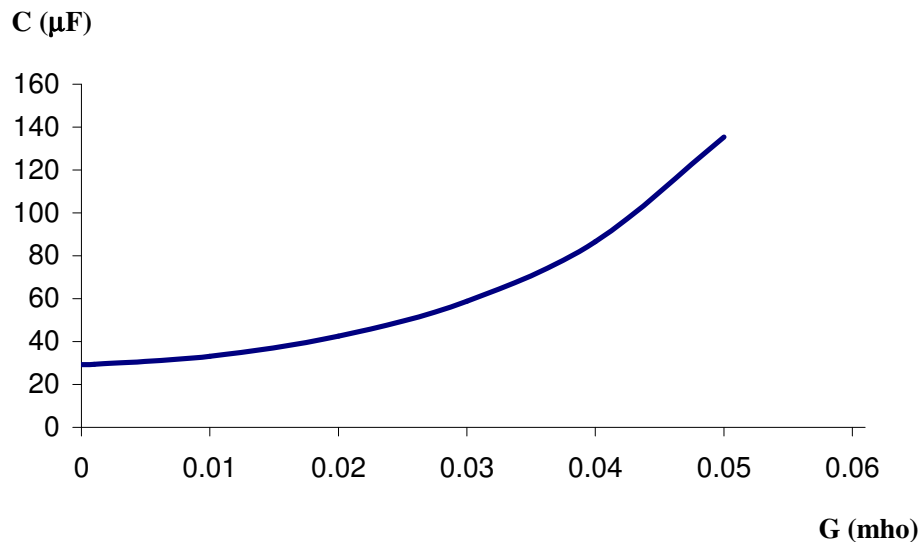
Figure 2.18 C versus G plane for the existence self-excitation at a constant frequency solution from the resonance condition (M=0.1578 mH constant).

On the other hand, since at steady-state, the frequency is required to stay constant at 50 Hz, the excitation capacitance should be modified according to the load variations. Fig. 2.19 shows the capacitance values versus the load conductance for the IG to self-excite at 50 Hz.
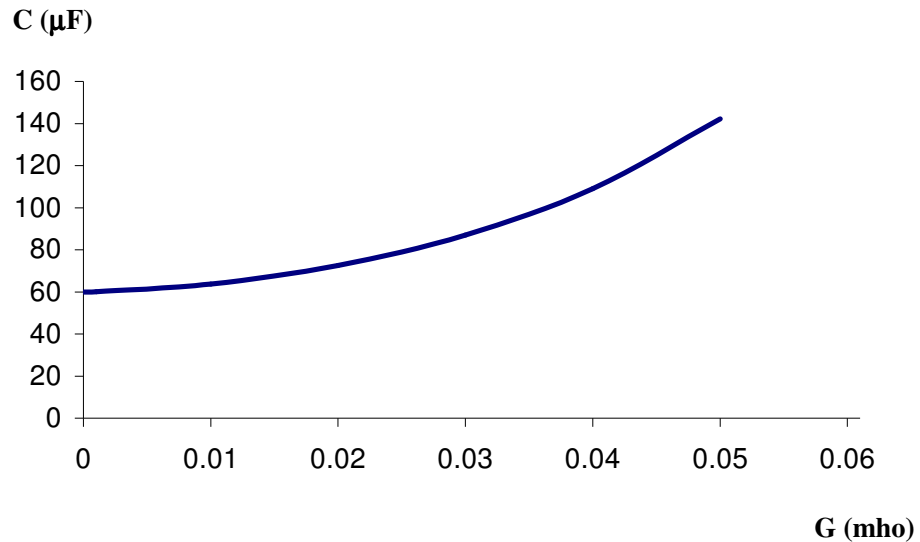
Figure 2.19 C versus G plane for the existence of Self-excitation at 50 Hz (M=0.1578 mH constant).

Also, a region can be determined in terms of the load G and the wind speed v for the existence of the self-excitation. Fig.2.20 shows such a region on the assumption that M, R_r and C are constant at their values corresponding to rated voltage and frequency at rated load and wind speed.

Figure 2.21 shows wind speed (v) versus load (G) curves for the self-excitation at rated voltage and frequency (M=0.1578 mH constant) for different rotor resistance values.
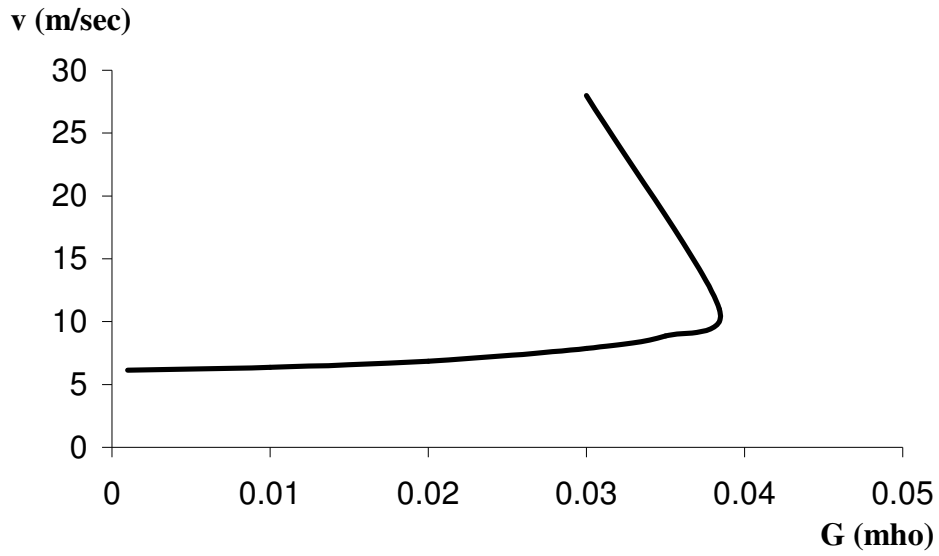
Figure 2.20 v versus G plane for the existence of a Positive Turbine Torque (M=0.1578 mH constant).
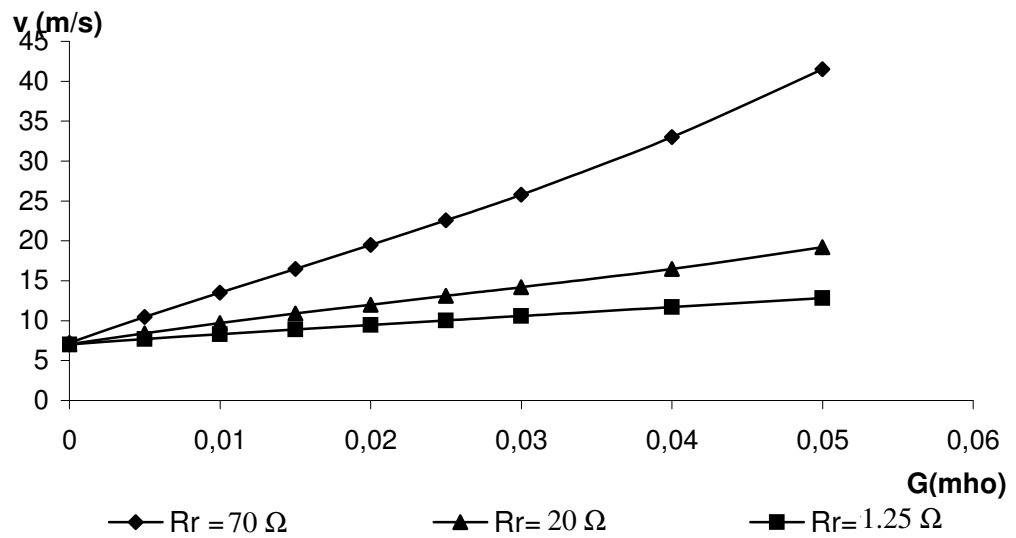
Figure 2.21 v versus G curves for the self-excitation at rated voltage and frequency (M=0.1578 mH constant).

It is worth mentioning that both the results presented in [7] and the steady-state conditions derived in the previous section indicate that single loop control methods are inadequate in order to satisfy CVCF operation of the VAWT-SEIG combination whenever the load and/or the wind speed changes, and thus multi-variable control - strategies have to be developed.

As a conclusion, in this chapter, a general mathematical model is derived for the VAWT-SEIG-load combination. This model can be used to predict the steady-state and the transient behaviors of the system.

In the next chapter the transient behavior of the SEIG and the control strategies developed in [7] will be modeled in Matlab/Simulink. Besides, the control strategies for the cage type IG will be developed and the control signal obtained from the controller will be used in the simulation of the system with SVC consists of a large fixed capacitor with Thyristor Controlled Reactor for frequency regulation. Voltage regulation, on the other hand will be done by eight resistive loads connected to the stator terminals in parallel having switches controlled by the controller to adjust the load value.

CHAPTER 3

SIMULATIONS AND RESULTS

3.1.   INTRODUCTION

In this chapter, the modeling of the IG, Wind Turbine, Controlled Excitation-Capacitance, Variable Resistive Load, and Controlled External Load combination are done with MATLAB 6.5 / Simulink 5.0 technical computing software which is one of the most popular simulations program. Based on the models obtained, simulations are done in a wide range of operation where the wind speed and the load can be varied below and above rated values.

First, the general model developed in Chapter 2 is simulated with the set of the seven differential equations given in Eq.2.27 and Eq.2.40. Saturation effect is added to the model by representing the saturation curve with the double-exponential function given in Eq.2.47.

Second, the dynamic responses of the output variables of the SEIG under various step type disturbance conditions in load and wind speed are simulated. Also, the responses of the feed-forward control are simulated by immediate adjustment of the control variables C and R_r.

Third, based on the steady-state analysis done in Chapter 2 and the dynamic responses of the system, control flowcharts are drawn for control strategies.

Fourth, the closed-loop controls proposed in [7] are applied to Wound Rotor IM. For

the Squirrel Cage IM, there are two possibilities for the frequency regulation, one with the variable excitation capacitance and the other with variable external load connected in parallel to the main load, since the resonance frequency in Eq.2.63 depends both on C and G. Also voltage regulation can be done with a variable capacitance or with a variable external load, since the steady-state terminal voltage depends both on C and G. The variables ξ, η and w contain C and G terms in Eq.2.62, which gives the equilibrium value of the stator voltage. Steady-state analysis of the C and G effects on voltage and frequency can be seen in Figures 2.10, 2.11, 2.14 and 2.15. In this study, voltage regulation is done with the external loads while the frequency regulation is done with the variable excitation capacitance. Control signals obtained for C and G is used in the further simulations.

Fifth, the standard Asynchronous Machine of the Power System Blockset of the Matlab is used for simulation. Information about the Matlab, Simulink and Power System Blockset is given in [16] and explained in Appendix B. Obviously, the model of the Matlab Asynchronous Machine is the same with the model given in Chapter 2. There are some differences between two models in evaluating the state variables. The Matlab model uses mutual fluxes in calculating the rotor and stator fluxes [15].

Saturation effect is not considered in Matlab's Asynchronous Machine model. Therefore the inner model of the machine is modified to add the saturation effect given in Eq.2.43, Eq2.45, Eq.246 and Eq.2.47. To do this, the saturation related equations are added to the "Mutual Fluxes" block of the machine whose variables are in p.u. values. The rotor and stator currents are converted from p.u. to SI variables to apply the related equations, and then the calculated mutual inductance value is converted to p.u. value.

After getting the saturation adaptive induction machine, variable excitation capacitance is modeled with a three phase Y-connected capacitor and Y-connected Thyristor Controlled Reactor (TCR). Operating principle of the TCR is given in [17] and explained in Appendix C.

Variable external load, on the other hand, is modeled with eight resistors connected parallel to the stator terminals of the IM. Their resistance values are 10000, 5000, 2500, 1250, 625, 312.5, 156.25, 78.125 ohms. They are controlled by 24 switches (eight switches for each phase), resulting in $2^8 = 256$ different switching possibilities. Each switching possibility results in a different resistance value. This type of operation is used as a frequency regulator in the demonstration of the wind power generation in Power System Blockset. As a last step, the whole model is simulated for the CVCF operation of the stand-alone SEIG application.

It should be noted that, operation of the SEIG with constant mutual inductance is only given in The Dynamic Responses of the SEIG part to compare it with saturation adaptive mutual inductance (Represented by Double-Exponential Representation of the Magnetization Curve given in Chapter 2). In the other parts, all the simulations are done with the saturation taken into account.

3.2.   MODEL OF THE INDUCTION MACHINE

Induction Machine (IM) can be modeled as a set of seventh order non-linear real algebraic differential equations given in Eqs.2.27 and 2.40 in Simulink. Saturation effect is added to the model with Eqs.2.44, 2.45, 2.46 and 2.47. The model of the IG is given in Figure 3.1. Calculation of the Mutual inductance is shown in Figure 3.2.

In Simulink, it is possible to see the characteristics of the all variables used in the model, including the state variables, differential of the state variables, and variation of the mutual inductance with saturation during the transient period.

The same machine parameters are used in all simulations as it is given in Chapter 2. By using this IM model we can see the dynamic responses of the SEIG under various disturbance conditions with a control applied or without any control applied.
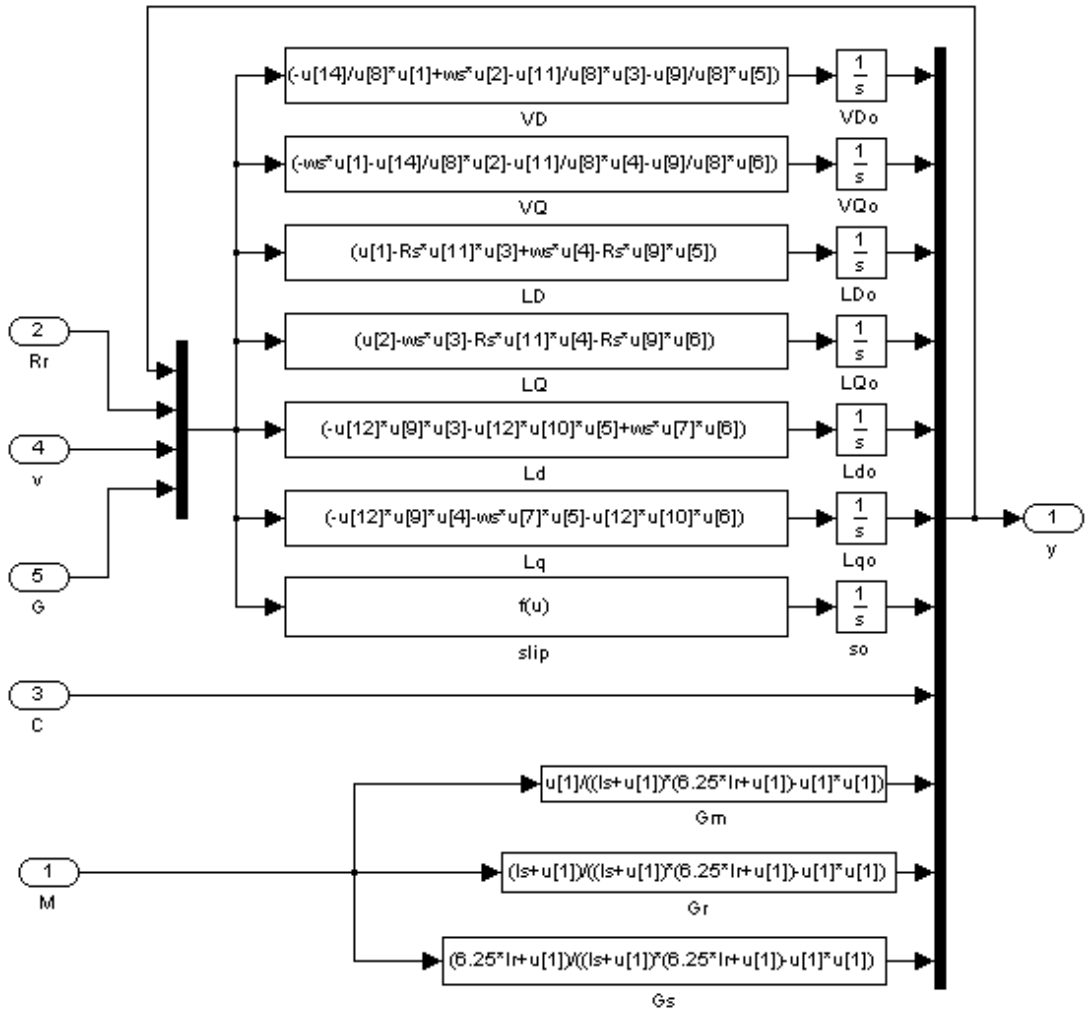
Figure 3.1 Model of the Induction Machine

In figure 3.1, the differential equations of the state variables are written in function blocks, the output of the function block is integrated with an integrator block whose transfer function is 1/s. It is important that the initial values of the state variables should be given to each integrator correctly. To obtain the correct initial values, the system is started with the random initial values for a specified C, R_r, G and v values. After the system is reached its equilibrium point, the state variables reach to their steady-state values. These steady-state values are the correct values of these operating conditions. There are infinitely many equilibrium states determined by the random initial conditions at the starting of the simulation. In the IG model given in Fig.3.1, Γ_m, Γ_r and Γ_s (represented as G_m, G_r and G_s) values are also calculated in

each integration step due to the saturation effect on the mutual inductance. C, R_r, G and v values are coming from the outside of the machine block which represent disturbance and control values, either they are constants or variable values.
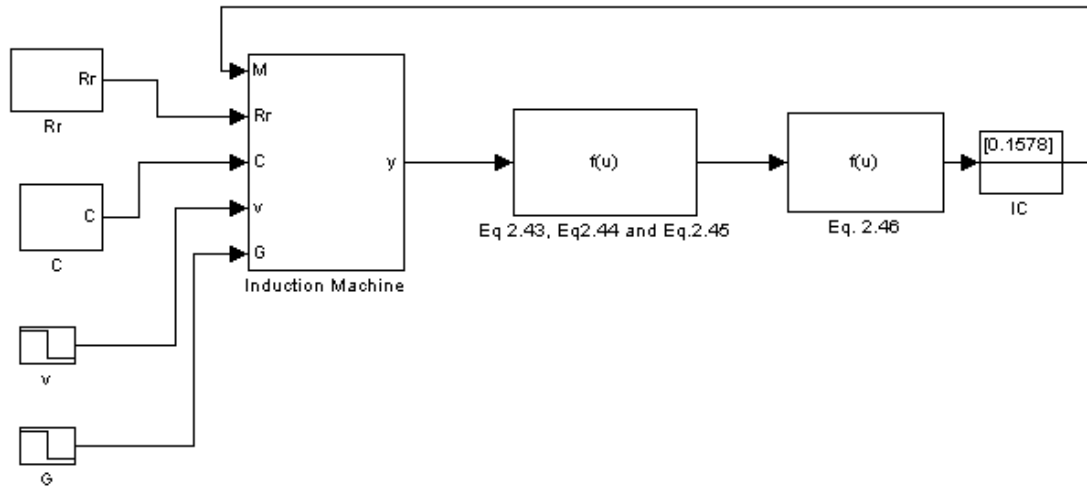
Figure 3.2 Calculation of the Mutual Inductance

In Figure 3.1 and Figure 3.2;

R_r is the rotor total resistance $r_r' + R_{ext}$

C is the excitation capacitance

v is the wind velocity, G is the load (1/R_{load})

IC block is initial condition block for the mutual inductance

LD is the flux linkage of stator D axis (λ_D) whose initial value is LDo.

3.3. THE DYNAMIC RESPONSES OF THE SEIG

The natural dynamic responses of the SEIG are obtained if there is no control on the control variables, C, R_r and G_{ext}. Various disturbance conditions in the load and in the wind speed are applied to the SEIG and the transient performances of the system are investigated. Due to the simplicity of the case and its closeness to real life situations, the load and the wind speed disturbances are assumed to be of step form. The circuit used in this part is shown in Figure 3.3. In the circuit, capacitor and rotor resistor values are fixed, while step type changes can be applied to the disturbances.
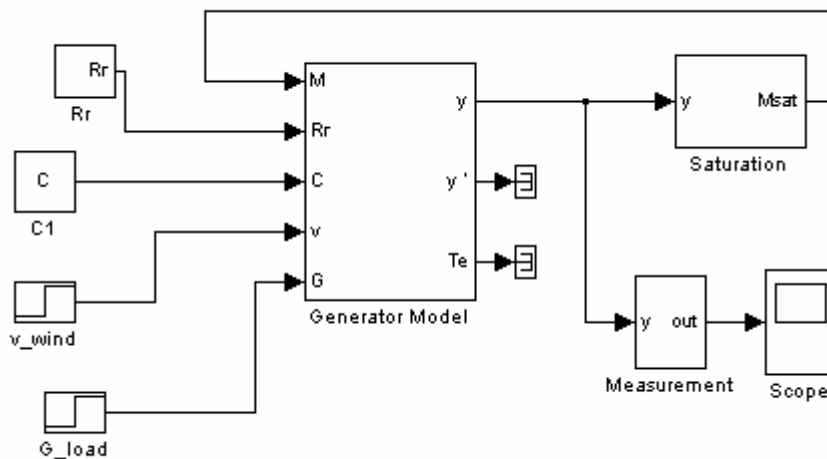
Figure 3.3 Dynamic Response Circuit Diagram of the General Model

In Fig.3.3, saturation effect can be neglected if it is wanted. To do this a constant value is connected to the M input (which represents mutual inductance) of the generator model. Te and y' output of the generator are not used. Te represents electrical torque of the machine whose equation is given in Eq.2.33, y' represents the derivatives of the state variables. The derivative of a variable is taken from the input of its integrator shown in Fig.3.1. Each parameter or variable can be analyzed by connecting a scope to its connecting wire. Measurement block is nothing but a selector of the output variables to be seen in the scope.

Step type disturbances are applied to the system and the results are shown in Figures 3.4-3.7. Before applying the disturbances we found the initial conditions of the state variables for the rated stator line-to-neutral voltage V_s =220Vrms and the rated frequency f=50Hz with the load G=0.0247mho and the wind speed v=10m/s. At these wind speed and load values, the values of the control variables are the capacitor C=78.518 μF and the rotor resistance Rr=1.25ohm. Now, it is ready for the simulation to be started.

Simulations are started with rated values, step type disturbances are applied at the specified times and the variation of the output variables are observed. Applied disturbance and its time are written in the figure names.

The simulations are done both with the constant mutual inductance and saturation effected mutual inductance. The saturation is represented with the double exponential representation of the magnetizing curve, which is explained in Chapter 2.
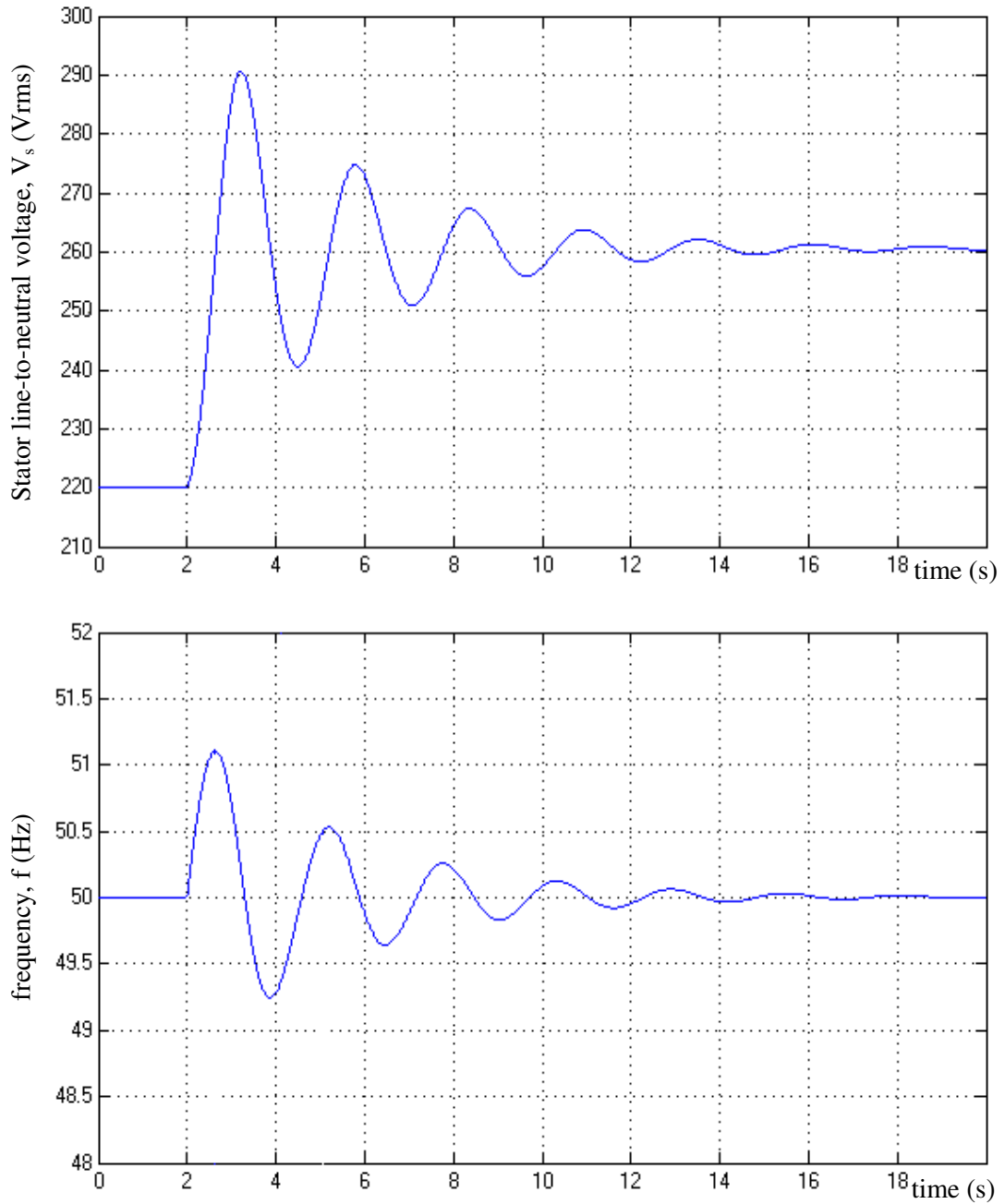
Figure 3.4 Stator line-to-neutral Voltage and frequency responses of the General Model corresponding to disturbance in the wind speed v=10m/s → 11m/s at t=2s, G=0.0247 mho constant (M=0.1578316 H Constant)

It is seen in Figure 3.4 that, 10 % increase in the wind speed will result in an increase in the stator voltage value. There is a big overshoot and the settling time is about 14-15 seconds. On the other hand, the oscillation in the frequency is less than the

voltage, and the frequency goes to its rated value 50 Hz at steady-state. These results are valid with the steady-state analysis done in Chapter 2.

The wind speed term v exists only in the mechanical torque T_m given in Eq.2.36, which is proportional with the cube of the wind speed. Since, T_m appears in the differential equation of the slip, ps given in Eq.2.40, the oscillation of the frequency during transients can be explained with this effect. Oscillations in the slip result in oscillations in the rotor flux linkages since the rotor flux linkages have slip term in their differential equations. Steady-state rotor flux value given in Eq.2.60 is proportional with the mechanical torque. Therefore, steady-state rotor flux value is increased with the increasing in the mechanical torque. These oscillations in the rotor flux linkages and the increase in rotor flux value explain the V_s response, since the differential equations of V_D and V_Q contain rotor and stator flux linkages and the steady-state stator voltage V_{so} given in Eq.2.62 is proportional with the rotor flux.

On the other hand, steady-state slip value s_o given in Eq.2.59 does not have torque related variable. s_o has R_r, Γ_m and δ values. δ contains G, C and machine parameters. Also, the resonance frequency, w, does not contain torque related variable. Therefore, the steady-state frequency does not change with the wind speed variations.

As a result, when we take the mutual inductance value as constant; variation in the wind speed changes mechanical input torque that results in a new steady-state stator voltage. However, variation in the wind speed does not change the steady-state slip, frequency and rotor shaft speed.
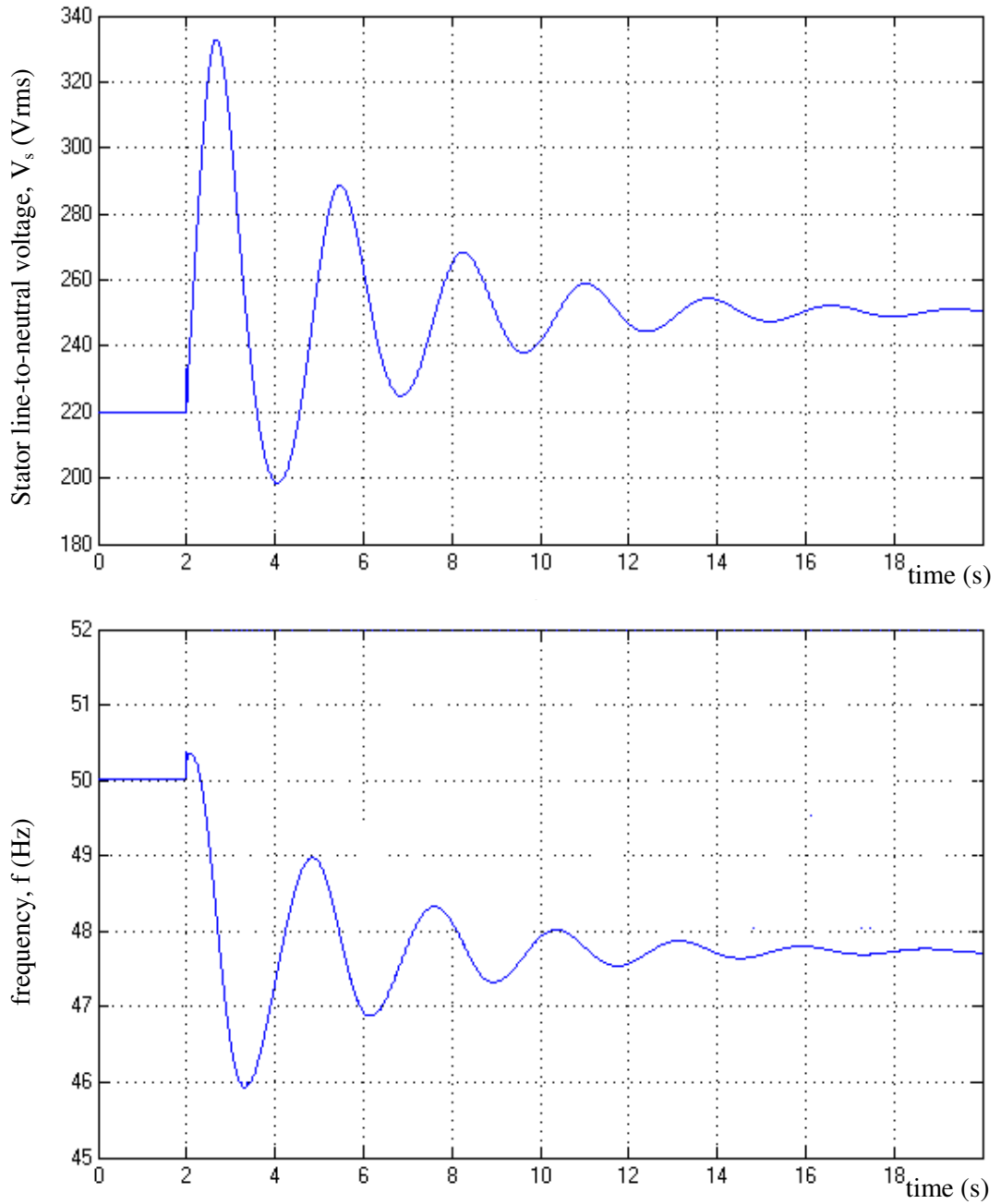
Figure 3.5 Stator line-to-neutral Voltage and frequency responses of the General Model corresponding to disturbance in the load G=0.0247mho → 0.0200mho at t=2s, v=10m/s constant (M=0.1578316 H Constant)

In Figure 3.5, the simulation is started with the rated values as explained for the Figure 3.4. Figure 3.5 represents 20% decrease at t=2s in the load value. This disturbance in the load affects both V_s and f during transient periods and steady state

53

f is determined by the resonance frequency given in Eq.2.58. γ in Eq.2.58 is independent of the state variables which is $\gamma = -\Gamma_r/\Gamma_m^2$. γ contains w, G, C and machine parameters. Variation in G will result in a variation in w, for fixed excitation capacitance, C at steady-state.

V_s on the other hand contains G value in the differential equation and its steady-state in Eq. 2.62 consists ξ, η and w which there of them are affected by G. Figure 3.4 and 3.5 represent constant mutual inductance value which is 0.15778316 H. This value is the linear approximation of the magnetizing curve at rated voltage and rated frequency when the load G=0.0247mho and the wind speed v=10m/s.

The same disturbances are applied to the model when the mutual inductance value is represented by the double-exponential function given in Eq.2.47. The corresponding transient responses are shown in Figures 3.6 and 3.7. At a first glance, it is seen that the basic difference between the constant and non-linear representation of the mutual inductance cases is that, in the latter case there is no oscillations in the output variables and the settling times are much lower (2.5-3 seconds).

Figure 3.6 shows the transient response of the output variables to % 10 increase in the wind speed at time t=2 s., when there is no control in the system as it is in the Figure 3.4. Steady-state value of the V_s is increasing since its value is proportional to mechanic torque input, which increases with the increase in the wind speed value. Besides, increase in the wind speed is resulted in an increase in the frequency, which is not seen in constant mutual inductance case. That is because of the fact that γ value in Eqn. 2.58 changes with Γ_m and Γ_r, reciprocal inductances; both of them contain mutual inductance term, which can be seen in Eq.2.26. Since increasing in voltage and fluxes will decrease mutual inductance M, therefore γ will change with the increase in V_s. γ consists of G, C, w and machine parameters. For a fixed G and a fixed C, a variation in γ value because of the saturation effect, is resulted in a different w value. This result is also valid with the steady-state analysis shown in Fig.2.12.
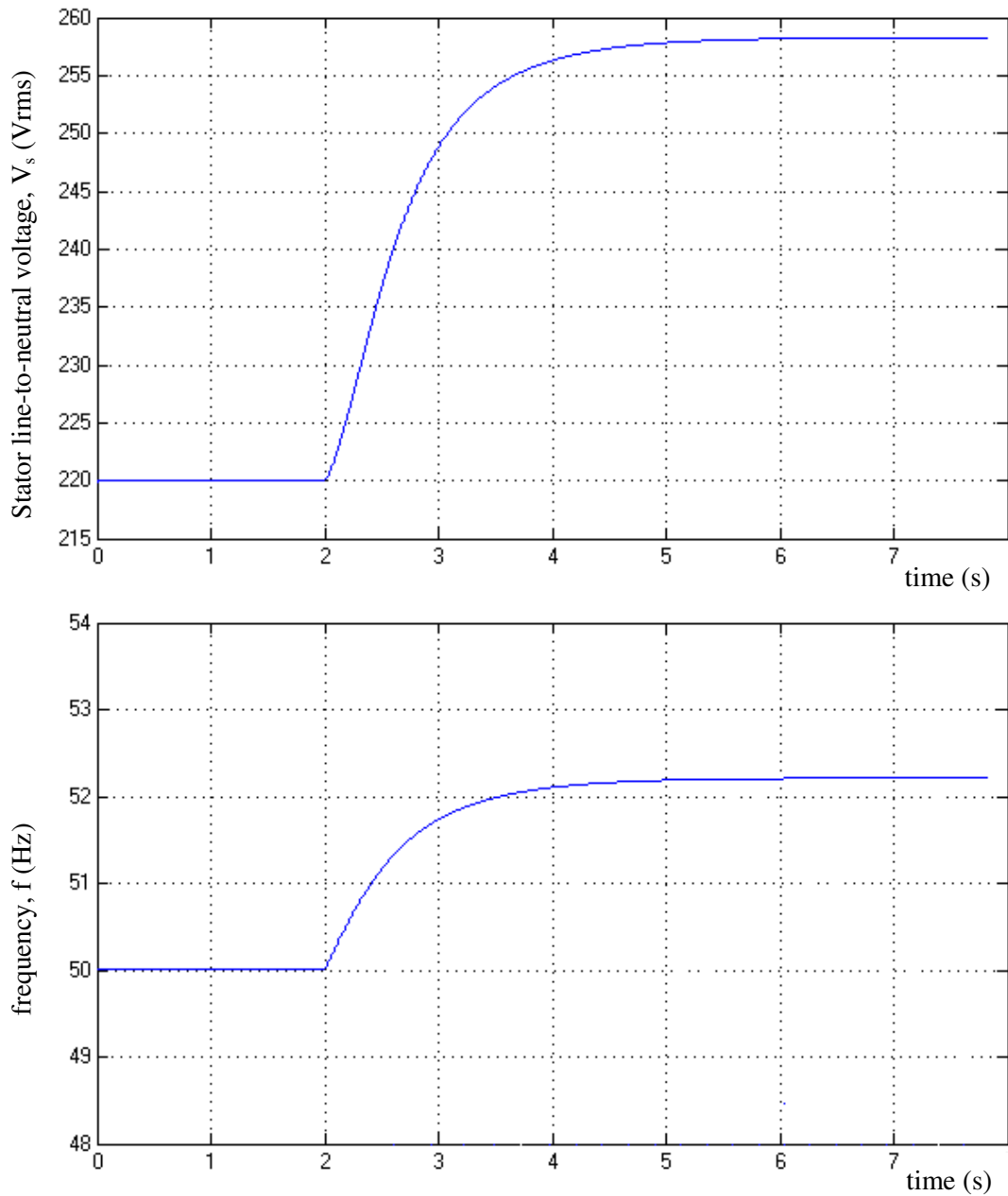
Figure 3.6 Stator line-to-neutral Voltage and frequency responses of the General Model corresponding to disturbance v=10m/s → 11m/s at t=2s G=0.0247 mho constant (Double-Exponential Representation of the Magnetization Curve)
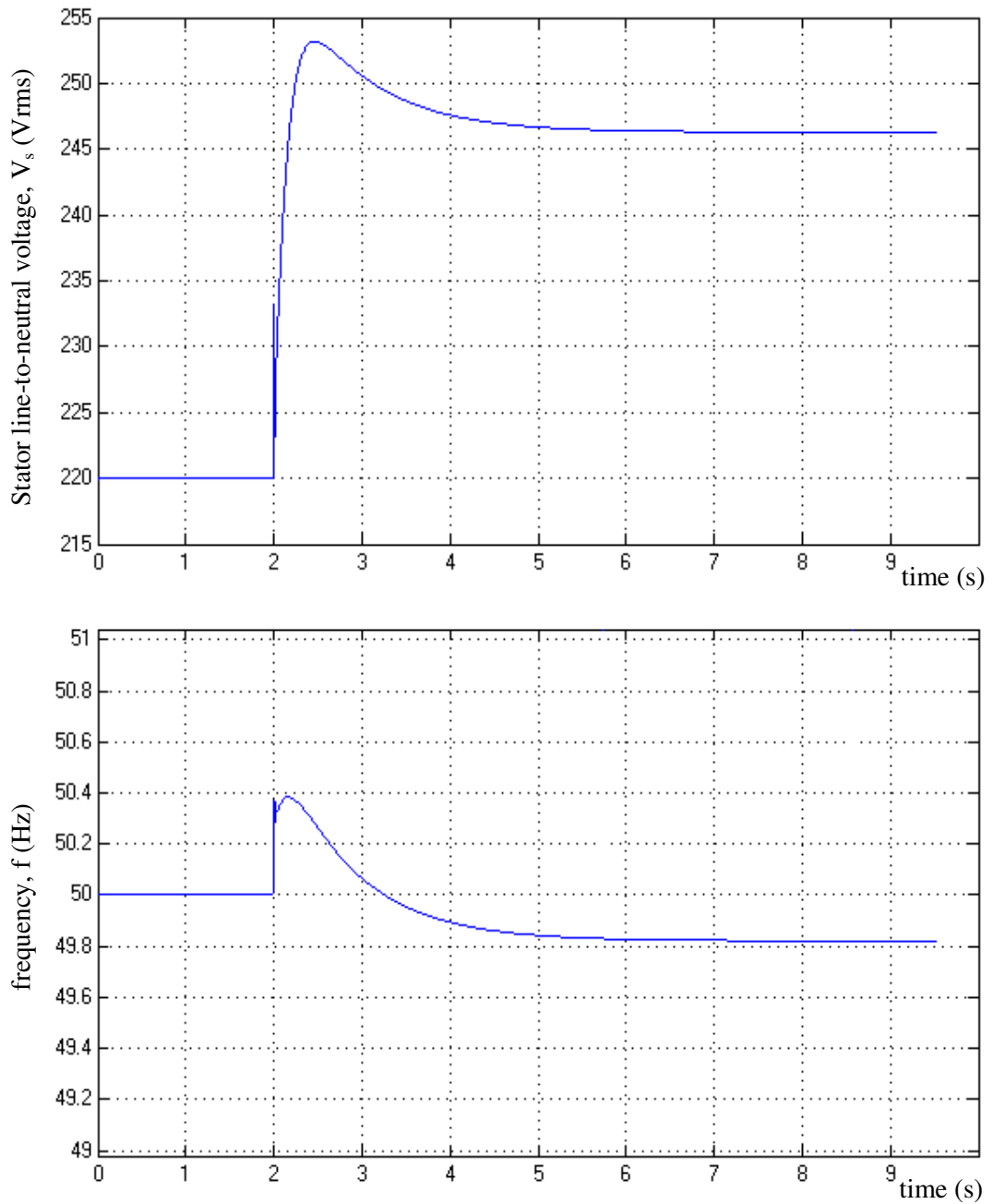
Figure 3.7 Stator line-to-neutral Voltage and frequency responses of the General Model corresponding to disturbance G=0.0247mho → 0.0200mho at t=2s, v=10m/s constant (Double-Exponential Representation of the Magnetization Curve)

Figure 3.7, on the other hand, shows the transient responses of the output variables when there is a 20% change in the load value at time t=2 s when there is no control applied to the system. As in the constant mutual inductance case, the steady-state

voltage value V_{so} is increasing with a decrease in the load. Because V_{so} contains ξ, η and w values which are affected by the load G. This result is validated with Figure 2.11.

Frequency response on the other hand, shows difference from the constant mutual inductance case given in Figure 3.5. The same disturbances in the load changes frequency from 50 Hz to 47.8 Hz in the constant mutual inductance case but in the saturation effected mutual inductance case frequency changes from 50 Hz to 49.8 Hz very little deviation from the rated value. The saturation affects the frequency changes in an opposite way, when there is a disturbance in the load. This is shown in Table 2.2 and Figure 2.10. This can be explained as, when there is a decrease in the load value at the constant wind speed, voltages and fluxes are increasing which result in a decrease in the mutual inductance, which tends to increase the frequency. This can be analyzed with the matlab file given in Appendix A. Variation of w for different M values can be seen in the solution of the Eq2.63 in Appendix.

From the natural response simulation results, it can be concluded that

a) If the constant mutual inductance is used in the model, the effects of wind speed on the stator frequency, slip and the rotor speed are not seen in steady-state. These are verified also in steady-state analysis in Chapter 2. For rated load, capacitance and rotor resistance values, frequency does not change with the wind speed above 7.25 m/s, which is the sub-limit for loss of excitation.

b) When using constant mutual inductance in simulations, there are big oscillations in the responses of the output variables, especially in the stator voltage, V_s. Besides, the settling times are long about 14-15 seconds. On the other hand, if the double exponential representation of the magnetizing curve is used in the simulations, there are no oscillations and the settling times are 3-4 seconds.

c) In the double-exponential representation of the magnetizing curve the deviation on the frequency is bigger with the wind speed disturbances than the load disturbances, this is because of the fact that increasing the mutual inductance will increase the frequency, and this can be shown in Fig.2.12. Without saturation, decrease in the load will decrease frequency. With saturation this disturbance will increase the mutual inductance that tends to increase the frequency, opposite to the load disturbance.

d) It is seen that, wind speed disturbances affect the system (both the voltage and frequency) more than the load disturbances of the same order of magnitude. (In simulations, 10% wind disturbance affects the system more than 20% load disturbance). It can be explained as; the power extracted from the wind is proportional to the cube of the wind speed [7].

e) With the above considerations, it is concluded that, saturation has an utmost importance for the transient performance, and for reaching the correct steady-state value of the frequency. Therefore, since IM's are normally operated in a saturated mode, a linear magnetization characteristic comes out to be an unstable approximation for dynamic studies.

At this point, the responses of the very simple method of feed-forward control can be analyzed. This simple feed-forward control corresponds to the immediate adjustment of the capacitor and the rotor external resistor values according to the eventual variations in the wind speed and/or the load disturbances. Figures 3.8, 3.9 and 3.10 show the responses of the feed-forward control. In Figure 3.8, the simulation starts with G=0.019 mho, v=10 m/s, C=71.344µF and R_r=6.55ohm. The capacitance C and the rotor resistance R_r values are adjusted so that the SEIG operates at rated voltage and frequency when the load G=0.019 mho and wind speed v=10 m/s. Before starting the simulation the initial values of the state variables are found for these starting control and disturbance variables. As can be seen from the Figure 3.8, simulation starts with rated voltage and rated frequency. At time t=2 s. the load G changes from 0.019 mho to 0.0247 mho, capacitor value C changes from 71.344 µF

to 78.518 μF the rotor resistance value R_r changes from 6.55 ohm to 1.25 ohm at the same time. In the simulation, double-exponential representation of the magnetization curve is used.
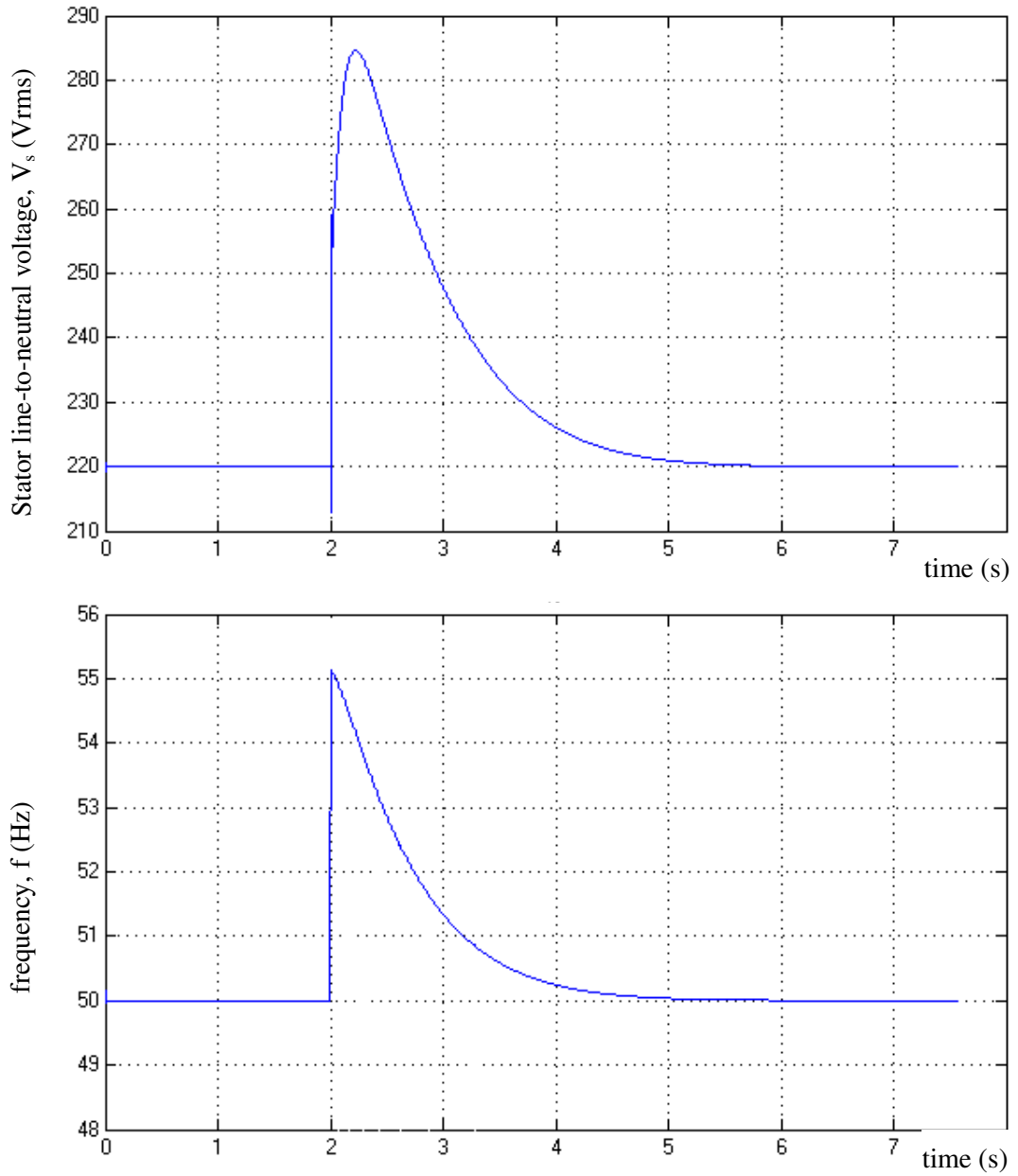
Figure 3.8 Stator line-to-neutral Voltage and frequency variations in case of the Feed Forward control corresponding to disturbance G=0.019mho → 0.0247mho at t=2s, v=10m/s constant (Double-Exponential Representation of the Magnetization Curve)
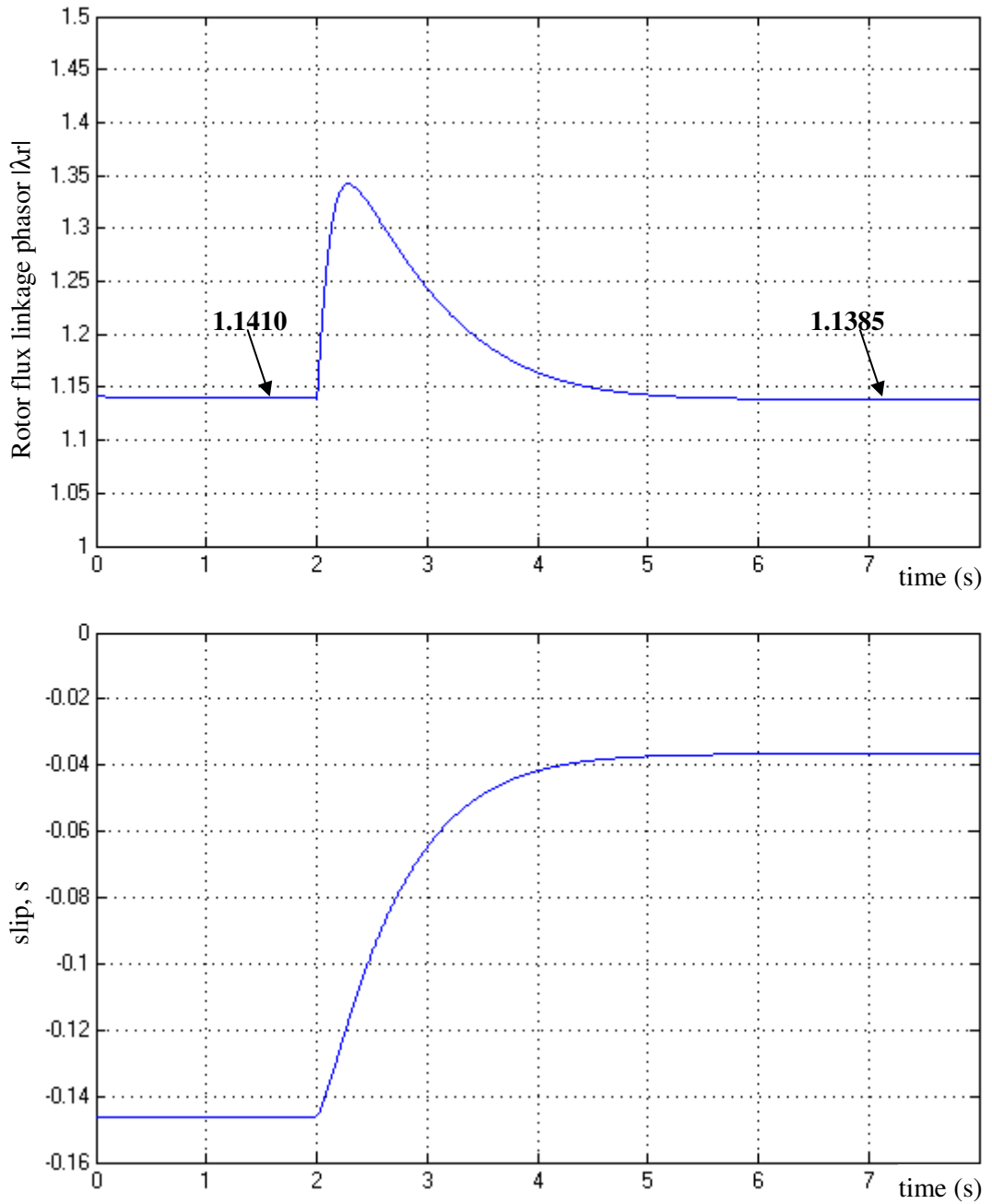
Figure 3.9 Rotor flux linkage phasor and slip variations in case of the Feed-Forward control corresponding to disturbance G=0.019mho → 0.0247mho at t=2s, v=10m/s constant (Double-Exponential Representation of the Magnetization Curve)

In Figure 3.9, the rotor flux linkage phasor |λ$_r$| and the slip variations are given for the load disturbance as in the Figure 3.8. It is seen that the rotor flux is not constant for the case of the load disturbances. Therefore, keeping the rotor flux constant will not ensure CVCF operation of the SEIG.
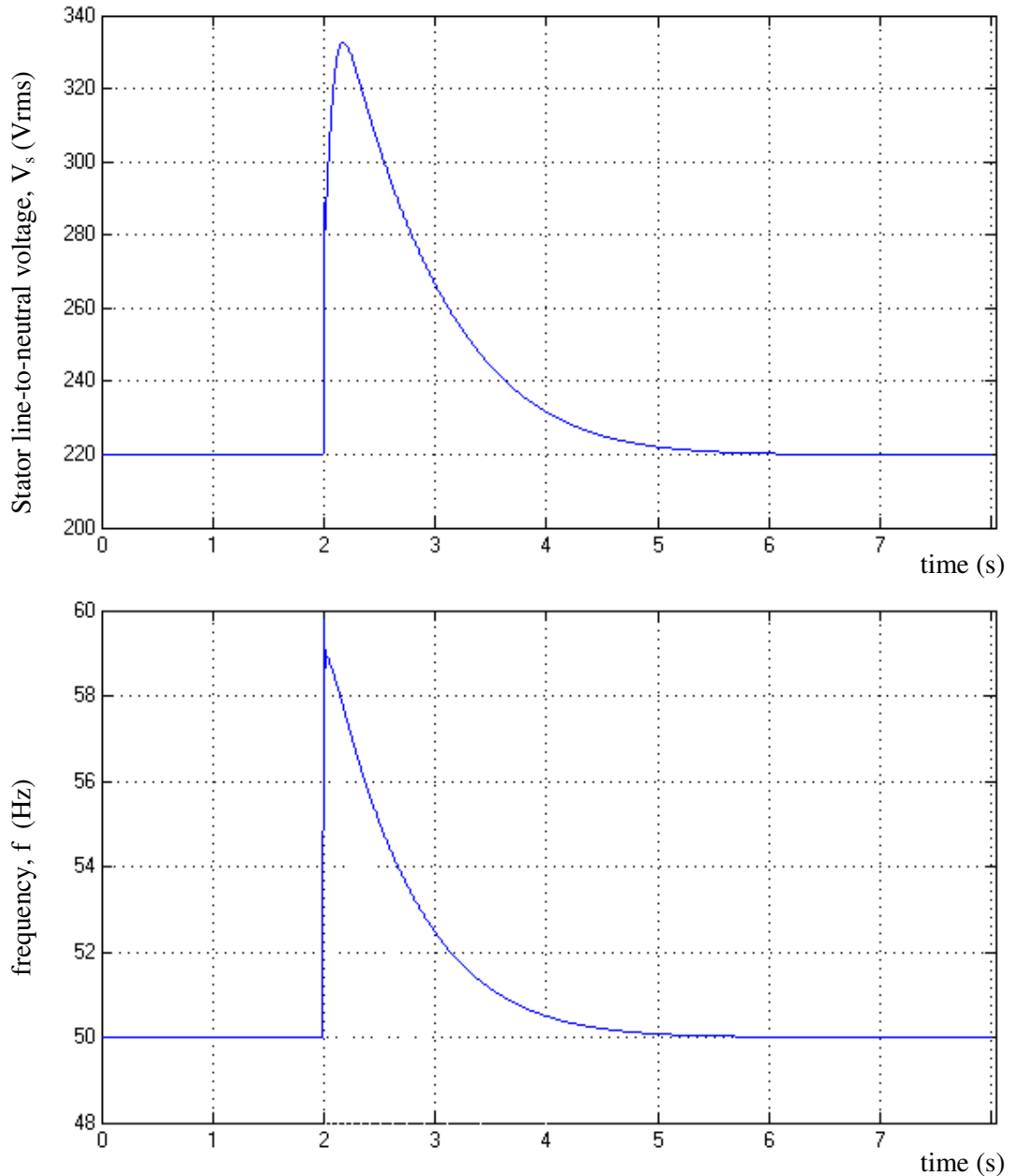
Figure 3.10 Stator Voltage and frequency variations in case of the Feed-Forward control corresponding to disturbance v=11m/s → 10m/s at t=2s, G=0.0247mho constant (Double-Exponential Representation of the Magnetization Curve)

In Figure 3.10, the same feed-forward control is applied for the wind speed disturbance from v=11 m/s to its rated value v=10 m/s. Again, first, the required capacitance and resistance values are calculated for the rated voltage and frequency for these disturbance values. They are found as C=78.518 and R_r =7.915ohm. The Load is rated load G=0.0247. Initial conditions of the state variables are found for these sets of variables. Then simulation is started. At time t=2 s, all variables go to their rated values C=78.518 μF, R_r=1.25 ohm, v=10 m/s.

It can be seen from the figure 3.10 that, adjustment of R_r is enough for voltage and frequency regulation for the wind speed disturbances above the rated value for the rated load. This is also concluded in [7]. Rotor external resistance does not affect the frequency steady-state value, if the stator voltage value is kept in its rated value. Otherwise, if the stator voltage is different from its rated value, change in rotor resistance will change the mutual inductance value because of the saturation effect, which will change the frequency.

From the simulation results, it is seen that, the basic feed-forward control technique is far from satisfying the requirements of a CVCF output during the transient period. Feed-forward responses look like the natural responses of the system for the saturated machine case. For the constant mutual inductance case, also the responses, which are not given here, look like the natural responses, having oscillations and long settling times.

It is concluded that, the feed-forward control strategy, besides of being impractical, since it requires wind speed measurement is far from satisfying the basic demands during the transient period. Therefore, it is clear that some kind of a closed-loop control should be applied for the proper operation of a variable speed SEIG.

3.4.   CONTROL FLOWCHARTS OF THE SEIG OPERATION

From the dynamic responses of the system given in previous part, it is seen that, if the system is operated as an open-loop one, i.e, without any control applied to the capacitance and/or to the external resistances, even relatively small disturbances in either the load or the wind speed result in substantial deviations of the voltage and frequency from their rated values. Also, feed-forward control is investigated which corresponds to the immediate adjustment of the capacitor and the rotor external resistor values according to the eventual variations in the disturbances (load and wind speed). But, still, the results in Figures 3.8-3.10 show that such a control strategy, besides of being impractical, since it requires wind speed measurement, is far from satisfying the basic demands during the transient period. Therefore, it is clear that some kind of a closed-loop control should be applied for the proper operation of a variable speed SEIG.

The control problem can be stated as; the excitation capacitance and the rotor/stator external resistance should be adjusted to keep the stator voltage and frequency of the SEIG at their rated values with varying load and/or wind speed conditions. The control flowcharts shown below are derived from steady-state operation of the system in Chapter 2.

In the flowcharts (+) means that, change in the previous parameters will change the next parameter in the same manner. (─) means that, change in the previous parameters will change the next parameter in the opposite manner. For example, in Figure 3.11, increasing in the load (G) will increase the frequency (w), increasing in w should be regulated by increasing the capacitance (C), increasing in C will result in an increase in the stator voltage (V_s), also increasing in G will result in a decrease in V_s. If total effect leads in an increase in V_s, it should be regulated by increasing R_r. Increasing in R_r will decrease the frequency due to the saturation effect. Increases and decreases in the variables continue until the steady-state values are reached.
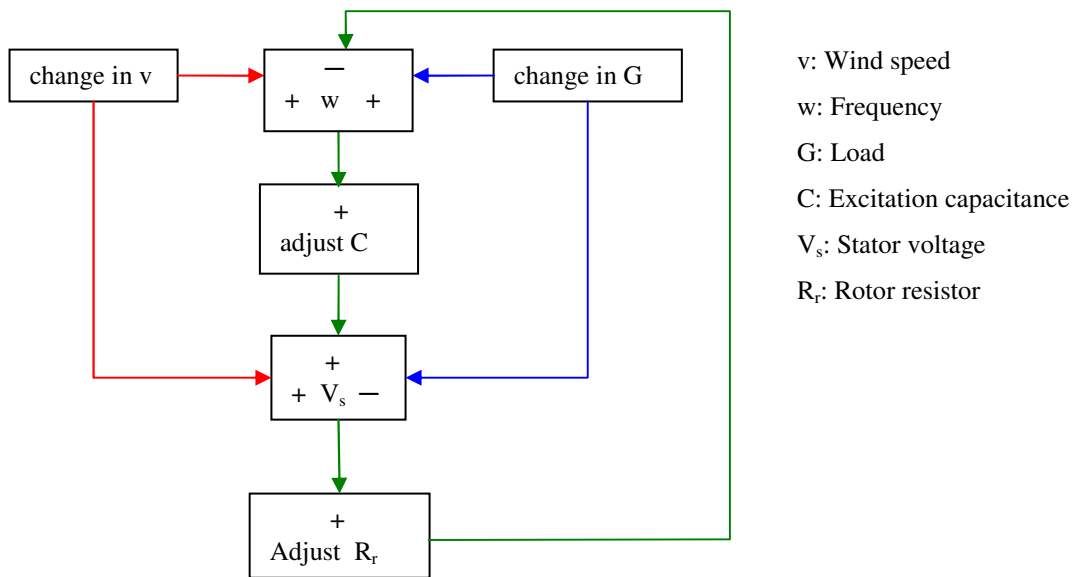
Figure 3.11 Control Flowchart of the SEIG when using rotor external resistors as the voltage regulator (Double-Exponential Representation of the Magnetization Curve)
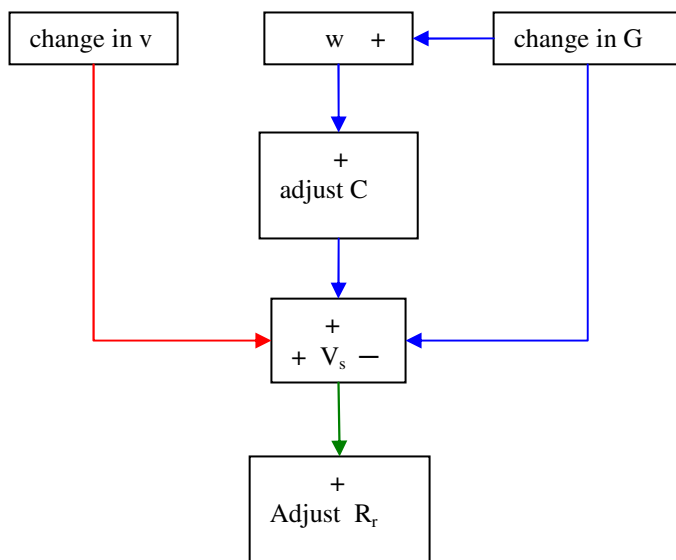
Figure 3.12 Control Flowchart of the SEIG when using rotor external resistors as the voltage regulator (M=0.1578316 H Constant)
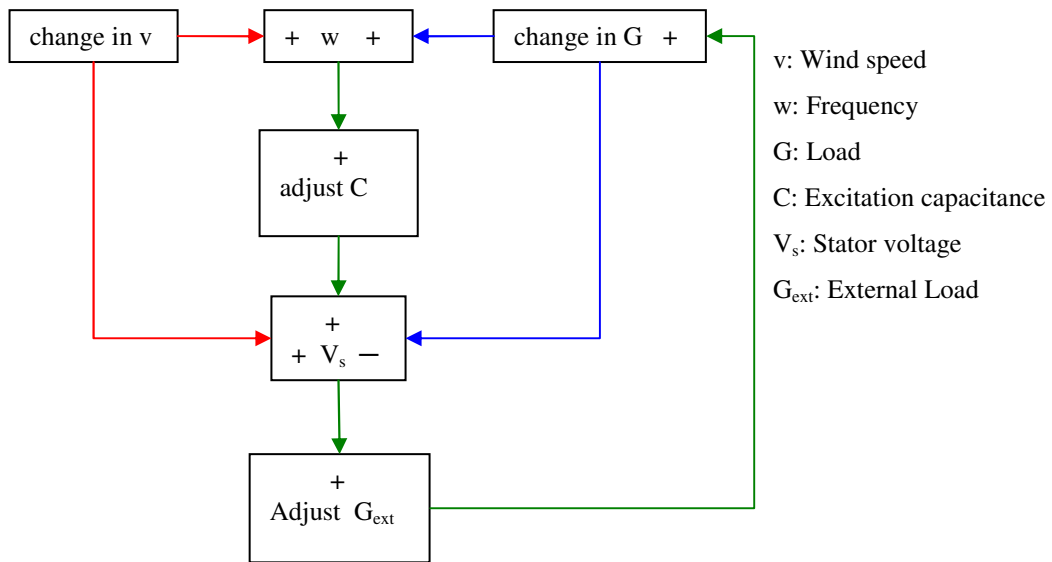
Figure 3.13 Control Flowchart of the SEIG when using stator external resistors as the voltage regulator (Double-Exponential Representation of the Magnetization Curve)
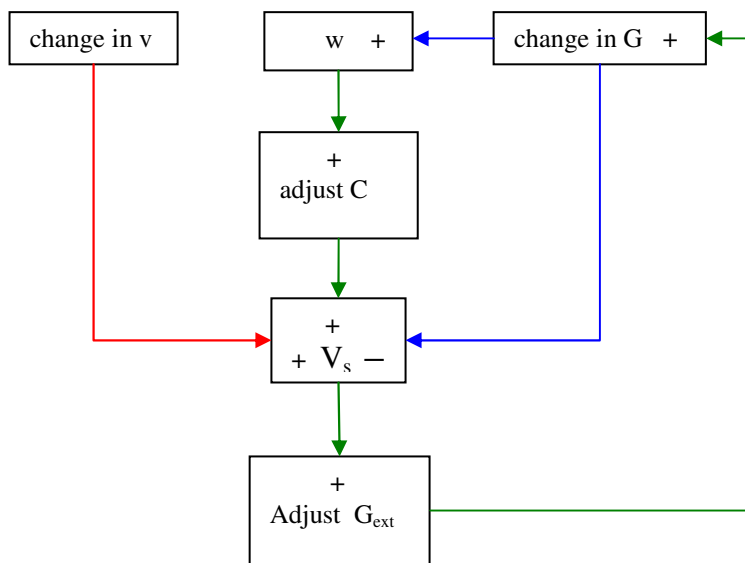
Figure 3.14 Control Flowchart of the SEIG when using stator external resistors as the voltage regulator (M=0.1578316 H Constant)

3.5. FREQUENCY REGULATION WITH EXCITATION CAPACITANCE

The previous steady-state and dynamic analyses and the studies carried out in [7] have shown that the correct choice of the excitation capacitor value is fundamental in the setting of both the stator voltage and the frequency to their rated values. From the resonance condition, it is obvious that the steady-state frequency value depends on the excitation capacitance and the load. Therefore, the excitation capacitance should be adjusted at each step where the load and/or the wind speed have a deviation from their values, to ensure a constant frequency at steady-state. Control of the excitation capacitance value is done by frequency error. Therefore frequency error should be derived from the measured state variables. Frequency can be calculated by the stator voltage phasor, stator flux phasor or rotor flux phasor. Besides, the frequency can be calculated by measuring the stator voltage and calculating the time between the zero crossings of the voltage. In this study, the frequency value is calculated from the rotor flux phasor, which tends to change more slowly than the other variables.
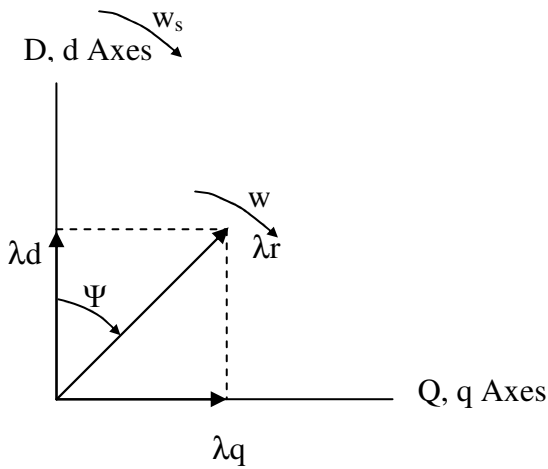
Figure 3.15 Rotor Flux Phasor with Synchronously Rotating Reference Frame

The phase term of the rotor flux phasor can be defined with the help of Fig.3.15 as;

$$\Psi = \tan^{-1}(\lambda_q / \lambda_d) \tag{3.1}$$

Ψ is the phase angle of the rotor flux phasor with respect to the synchronously rotating reference frame axis. If at steady-state, the system oscillates at the synchronous speed w_s, it is obvious that the rotor flux phasor will assume a constant value depending on the initial conditions and phase angle Ψ is constant. Any variation in the system frequency (w) will change the phase angle. Therefore, the time rate of change of the phase angle, $p\Psi(t)$, can be considered as the speed variations of the rotor flux phasor with respect to the reference frame speed and hence represents the deviation of the angular velocity of the electrical variables from that of the reference frame.

$$p\Psi(t) = w(t) - w_s \tag{3.2}$$

Thus a rigorous frequency control requires the right hand-side of the Eqn to be equal to zero both during the transient period and at steady state for a choice of w_s corresponding to the rated frequency.

Based on these considerations the control signal for the excitation capacitance is assumed to be derived for the variable Ψ and be of the form.

$$C(t) = k_i \, \Psi(t) \tag{3.3}$$

Since, rotor flux linkages can not be measured, they should be calculated from the measured values, stator voltage V_A, V_B, V_C and stator currents I_A, I_B, I_C. First, stator flux linkages are calculated, then the rotor currents are calculated and then the rotor flux linkages are calculated. The related equations are given below;

$$p\lambda_D = V_D - R_s \cdot I_D + w_s \cdot \lambda_Q \tag{3.4}$$
$$p\lambda_Q = V_Q - R_s \cdot I_Q - w_s \cdot \lambda_D \tag{3.5}$$

$$I_d = (\lambda_D - L_s \cdot I_D) / M \tag{3.6}$$
$$I_q = (\lambda_Q - L_s \cdot I_Q) / M \tag{3.7}$$

$$\lambda_d = L_r \cdot I_d + M \cdot I_D \tag{3.8}$$

$$\lambda_q = L_r \cdot I_q + M \cdot I_Q \tag{3.9}$$

Frequency Regulation Circuit diagram is given in Figure 3.16. First, the stator ABC voltages and currents are converted to DQ variables with the transformation given in Eq. 2.14. However, in this model DQ variables are state variables and coming directly from the Generator Model block. The stator flux linkages and the rotor flux linkages are calculated in Figure 3.17, 3.18 and 3.19.
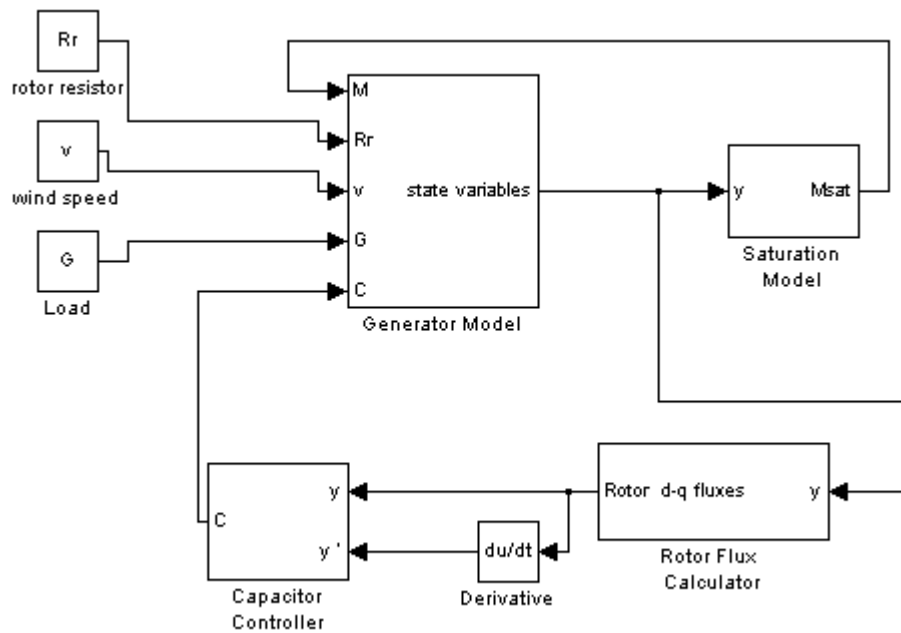
Figure 3.16 Frequency Regulation with Excitation Capacitance Circuit Diagram
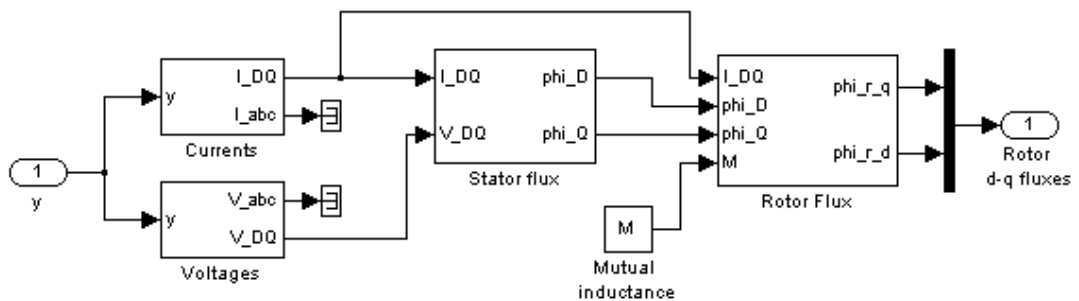
Figure 3.17 Rotor Flux Calculator Circuit Diagram
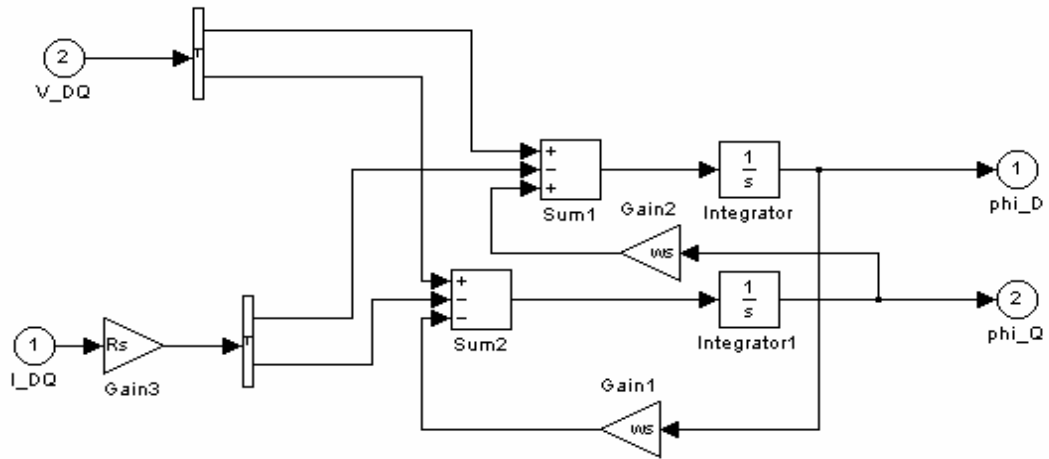
Figure 3.18 Stator Flux Calculation Block
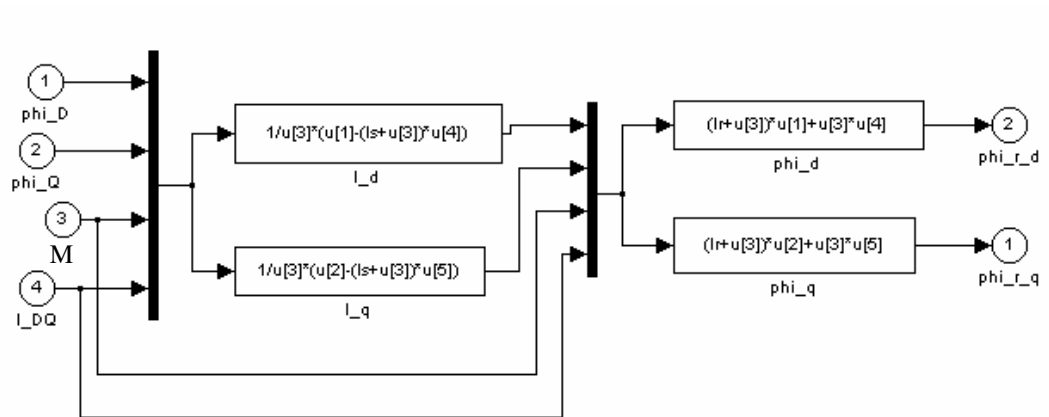
Figure 3.19 Rotor Flux Calculation Block

After obtaining the rotor flux linkages, the frequency error is obtained with the Eq. 2.42. The frequency error is the input of the PI controller of the capacitor, the related circuit is given in Figure 3.20, where y is the rotor flux linkages (λ_d and λ_q) and y' is the derivative of the rotor flux linkages ($p\lambda_d$ and $p\lambda_q$).

69
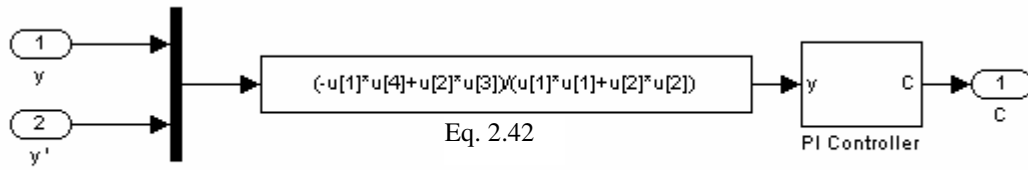
Figure 3.20 Generating the Capacitance command to the PI controller

In rotor fluxes calculation, constant mutual inductance value is used although the IG uses saturated mutual inductance. Using constant mutual inductance in the calculations gives acceptable results, since the system works at the rated values of the output variables.

In PI controller only the integral term is active. k_i parameter of the integral can be selected in a wide range, it is optimized by selecting ki=0.001 and giving initial condition for the capacitance as C_0=78.518 μF in the controller.
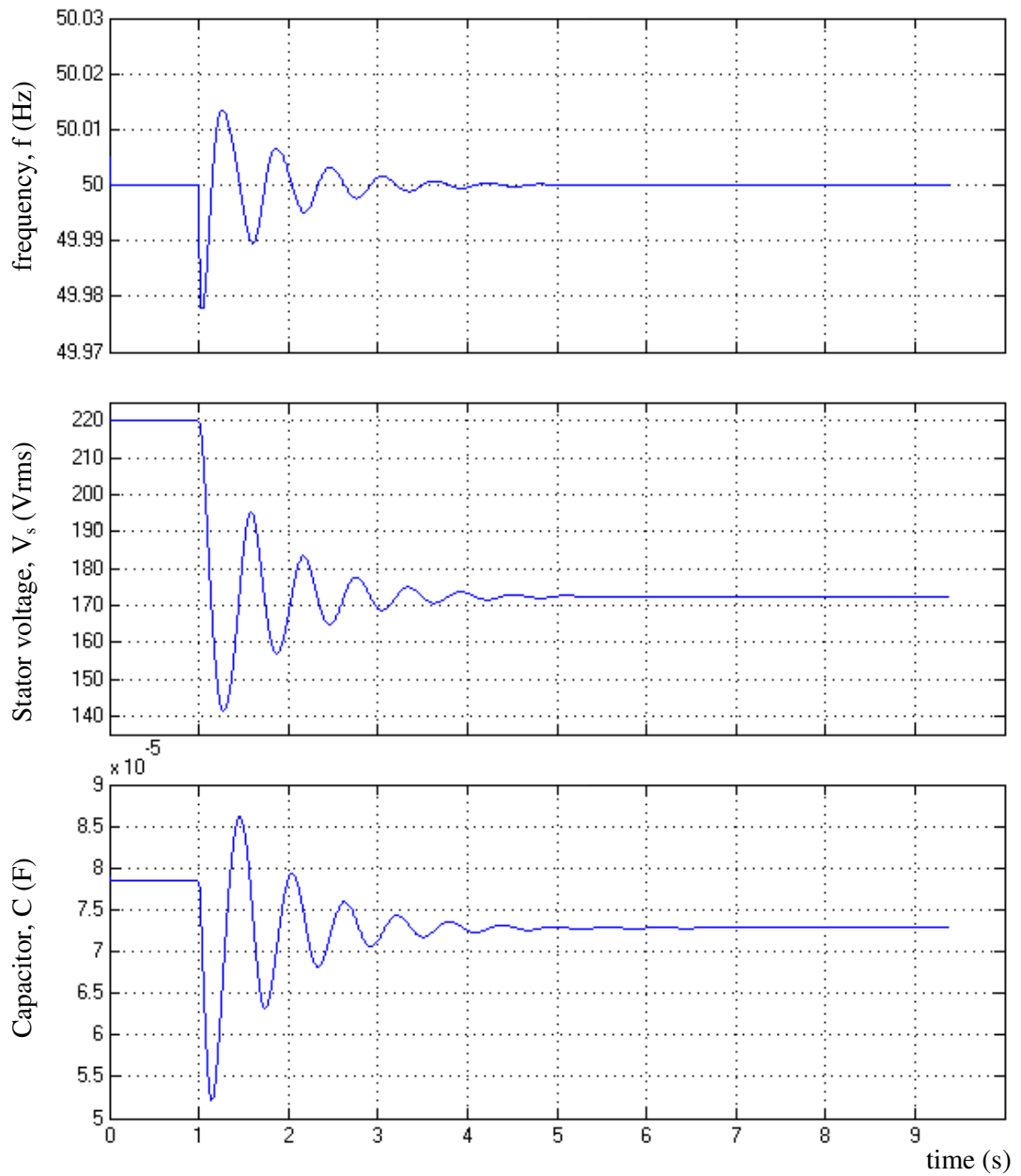
Figure 3.21 Frequency, Stator line-to-neutral voltage and Capacitor variations in case of the PI control of the Excitation Capacitance C (v=10m/s → v=9m/s at t=1s, G=0.0247 constant)
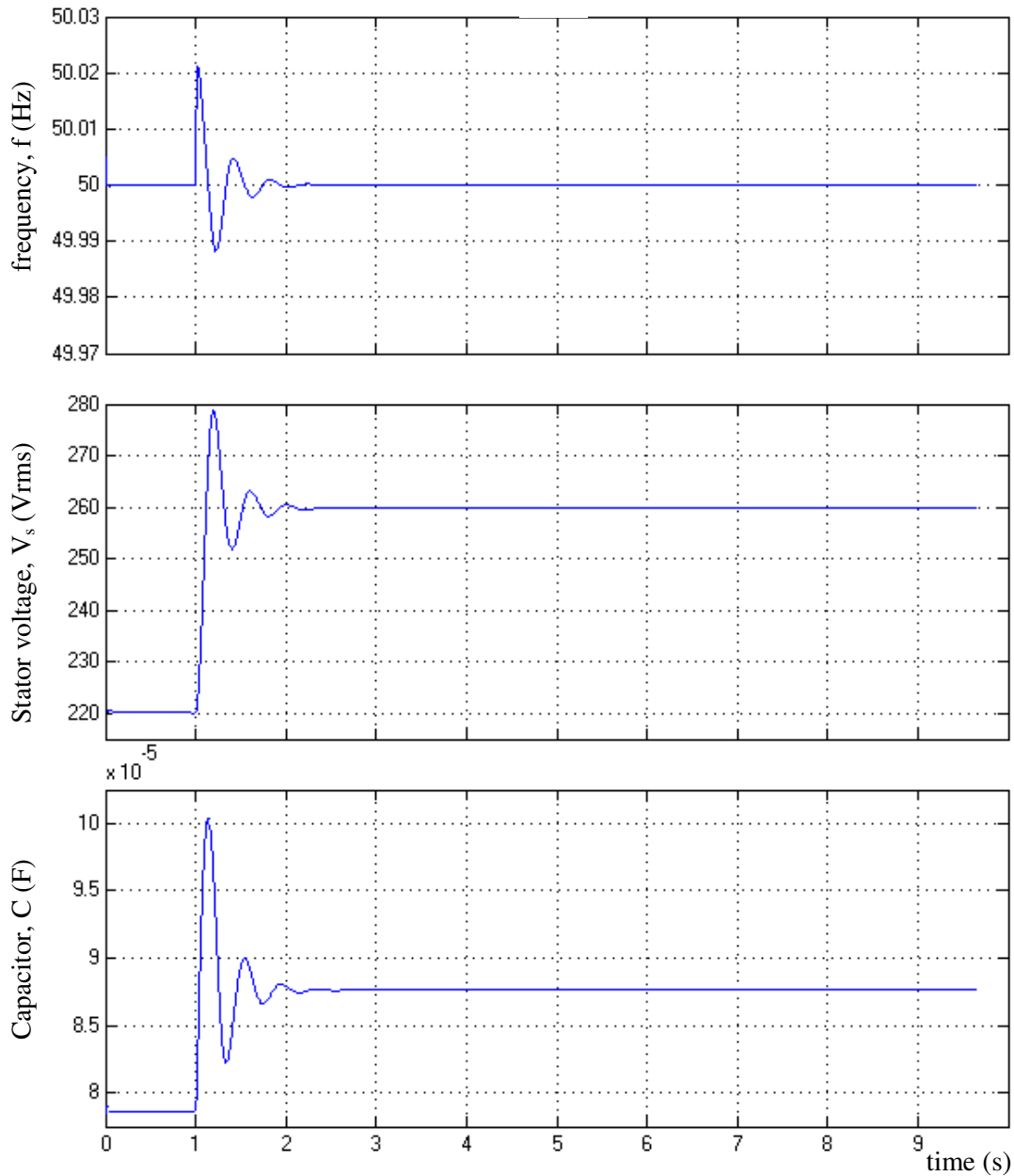
Figure 3.22 Frequency, Stator line-to-neutral voltage and Capacitor variations in case of the PI control of the Excitation Capacitance C (v=10m/s → 11m/s at t=1s, G=0.0247mho constant)

The performance of the controller is controlled with all types of disturbances shown in the Figures 3.21-3.24. In this part, the simulations are done with the double-exponential representation of the magnetizing curve.

In Figure 3.21 system starts with the rated values of the output and control variables at time t=0. At time t=1 step type disturbance is applied to the wind speed, changing from v=10 m/s to v=9 m/s. Load G=0.0247 mho and rotor resistance R_r = 1.25 ohm are fixed during the simulation.

In figure 3.21, it is seen that, decrease in the wind speed results in a decrease in V_s. Stator frequency f, on the other hand remains constant at steady state, with a few oscillations about 0.02 Hz in magnitude. Normally as it is seen in Figure 3.6, frequency tends to change in the same manner with the wind speed disturbances. However, in Figure 3.21 frequency is kept constant by decreasing the capacitance value. That is shown in Figure 2.15, to increase the frequency, the capacitance value should be decreased.

In Figure 3.22, again the wind speed disturbance applied at t=1 s but in that case wind speed is increased from v=10 m/s to v=11 m/s. As expected V_s is increasing, since there is no control for voltage. Frequency tends to increase but the controller increases the capacitance value to regulate the frequency. This result also verifies the results in Figure 2.15.

Figure 3.23 shows step type decrease in the load G. The expected results are; increase in V_s and decrease in f as can be seen in Figure 3.7. Voltage V_s is increasing as it is expected with a big overshoot, since there is no control on V_s. Frequency is kept constant by a small adjustment (in a decreasing manner) of excitation capacitance. This results verify the results in figure 3.7, since the deviation in frequency in figure 3.7 is very small (0.1 Hz) so the compensation capacitance value is also small (~1 μF).

The same conclusions can be done for figure 3.24 which shows an increase in load value G at time t=1s. As expected, steady-state voltage value is smaller than the rated value. Frequency is kept constant by increasing the capacitance value. This result validates Figure 3.7.
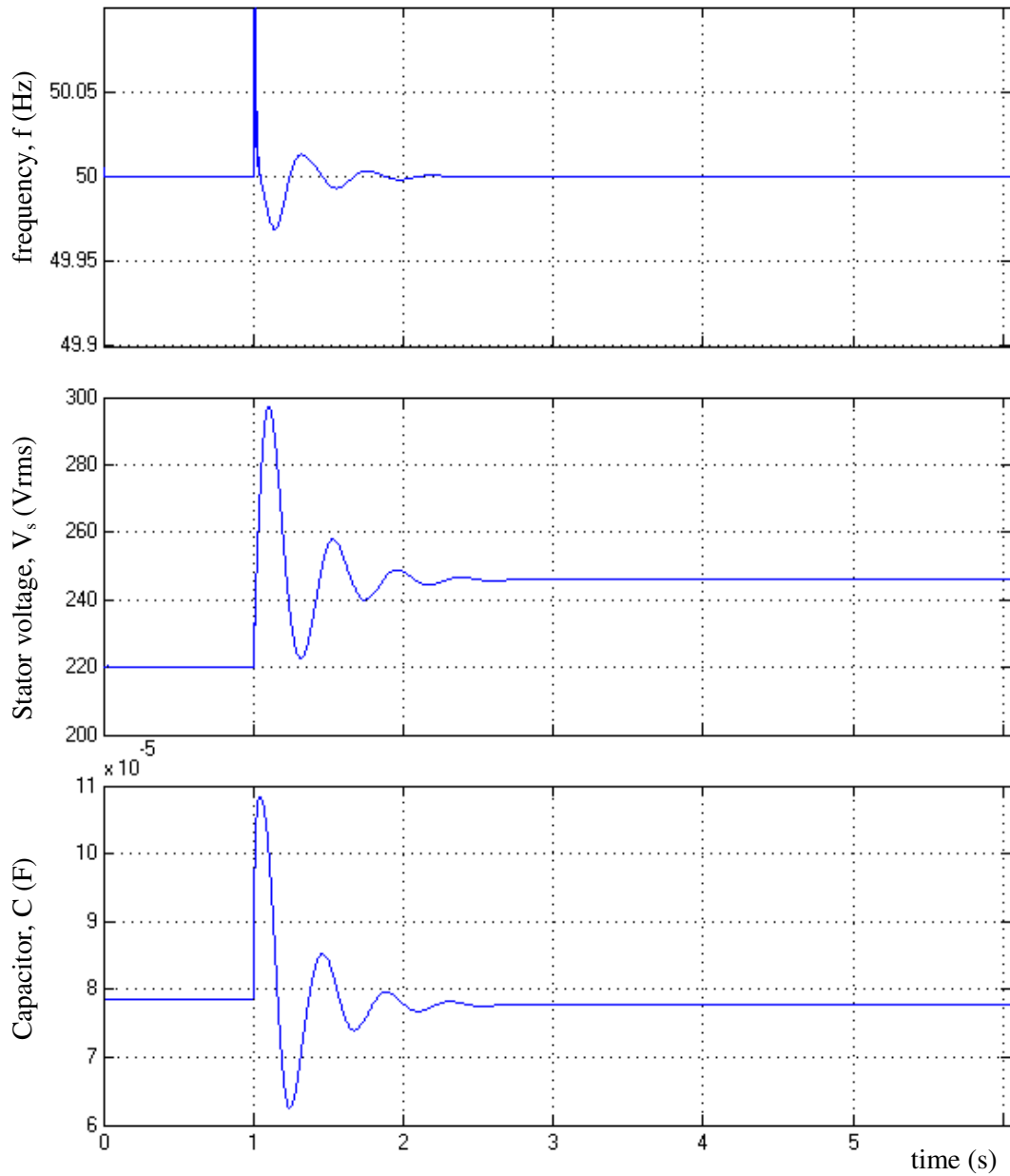
Figure 3.23 Frequency, Stator line-to-neutral voltage and Capacitor variations in case of the PI control of the Excitation Capacitance C (G=0.0247mho → 0.0200mho at t=1s, v=10m/s constant)
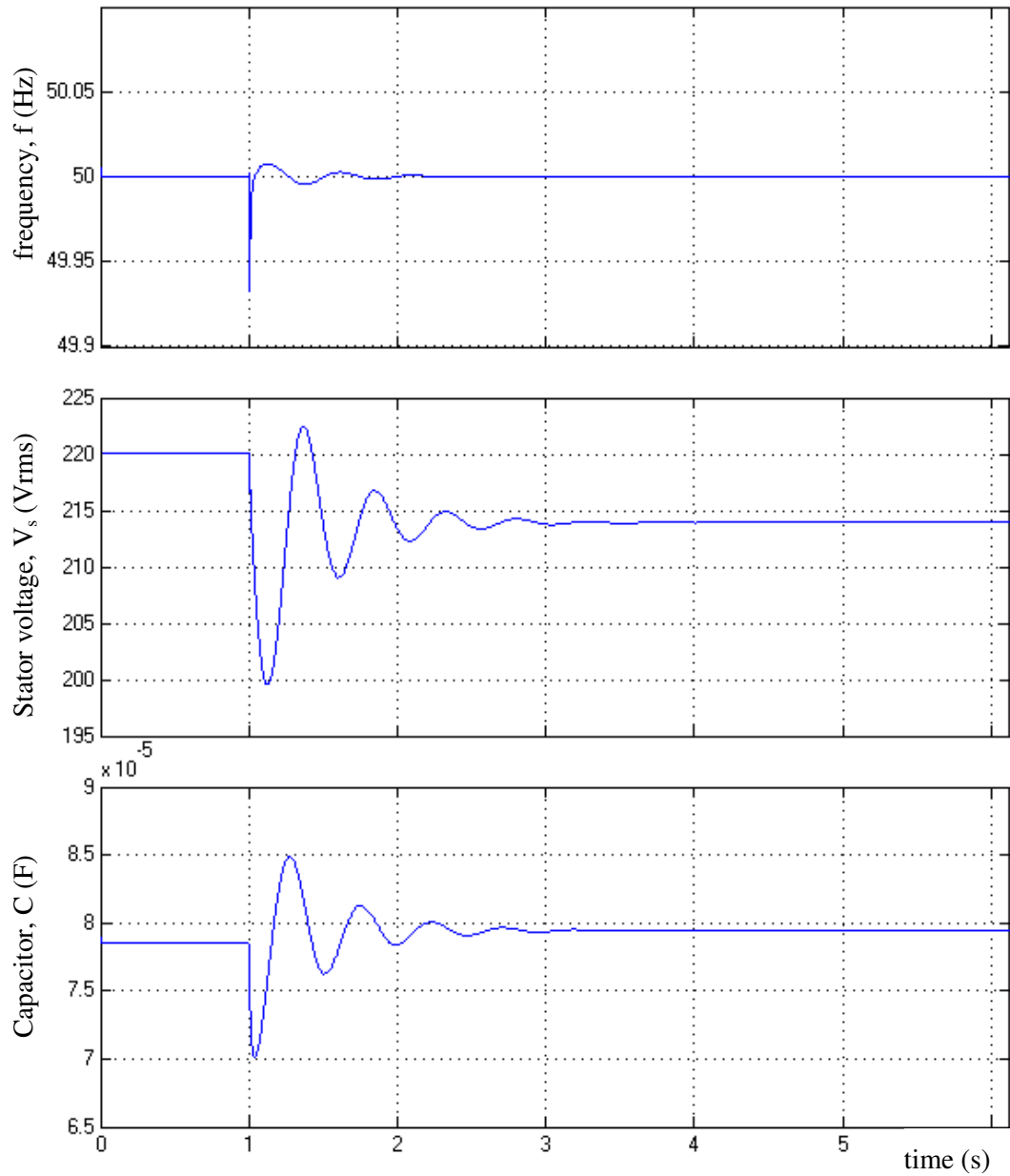
Figure 3.24 Frequency, Stator line-to-neutral voltage and Capacitor variations in case of the PI control of the Excitation Capacitance C (G=0.0247mho → 0.0260mho at t=1s, v=10m/s constant)

3.6.   VOLTAGE REGULATION WITH ROTOR EXTERNAL RESISTORS

Stator voltage, V_s can be controlled with variable rotor resistance. This is shown in Chapter 2, steady-state performance of system in Figure 2.16. It is seen that whenever there is an increase in the stator voltage V_s, it can be decreased by increasing the rotor resistance R_r. In this part of the study the transient analysis of the voltage control with rotor external resistors is analyzed. The controller suggested in [7] is used in the simulation. Rotor external resistor value is adjusted by proportion of the slip and integral of the voltage error. The details of the controller are given in [7]. Voltage circuit diagram used in the simulation is given in Figure 3.25.
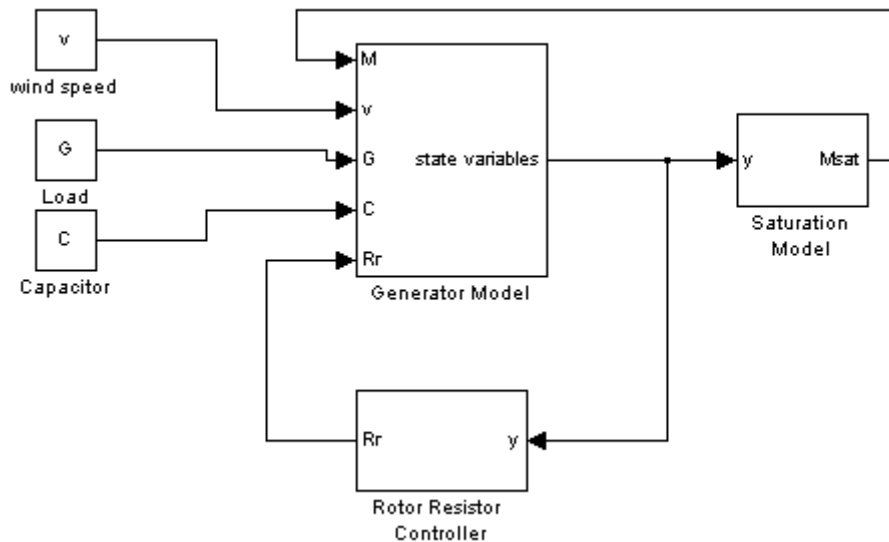
Figure 3.25 Voltage Regulation with Rotor External Resistors Circuit Diagram

The Rotor Resistor Controller controls the effective value of the rotor resistance. It is a type of PI controller working with proportion of the slip and the integral of the voltage error between the measured and reference value.

$$R_r(t) = k_p \, s(t) + \int k_{i2} \, [(V_s(t))^2 - (V_{ref})^2]$$

k_p and k_{i2} values are given in [7] as, $k_p = -34$ and $k_{i2} = 0.063$
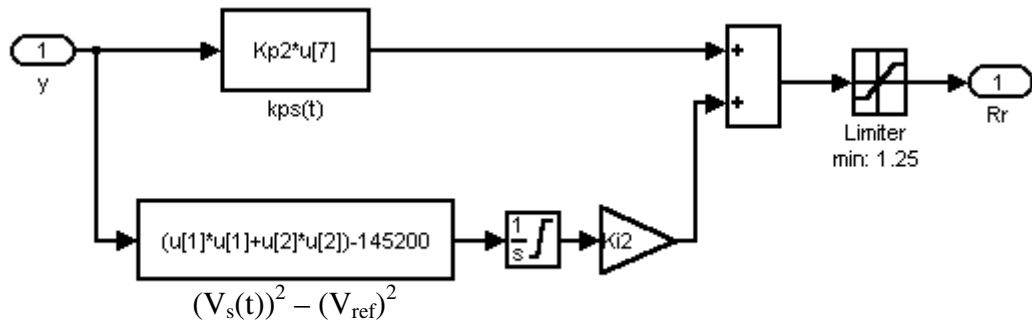
Figure 3.26 Rotor Resistor Controller

The Rotor Resistor Controller is shown in Figure 3.26. Minimum R_r value is 1.25 ohm, which is the resistor value of the rotor winding (r_r'). For this purpose a limiter is used at the output of the controller.

It is obvious that this controller will not take action if there is a disturbance resulted in a decrease in steady state voltage value. Therefore this controller is analyzed only for step type increase in the wind speed and for step type decrease in the load. The results are shown in Figure 3.27 and Figure 3.28.

In Figure 3.27 it is seen that, adjustment of R_r is enough for voltage and frequency regulation in case of the wind speed disturbances. The rotor external resistance does not affect the frequency steady-state value, if the stator voltage value is kept in its rated value. The same conclusion was done for Fig.3.10.
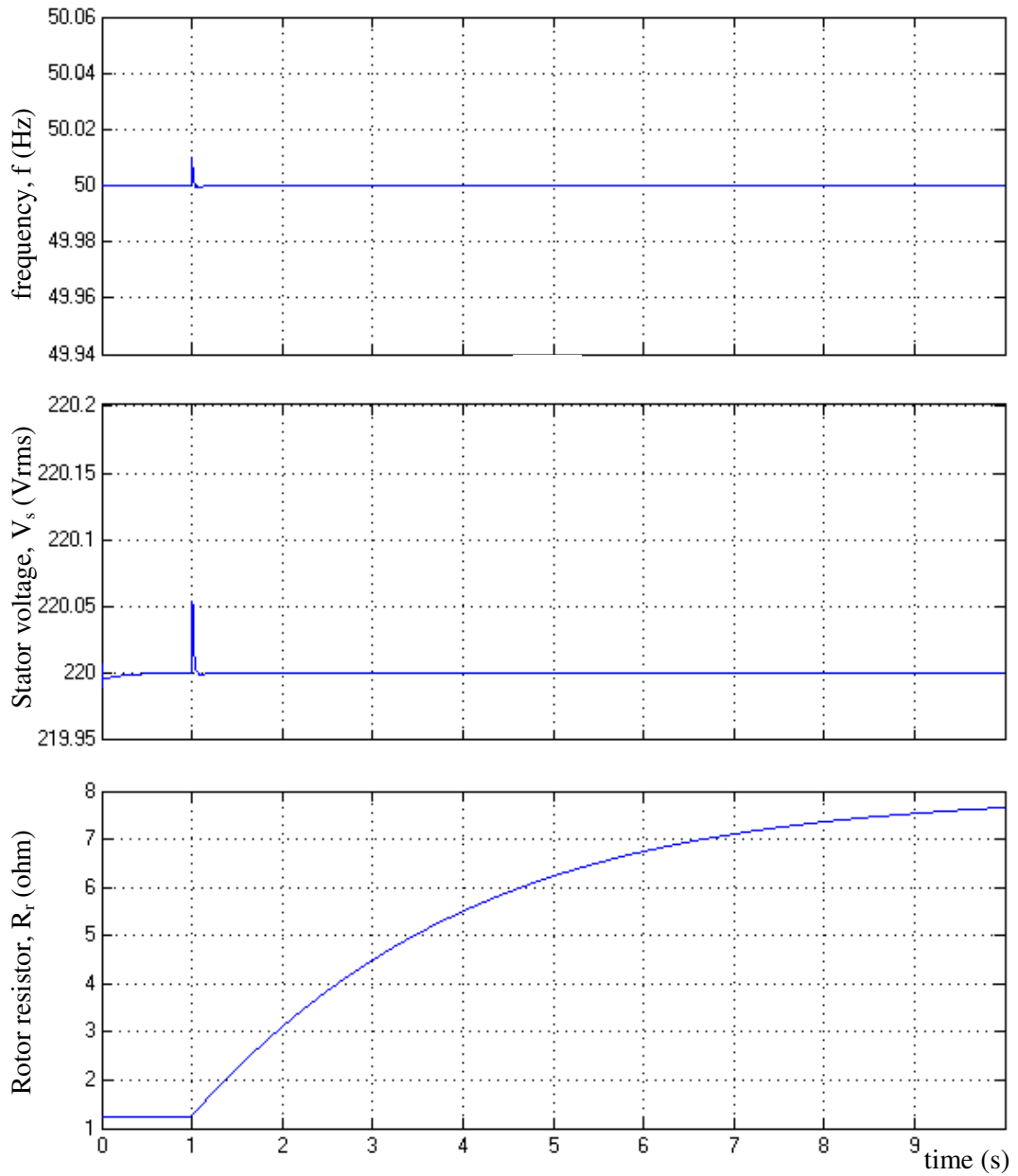
Figure 3.27 Frequency, Stator line-to-neutral Voltage and Rotor Resistor variations in case of the PI control of the Rotor Resistor R_r (v=10m/s $\rightarrow$ 11m/s at t=1s, G=0.0247mho constant)
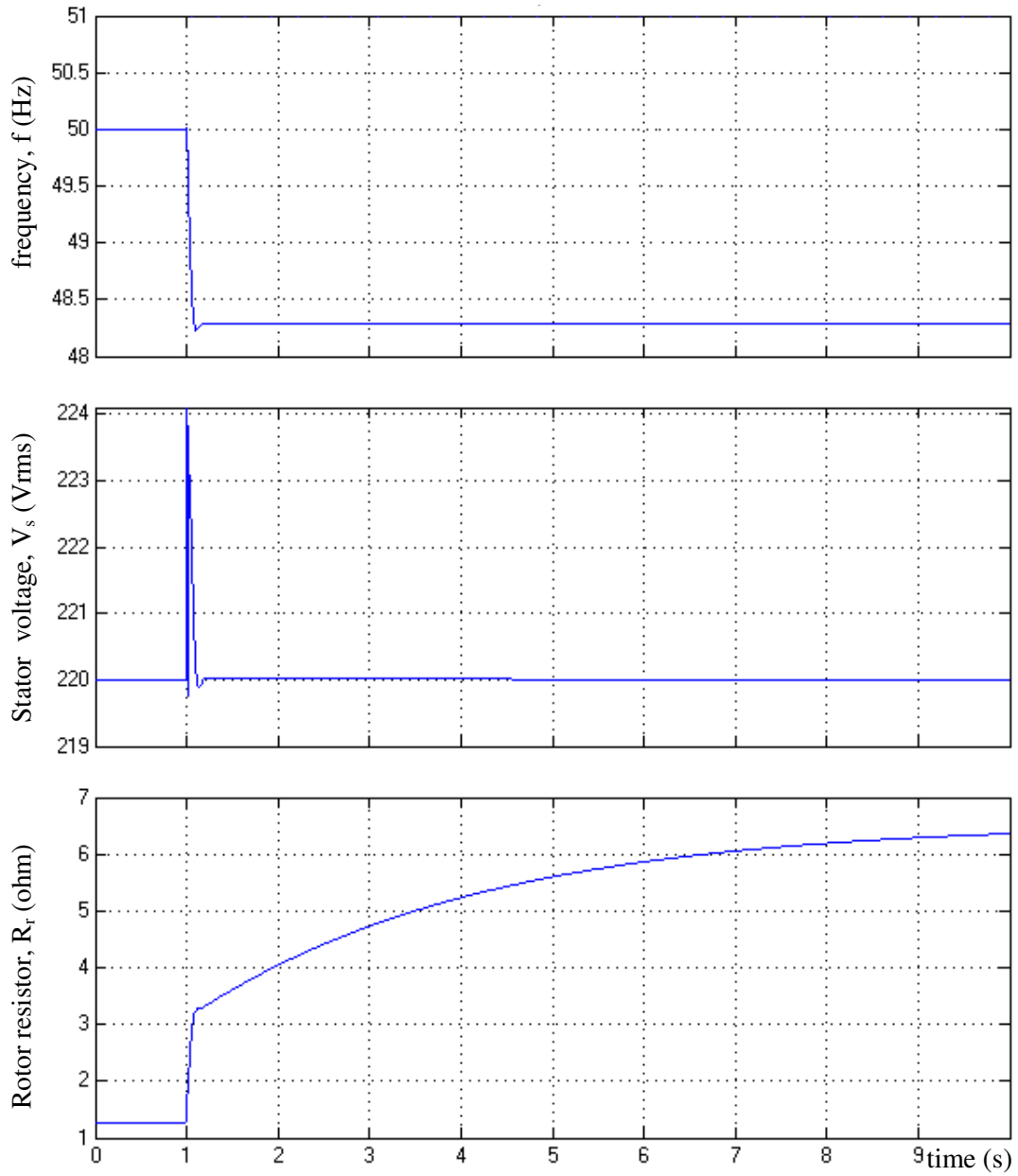
Figure 3.28 Frequency, Stator line-to-neutral Voltage and Rotor Resistor variations in case of the PI control of the Rotor Resistor R_r (G=0.0247mho $\rightarrow$ 0.0200mho at t=1s, v=10m/s constant)

3.7. VOLTAGE REGULATION WITH EXTERNAL LOADS

Voltage control can be done with variable external loads connected in parallel with the load. This scheme is preferred for the Squirrel Cage Induction Generator applications. In this case a variable resistor is connected parallel to the stator terminals. Whenever an increase in the voltage, we decrease the resistance value to extract the excess active power from the system. The flowcharts of this control are shown in Figs.3.13 and 3.14. As can be seen from the flowcharts, in this control scheme, for any disturbance it is required to make control on both of the control variables, capacitor (C) and external load G_{ext}. However, in this part of the study only the voltage regulation is simulated with external load control.
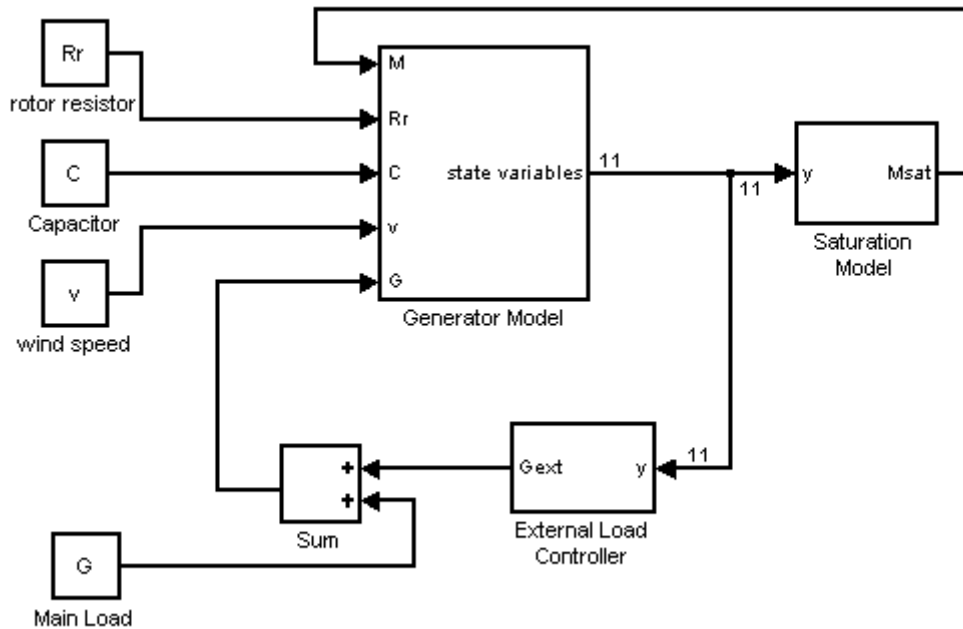
Figure 3.29 Voltage Regulation with External Loads Circuit Diagram

External load controller shown in Figure 3.29 is a PD type controller. The controller uses voltage error signal as input and produce control signal for the external load. The detail of the developed PD controller is given in Figure 3.30.
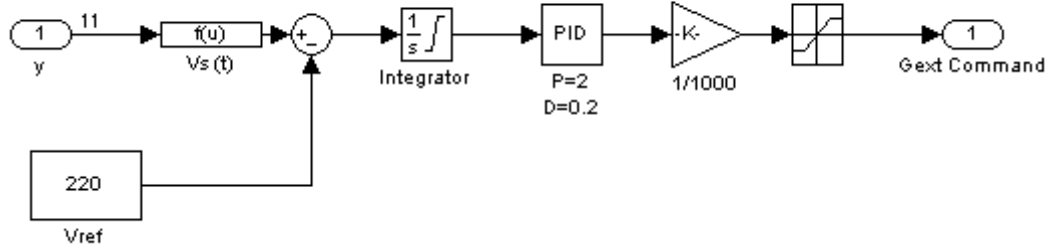
Figure 3.30 Proposed PD controller for External Load Control

The performance of this controller is analyzed in the Figures 3.31 and 3.32 for different type of disturbances.

Figure 3.31 shows Frequency, Stator line-to-neutral Voltage, Total Load and External Load variations in case of the PD control of the external load G_{ext}. Two disturbances are applied; wind speed changes from v=10m/s to 11m/s at t=1s and the load changes from G=0.0247mho to 0.0321mho at t=4s. It is seen that 10% increase in the wind speed generates enough active power for 30% of the rated load.

Figure 3.32 shows Frequency, Stator line-to-neutral Voltage, Total Load and External Load variations in case of the PD control of the external load G_{ext}. Two disturbances are applied as in Figure 3.31 but inversely; wind speed changes from v=10m/s to 9m/s at t=1s and the load changes from G=0.0247mho to 0.0173mho at t=4s. It is seen that 10% decrease in the wind speed is compensated with 30% decrease in the rated load.
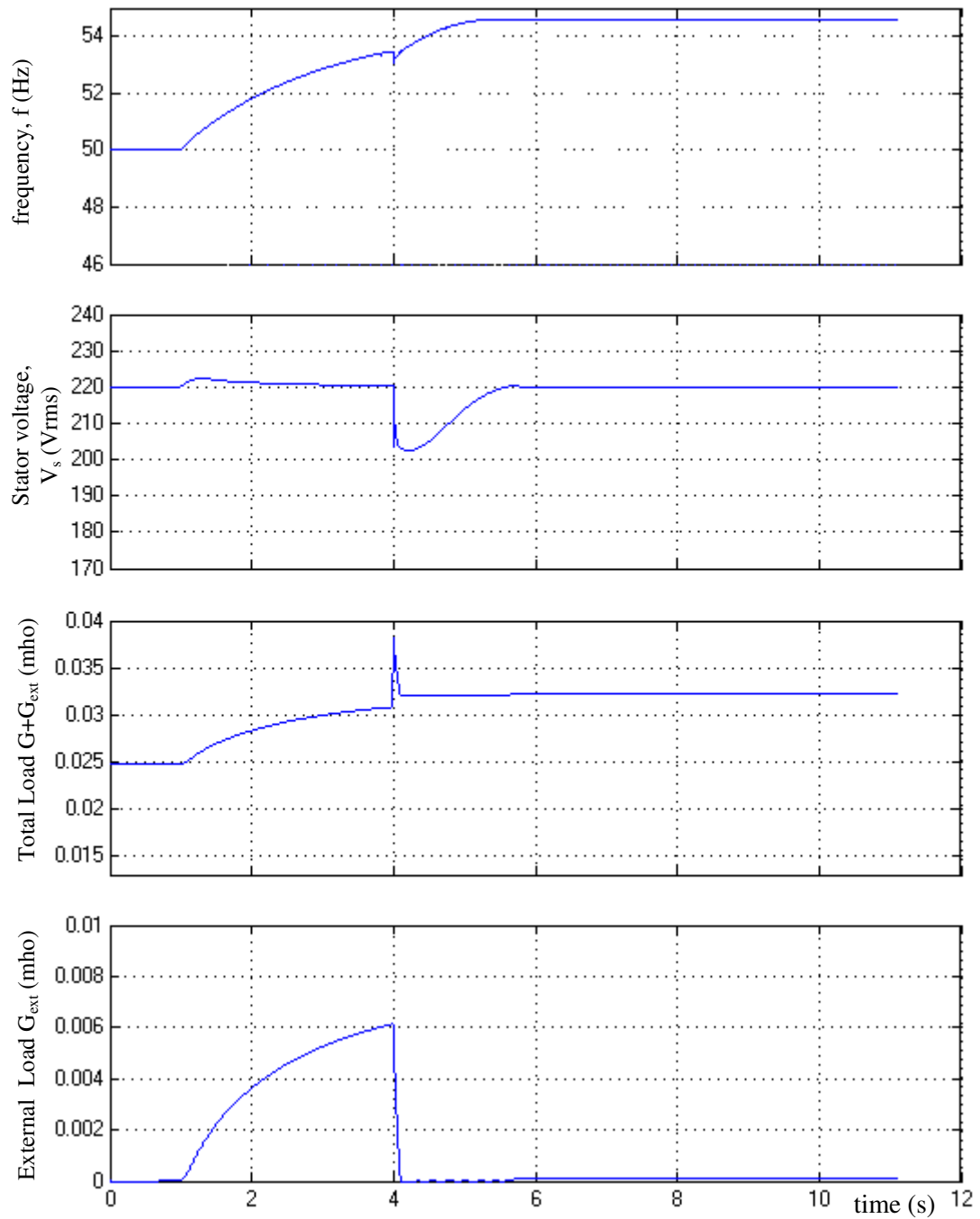
Figure 3.31 Frequency, Stator line-to-neutral Voltage, Total Load and External Load variations in case of the PD control of the external load G_{ext} (v=10m/s $\rightarrow$ 11m/s at t=1s and G=0.0247mho $\rightarrow$ 0.0321mho at t=4s)
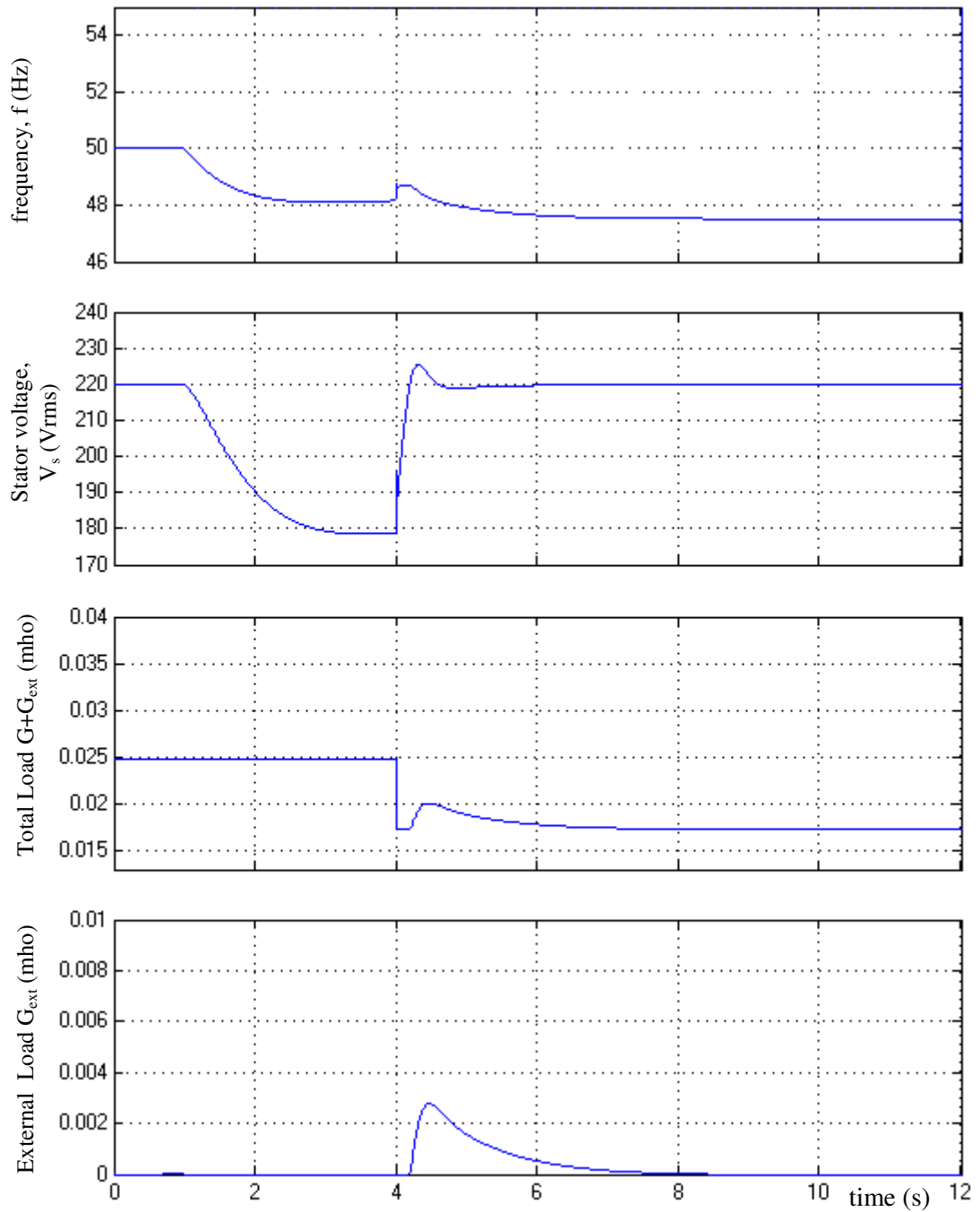
Figure 3.32 Frequency, Stator line-to-neutral Voltage, Total Load and External Load variations in case of the PD control of the external load G_{ext} (v=10m/s $\rightarrow$ 9m/s at t=1s and G=0.0247mho $\rightarrow$ 0.0173mho at t=4s)

3.8. SIMULATION OF THE COMPLETE SYSTEM

From now on, the simulations can be done with the power electronics components of the Power System Blockset. The power electronics components available in this blockset are modeled by professionals. These models are proven ones, they simulate the components with the turn on time, turn off time, R_{on}, snubber circuit, V_{on}, etc. Making the simulations with these components are better that making with the equations. Control strategies developed and control signals obtained in the previous part are ready to use in Power System Blockset.

There are three parts that should be simulated. The first one is the saturation adaptive induction machine, the second one is the frequency regulator, which should supply variable capacitance to the SEIG, and the third one is the voltage regulator, which should supply variable load to the SEIG.

3.8.1. Saturation Adaptive Asynchronous Machine Model

The Power System Blockset (PSB) has an Asynchronous Machine model. It can be seen that, the model of the PSB Asynchronous Machine is the same with the model given in Chapter 2. There are some differences between two models in evaluating the state variables. The PSB model uses mutual fluxes in calculating the rotor and stator fluxes [15]. The outputs of the two models are the same for the same operating conditions. However, saturation effect is not considered in PSB Asynchronous Machine model. Therefore the inner model of the machine should be modified to add the saturation effect given in Eq.2.43, Eq2.45, Eq.246 and Eq.2.47. PSB Asynchronous Machine model is shown in the Figures 3.33 and 3.34.
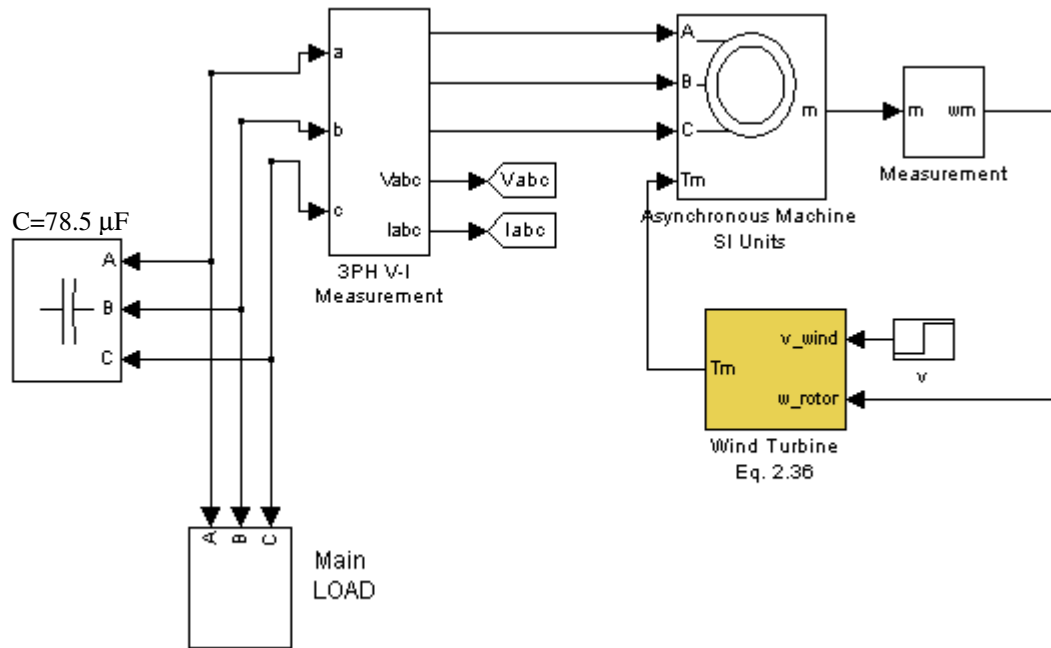
Figure 3.33 Dynamic Response Circuit Built with Power System Blockset
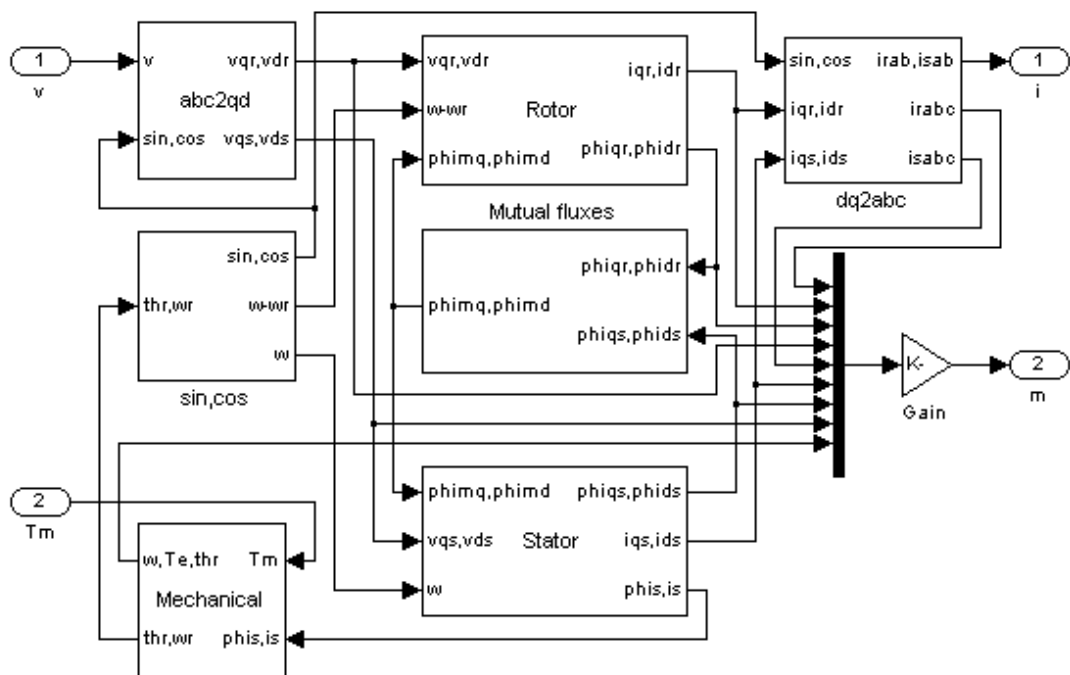
Figure 3.34 Asynchronous Machine model of the Power System Blockset

Saturation related equations are added to the "Mutual Fluxes" block of the machine, since the mutual inductance variable is used only in this block. Variables are

converted from p.u. to SI variables to apply the related equations, then the calculated mutual inductance value is converted to p.u. value. Detailed information about the p.u. machine model is given in [14]. The original Mutual Fluxes Block and the modified saturation adaptive Mutual Fluxes Block are shown in Figures 3.35 and 3.36, respectively.
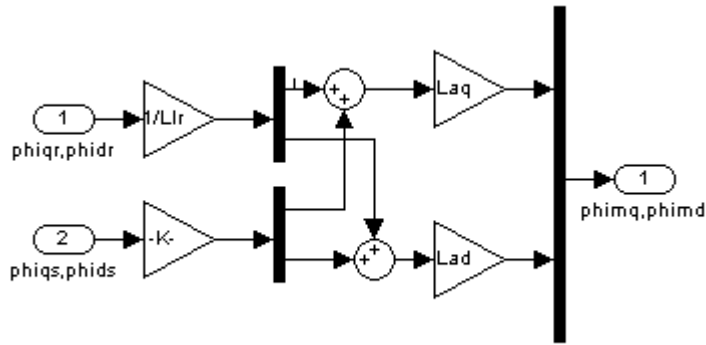
Figure 3.35 Model of the Mutual Fluxes Block

In Figure 3.35 Laq=Lad=L_M

$1/L_M=1/M+1/ls+1/lr$

M is the mutual inductance

ls and lr are stator and rotor leakage inductances, respectively.
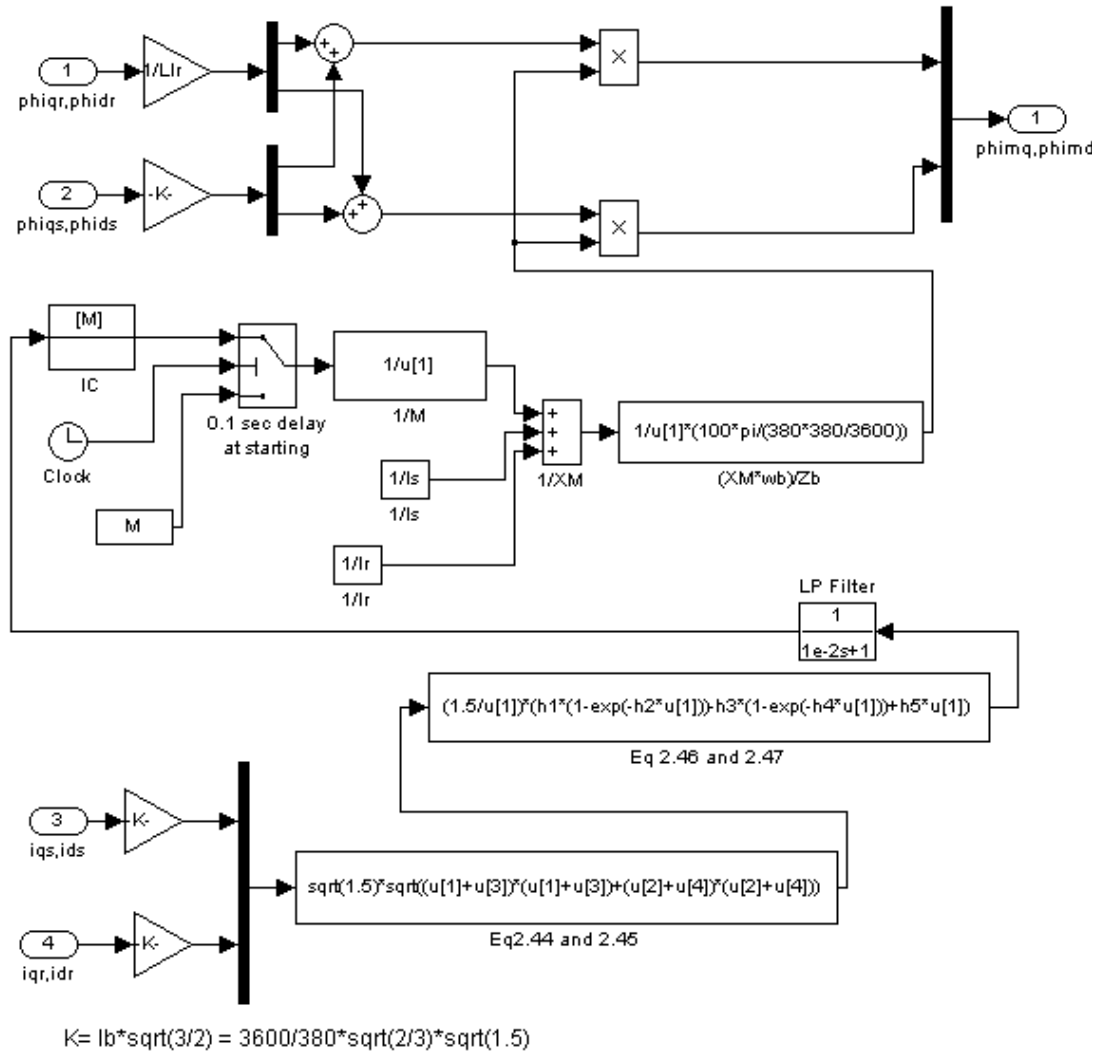
Figure 3.36 Saturation Adaptive Model of the Mutual Fluxes Block

The performance of the PSB original machine model and the modified machine is given in Figures 3.37 and 3.38, for the step type change in the wind speed as it is the case in Figures 3.4 and 3.6.
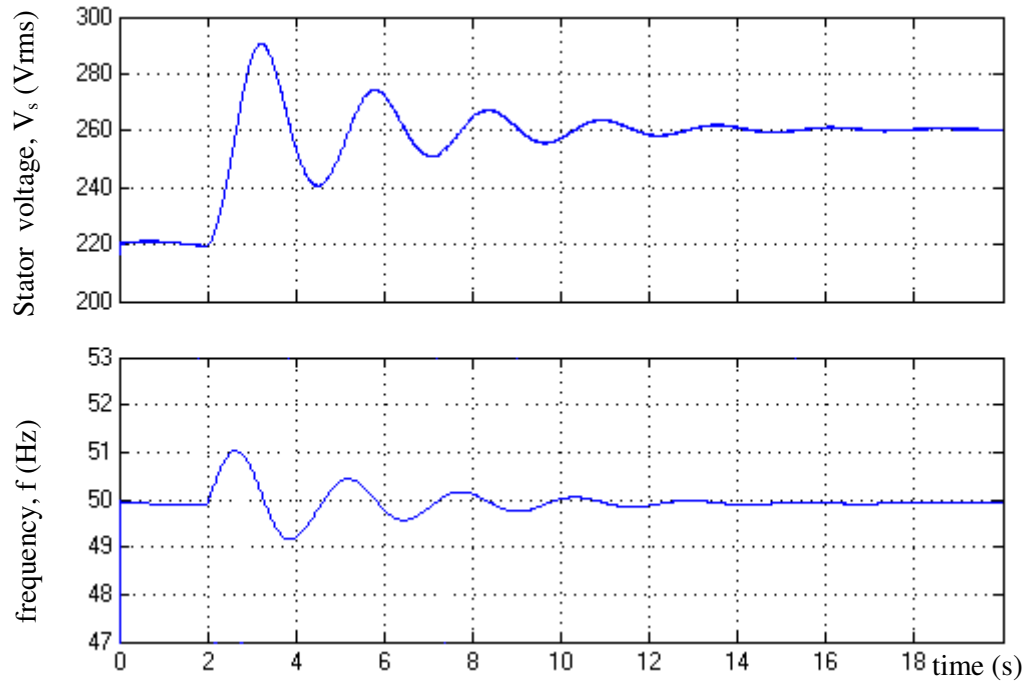
Figure 3.37 Stator line-to-neutral voltage and frequency responses of the Matlab PSB IM corresponding to disturbance v=10m/s → v=11m/s at t=2s(M=0.1578H Constant)
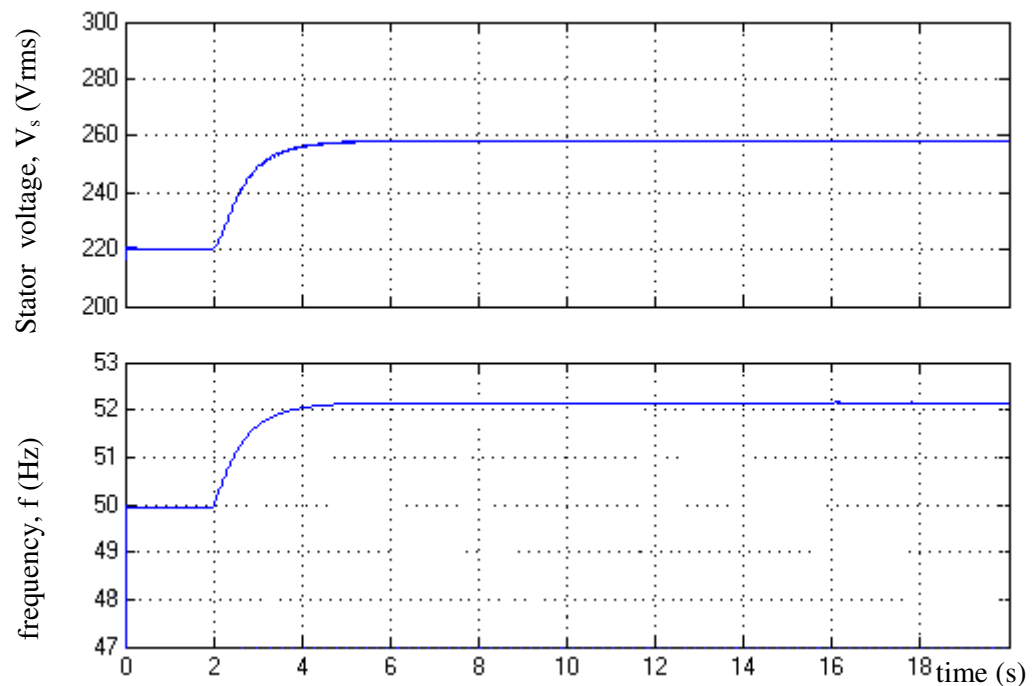
Figure 3.38 Stator line-to-neutral voltage and frequency responses of the Modified Matlab PSB IM corresponding to disturbance v=10m/s → v=11m/s at t=2 s (Double-Exponential Representation of the Magnetization Curve)

If the above figures are compared with the Figures 3.4 and 3.6, it is seen that the responses of the PSB machine model and the model given in Chapter 2 are the same for M=constant and M=saturated.

3.8.2. Frequency Regulation with TCR

The reactive volt-ampere (VAR) requirements of the IG and the load are supplied by means of VAR Generator connected to the stator terminals. In this study the Thyristor-controlled reactor connected in parallel to a fixed capacitor scheme is selected to meet the reactive power requirements of the SEIG. Operation principle of the TCR is explained in Appendix C.
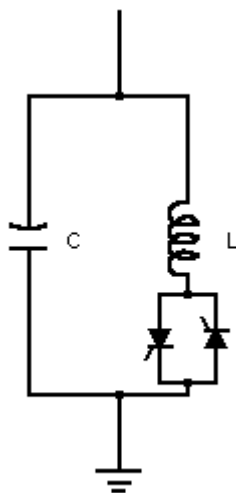
Figure 3.39 Proposed VAR Generator

The representation of the VAR Generator is shown in Figure 3.39. There are two elements; a relatively big fixed capacitor (C = 130µF), and an inductor (L=125mH).

The values of the C and L should be selected to suit the requirements of the SEIG. In this study, the induction generator used in the simulations is 5 kVA whose reactive power demand at rated wind speed (10m/s) and rated load (0.0247mho) is about 3.5 kVAR (C_{rated}=78.518 µF). 130 µF is chosen with the analysis of the dynamic

responses of the SEIG when it is disturbed. The variation of the excitation capacitance command signal is shown in Figures 3.21-3.24. From the Figures it is shown that C=130μF will suit the reactive power requirements during the transient and steady-state periods. The value of L, on the other hand should be selected according to the excess reactive power generated by the capacitor. This value can be calculated as;

$$wL = \frac{1}{w(C_{max} - C_{min})} \qquad (3.4)$$

Taking C_{max} = 130 μF and C_{min} = 50 μF resulted in L=126.7 mH. Then, choosing L=125 mH will be enough to absorb the excessive reactive power generated by the capacitor. C_{max} and C_{min} are the maximum and minimum capacitor requirements of the SEIG during transient periods of the disturbances.

Three phase Y-connected capacitor and Y-connected Thyristor Controlled Reactor (TCR) are used in the circuit. Arrangement of the Y-connected TCR with Y-connected capacitors is shown in Figure 3.40.
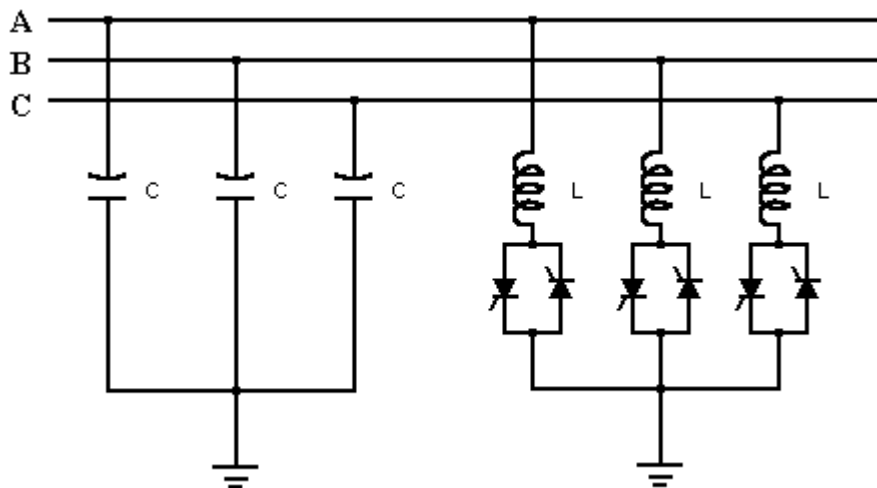
Figure 3.40 Three-phase Y-Connected TCR with shunt capacitors.
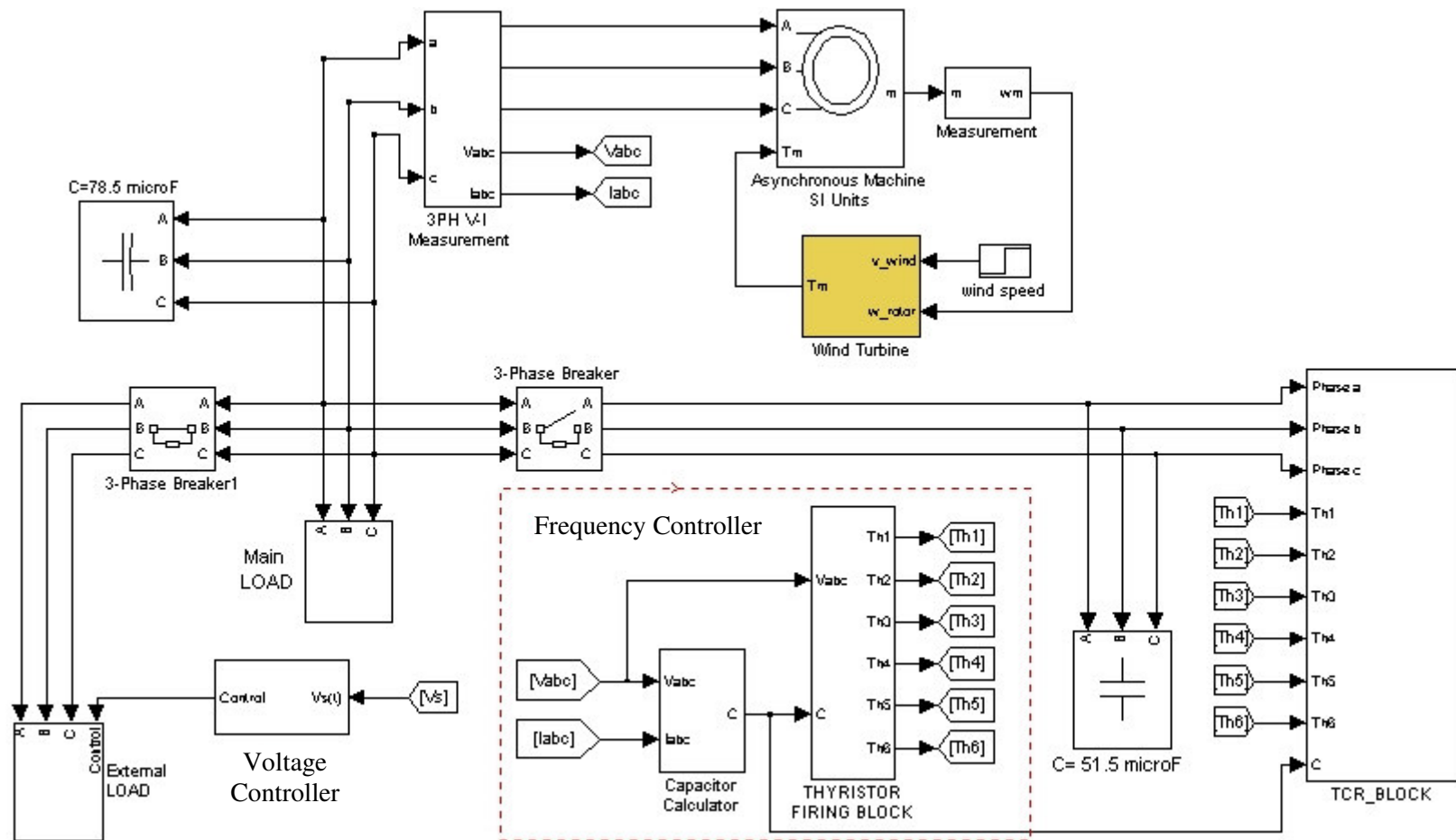
Figure 3.41 The Complete Simulation Circuit Diagram

The overall simulation circuit diagram is given in Figure 3.41 with Frequency Controller and Voltage Controller. The Operation of the Frequency Controller is as follows: There-phase voltages and currents measurements are converted to their D-Q components. Rotor flux linkages are calculated and used to generate excitation capacitance command, which is explained in the part 3.5 of this chapter. The Capacitance Command and the three-phase voltage measurements are connected to Thyristor Firing Block, which is shown in Appendix D.2. The required capacitance value extracted from the total capacitance value. This value should be absorbed by the TCR. Therefore, the conduction period of the inductor is adjusted according to this value. The generated firing pulses are sent to TCR Block whose circuit diagram is shown in Appendix D.2.

3.8.3. Voltage Regulation with Switched Resistors

Variable external load, on the other hand, is modelled with eight resistors connected parallel to the stator terminals of the IM. Their resistance values are 10000, 5000, 2500, 1250, ..., 78.125 ohms. Each phase is controlled by eight switches, resulting in 2^8 = 256 different switching possibilities. Each switching possibility results in a different resistance value. The proposed voltage controller is shown in Figure 3.42.
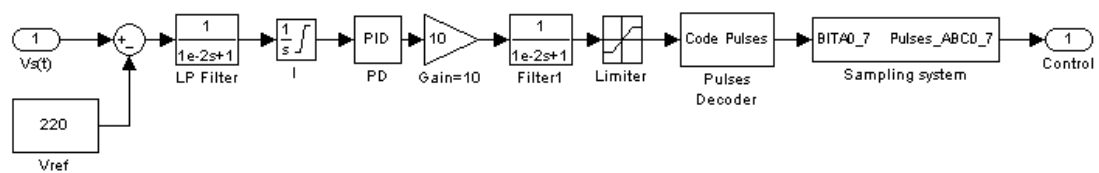
Figure 3.42 PD Type Voltage Controller with Pulse Decoder

This type of operation is used as a frequency regulator in the demonstration of the wind power generation in Power System Blockset.

The operating principle of the Voltage Controller is as follows; the generated external load command goes to Pulses Decoder whose circuit diagram is shown in Appendix D.1. Pulses Decoder, decode the input signal to eight-bit output signal with 256 different possibilities. The eight-bit signal goes to Sampling System block, which generates 3-phase pulses with zero crossing current of the phases. Therefore three phase current measurements are used in the Sampling System. Sampling System is firing the 24 switches (8 switches for each phase). Diagram of the all blocks are given in Appendix D.1.

3.8.4. Overall Simulation

As a last step, the whole model is simulated for the CVCF operation of the stand-alone SEIG application. The Circuit Diagram is given in Figure 3.41.

There are modified Asynchronous Machine, 3-phase V-I Measurement Block, Variable Main Load (which has two resistive loads connected in parallel with a circuit breaker between them), two fixed capacitors one has C_{rated}=78.5 μF and the other has C_{adjust}=51.5 μF, TCR which has an inductor L=125mH and two Thyristors in each phase, two circuit breakers used to activate and de-activate the controllers.

Integral control parameter in the Frequency Controller, k_i is optimized with k_i=0.001 and the PD parameters of the Voltage Regulator are optimized with P=2 and D=0.2.

All types of the disturbances are applied to the circuit and the results are shown in the Figures 3.43-3.53. The simulations start with the rated voltage and frequency values. Step type disturbances in the wind speed and the load are applied.
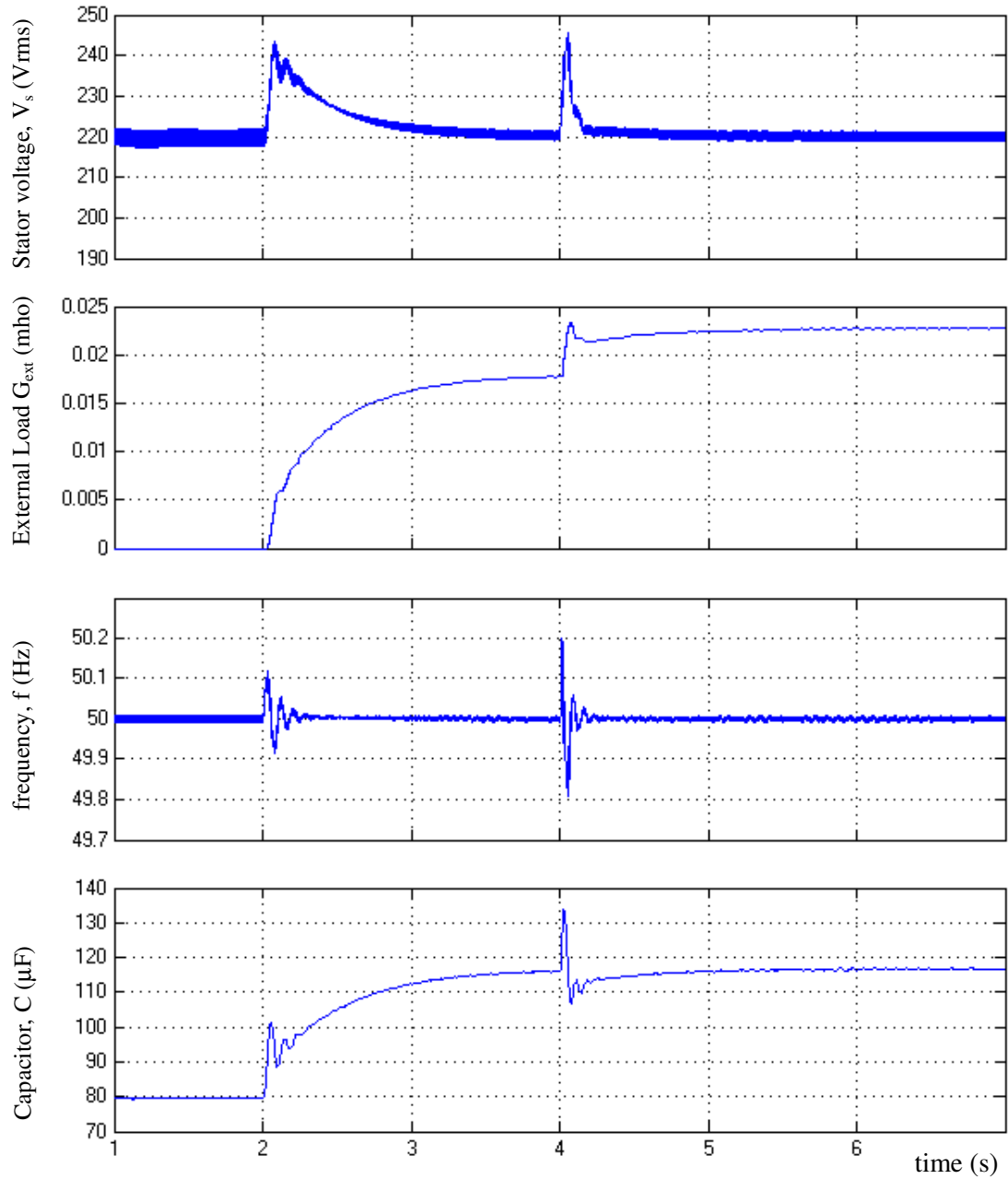
Figure 3.43 Stator line-to-neutral Voltage (V_s), External Load (G_{ext}), Frequency (f) and Required Excitation Capacitor (C) responses in case of the PD control of the external load G_{ext} and PI control of the Excitation Capacitor (v=10m/s → 12m/s at t=2s and G=0.0247mho → 0.0200mho at t=4s)

Figure 3.43 shows Stator line-to-neutral Voltage (V_s), External Load (G_{ext}), Frequency (f) and Required Excitation Capacitor (C). Required excitation capacitor is the control signal that the Capacitor Calculator in Figure 3.41 generates and sends to Thyristor Firing Block to adjust the reactor conduction angle. It can be said that, with this amount of large disturbance in wind (20%) maximum voltage error is about 10% of the rated value, which is acceptable for the power systems. This overshoot can be decreased by increasing the switching frequency of the switches of the external loads. However, keeping the switching frequency low (which is below 100 Hz) is better for the life of the switches. On the other hand the frequency regulation is also acceptable. The maximum error of the frequency is 0.4 % of the rated value.
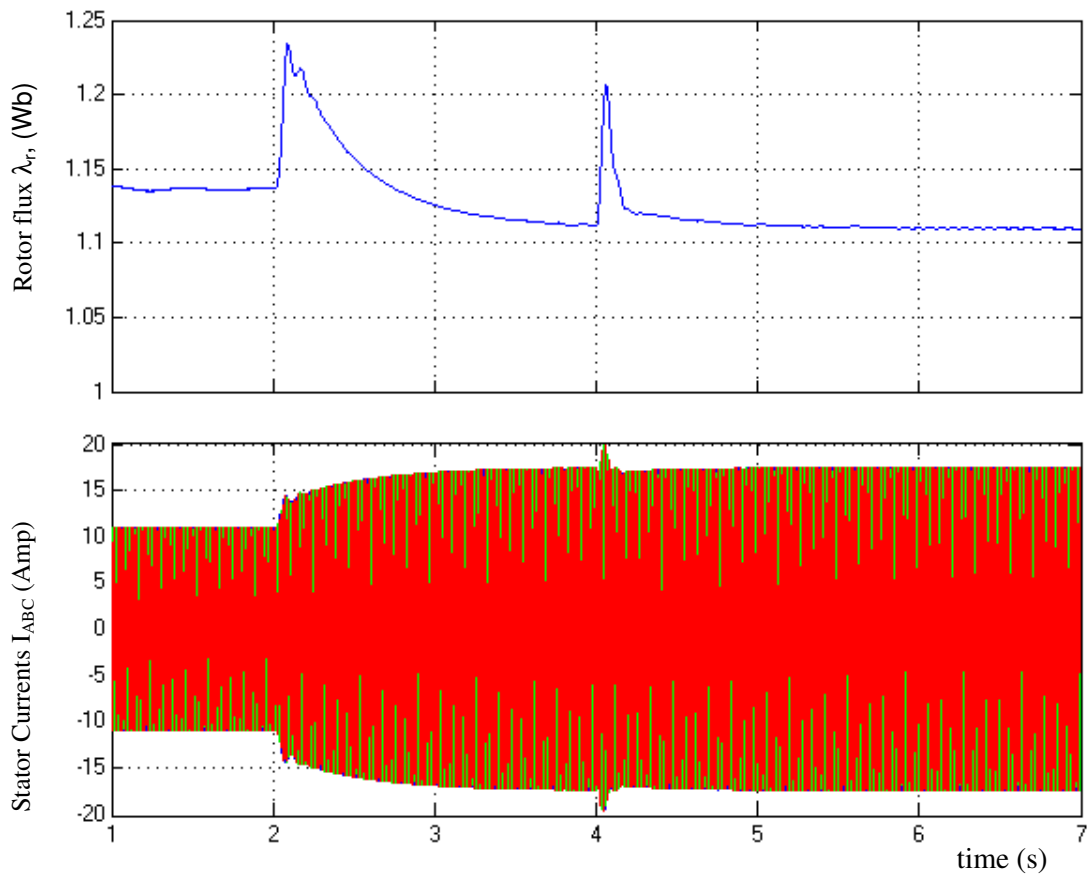
Figure 3.44 Rotor flux (λ_r) and Stator Currents (I_{ABC}) responses in case of the PD control of the external load G_{ext} and PI control of the Excitation Capacitor (v=10m/s → 12m/s at t=2s and G=0.0247mho → 0.0200mho at t=4s)

Fluxes and stator currents are shown in Figure 3.44. The rotor flux is not constant during the operation. Steady-state value of the rotor flux magnitude is changed with the wind speed disturbance, while it is constant with the load disturbance.
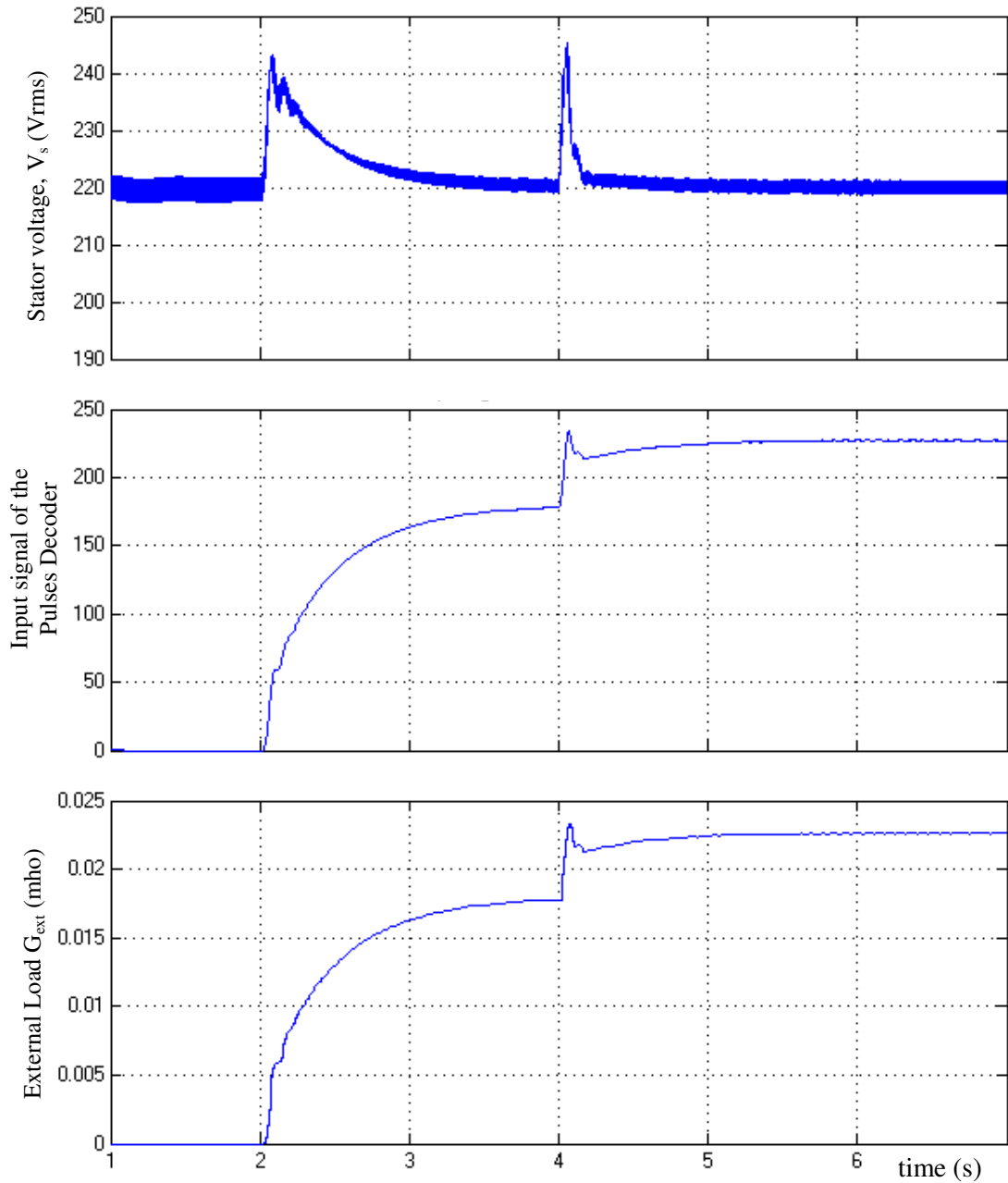
Figure 3.45 Stator line-to-neutral Voltage (V_s), Input Signal of the Pulses Decoder and External Load (G_{ext}) variations in case of the PD control of the external load G_{ext} and PI control of the Excitation Capacitor (v=10m/s $\rightarrow$ 12m/s at t=2s and G=0.0247mho $\rightarrow$ 0.0200mho at t=4s)
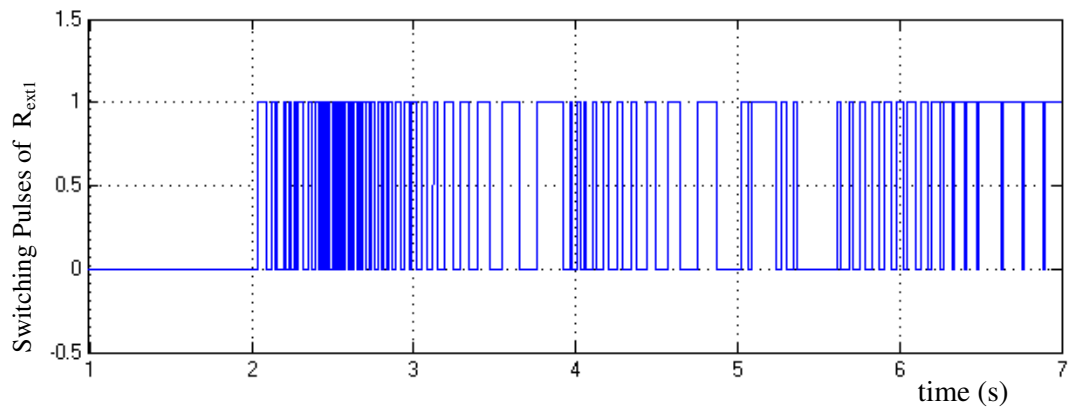
Figure 3.46 Switching Pulses of the Most Frequently switched External Resistor (R=10000 ohm) in case of the PD control of the external load G_{ext} and PI control of the Excitation Capacitor (v=10m/s → 12m/s at t=2s and G=0.0247mho → 0.0200mho at t=4s)

The performance of the Voltage Controller is shown in Fig.3.45. According to the stator voltage variation, PD controller shown in Fig. 3.42 generates control signal, which is limited between 0-255. This limitation is done for eight bit decoding $2^8 = 256$. Pulses Decoder decodes this signal to eight bit switching signal. Switching signals open or close the external resistances according to their 0 or 1 values. The measured external load also is shown in the figure as G_{ext} (mho). It is seen that Voltage Controller follows the voltage variations successfully.

Figure 3.46 shows the switching pulses of the most frequently switched external resistor whose resistance is R_{ext1} = 10000 ohm. It is the biggest external resistor connected to the stator. Therefore, it is the smallest load since the load is inversely proportional with the resistance value (G = 1/R). Since it is the smallest load, it is used most frequently to adjust the external load precisely.

The performance of the Frequency Controller is shown in Figures 3.47 – 3.49. The figures show the operation of the TCR. Although the Thyristor firing commands are sent with 10 ms delays to the thyristors, it is seen that current flow through the inductor follows the capacitance command.
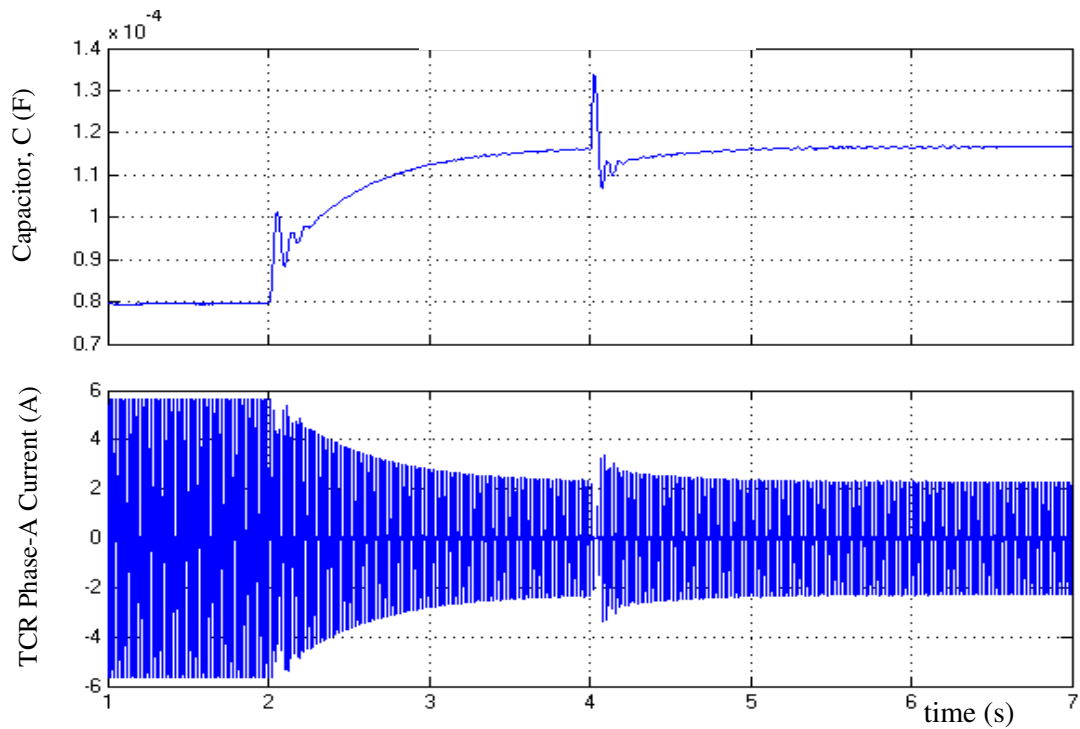
Figure 3.47 Required Excitation Capacitor (C) and phase current of TCR in case of the PD control of the external load G_{ext} and PI control of the Excitation Capacitor (v=10m/s → 12m/s at t=2s and G=0.0247mho → 0.0200mho at t=4s)

Figures 3.48 and 3.49 show the TCR operation with big conduction angle when the required capacitance is small between t=1s and t=2s and with small conduction angle when the required capacitance is big between t=4s and t=7s.
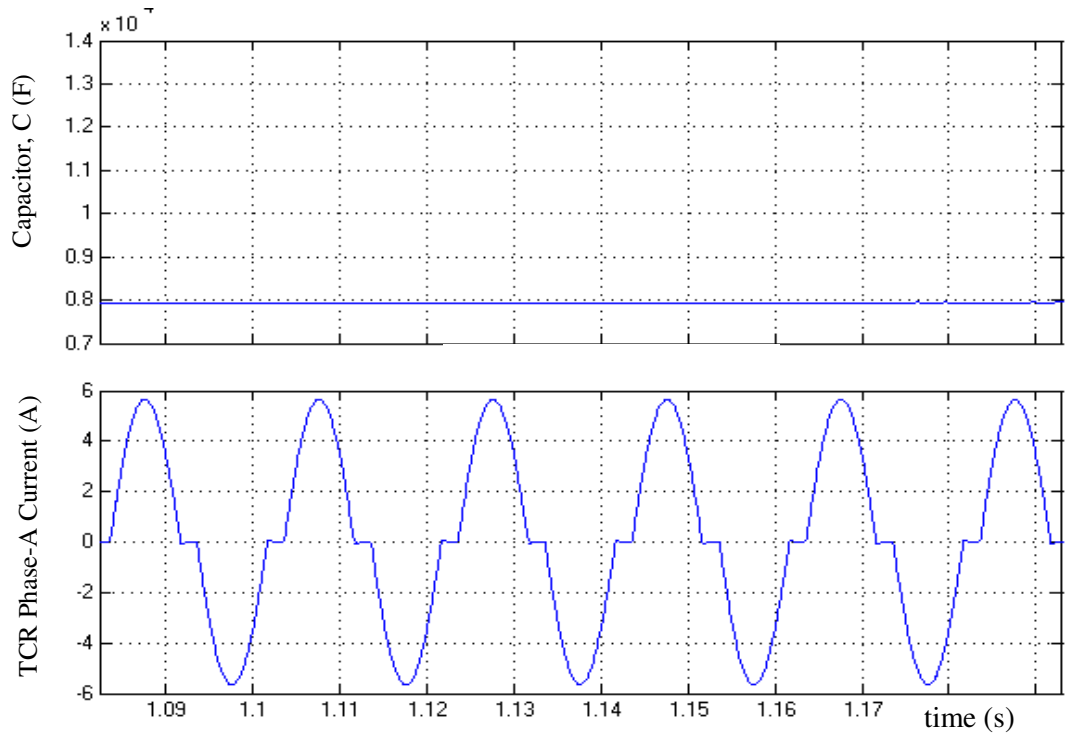
Figure 3.48 Required Excitation Capacitor (C) and phase current of TCR with big conduction angle (complete waveform is shown in Figure 3.47)
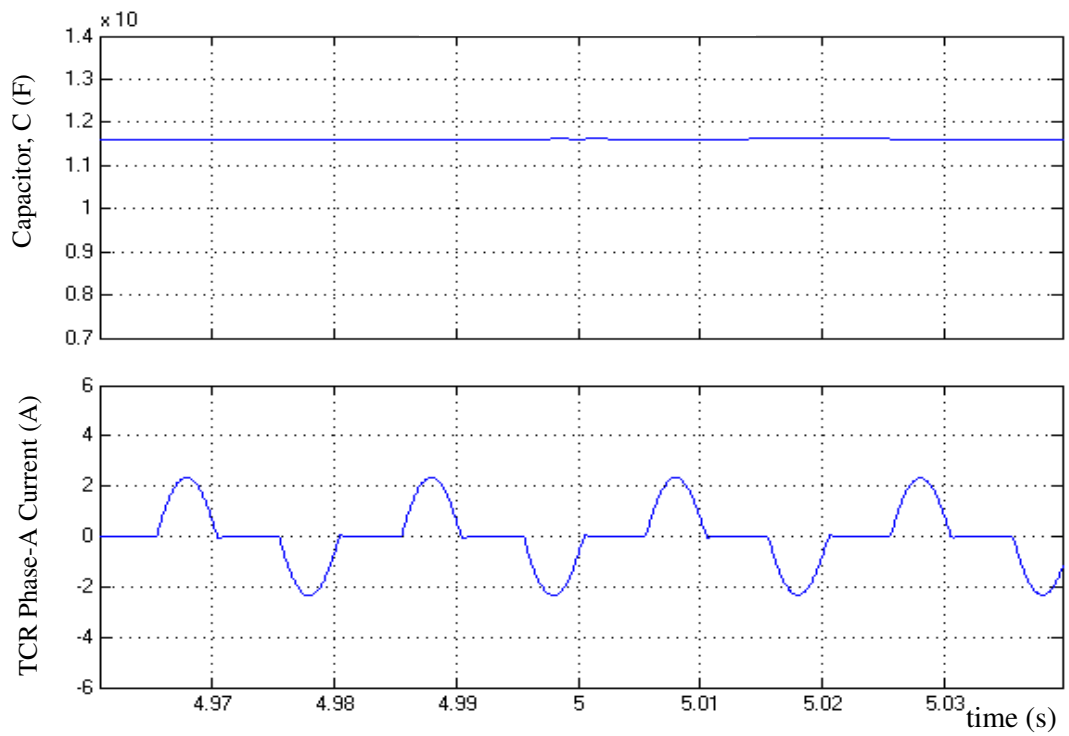
Figure 3.49 Required Excitation Capacitor (C) and phase current of TCR with small conduction angle (complete waveform is shown in Figure 3.47)

99

Similar simulations are done for the other type of the disturbances in the wind speed and in the load. In all simulations, it is seen that if there is no loss of excitation caused by low wind speed or very high loads, there are active and reactive power balances in the system. The Stator Voltage is kept at its rated value, provided that there is more or enough wind power for the corresponding load. Otherwise voltage will decrease and equilibrium state is reached below the rated voltage. Frequency is kept constant for all types of the disturbances.

Figure 3.50 shows the waveforms of the output and control variables; Stator line-to-neutral Voltage (V_s), Frequency (f), External Load (G_{ext}) and Required Excitation Capacitor (C) corresponding the disturbances in the wind speed v=10m/s → 11m/s (10% increase) and the load G=0.0247mho → 0.02717mho (10% increase). The controllers again work properly for these types of disturbances.

Figure 3.51 shows the waveforms of the output and control variables; Stator line-to-neutral Voltage (V_s), Frequency (f), External Load (G_{ext}) and Required Excitation Capacitor (C) corresponding the disturbances in the wind speed v=10m/s → 9m/s at t=2s (10% decrease) and the load G=0.0247mho → 0.0200mho at t=4s (20% decrease). The controllers again work properly for these types of disturbances.
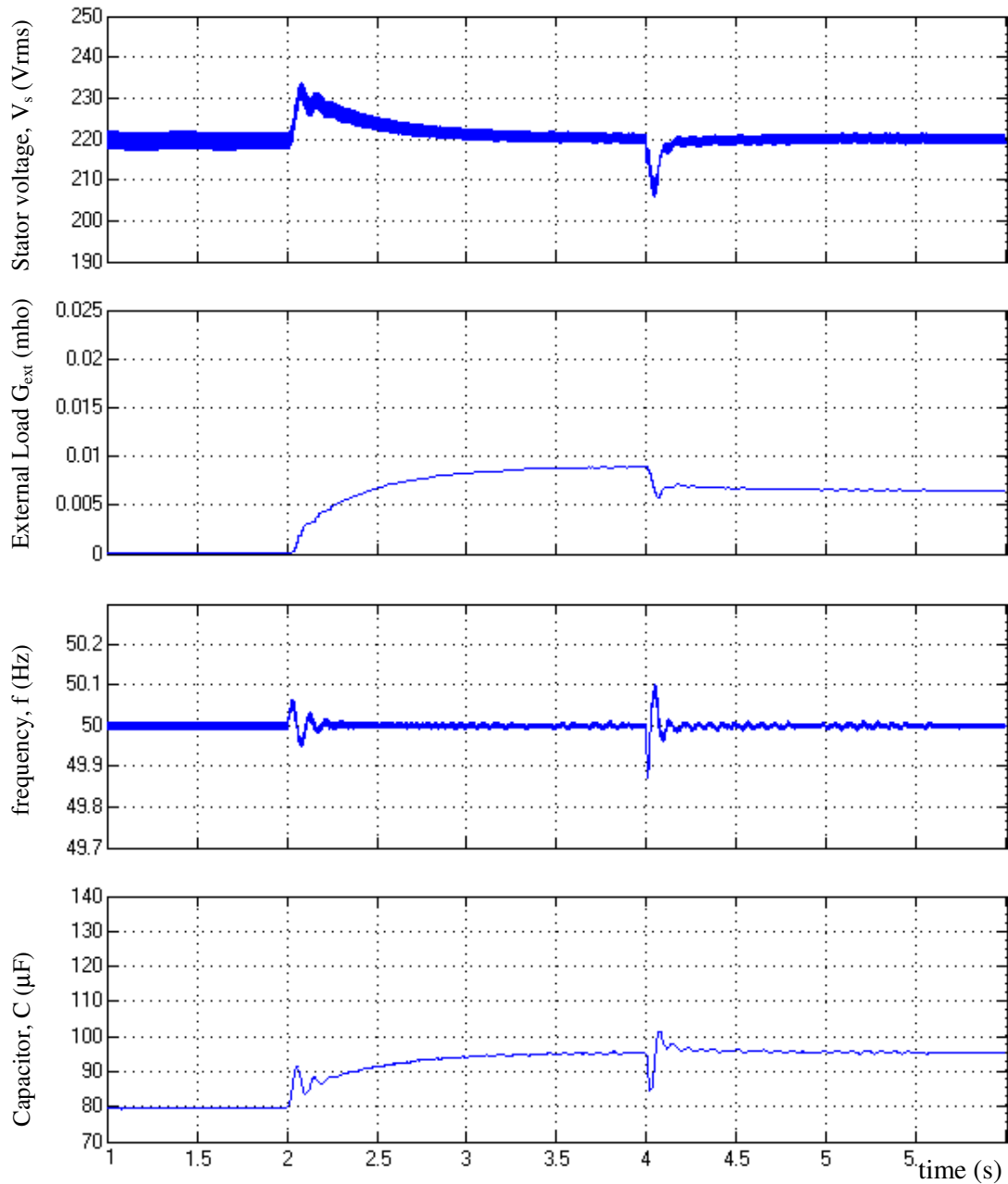
Figure 3.50 Stator line-to-neutral Voltage (V_s), External Load (G_{ext}), Frequency (f) and Required Excitation Capacitor (C) responses in case of the PD control of the external load G_{ext} and PI control of the Excitation Capacitor (v=10m/s → 11m/s at t=2s and G=0.0247mho → 0.0272mho at t=4s)
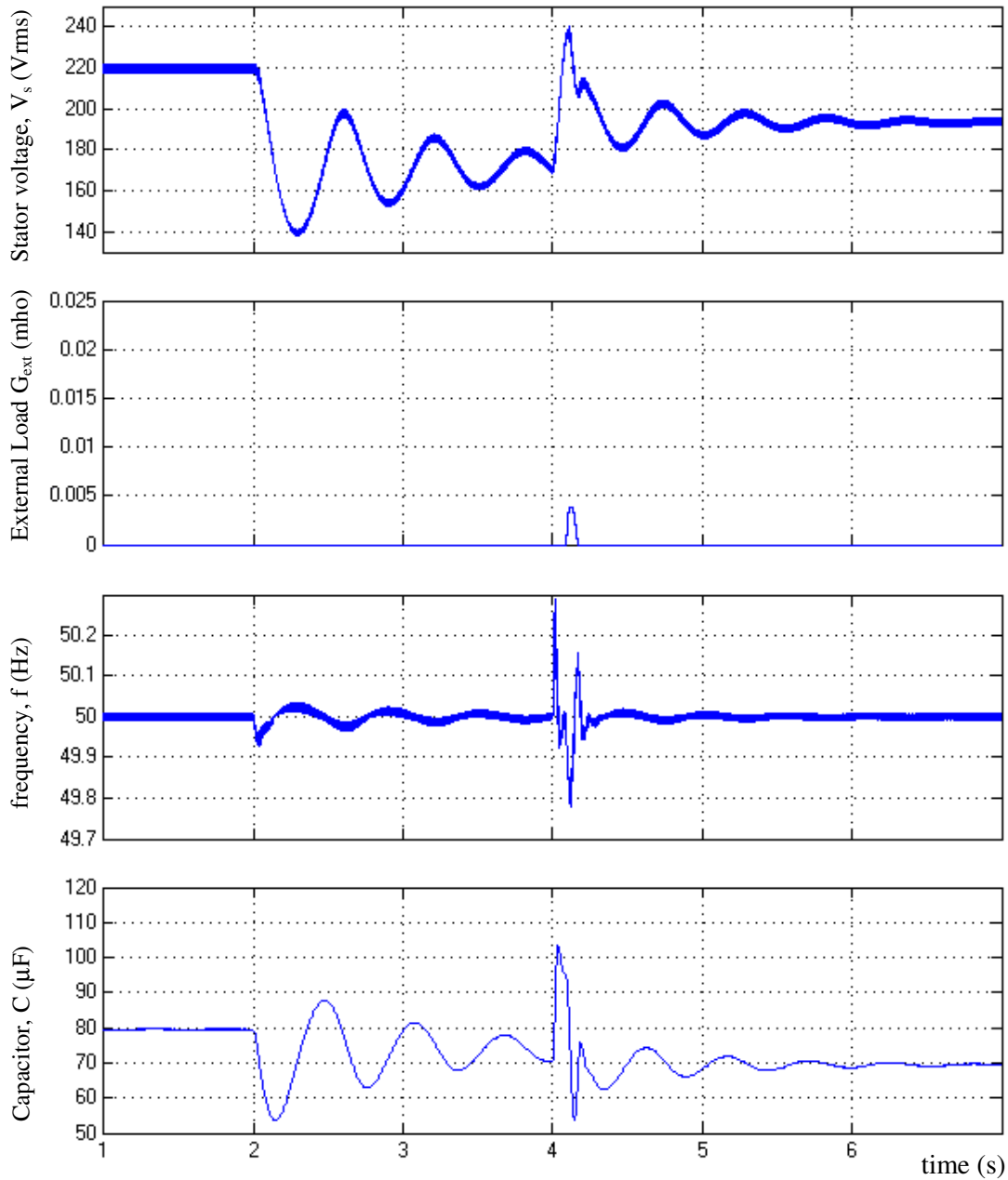
Figure 3.51 Stator line-to-neutral Voltage (V_s), External Load (G_{ext}), Frequency (f) and Required Excitation Capacitor (C) responses in case of the PD control of the external load G_{ext} and PI control of the Excitation Capacitor (v=10m/s → 9m/s at t=2s and G=0.0247mho → 0.0200mho at t=4s)
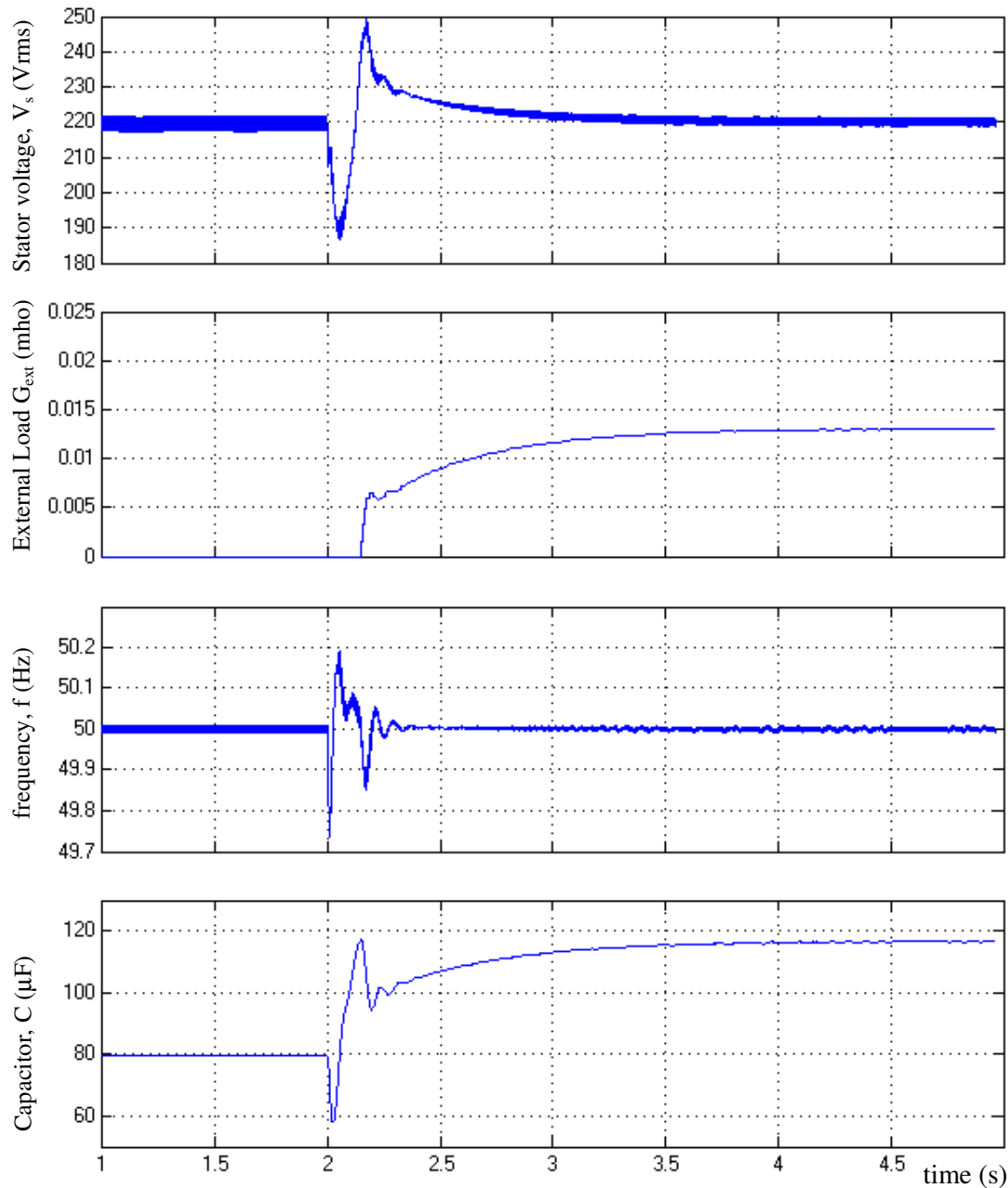
Figure 3.52 Stator line-to-neutral Voltage (V_s), External Load (G_{ext}), Frequency (f) and Required Excitation Capacitor (C) responses in case of the PD control of the external load G_{ext} and PI control of the Excitation Capacitor (double disturbance v=10m/s → 12m/s at t=2s and G=0.0247mho → 0.02964mho at t=2s)
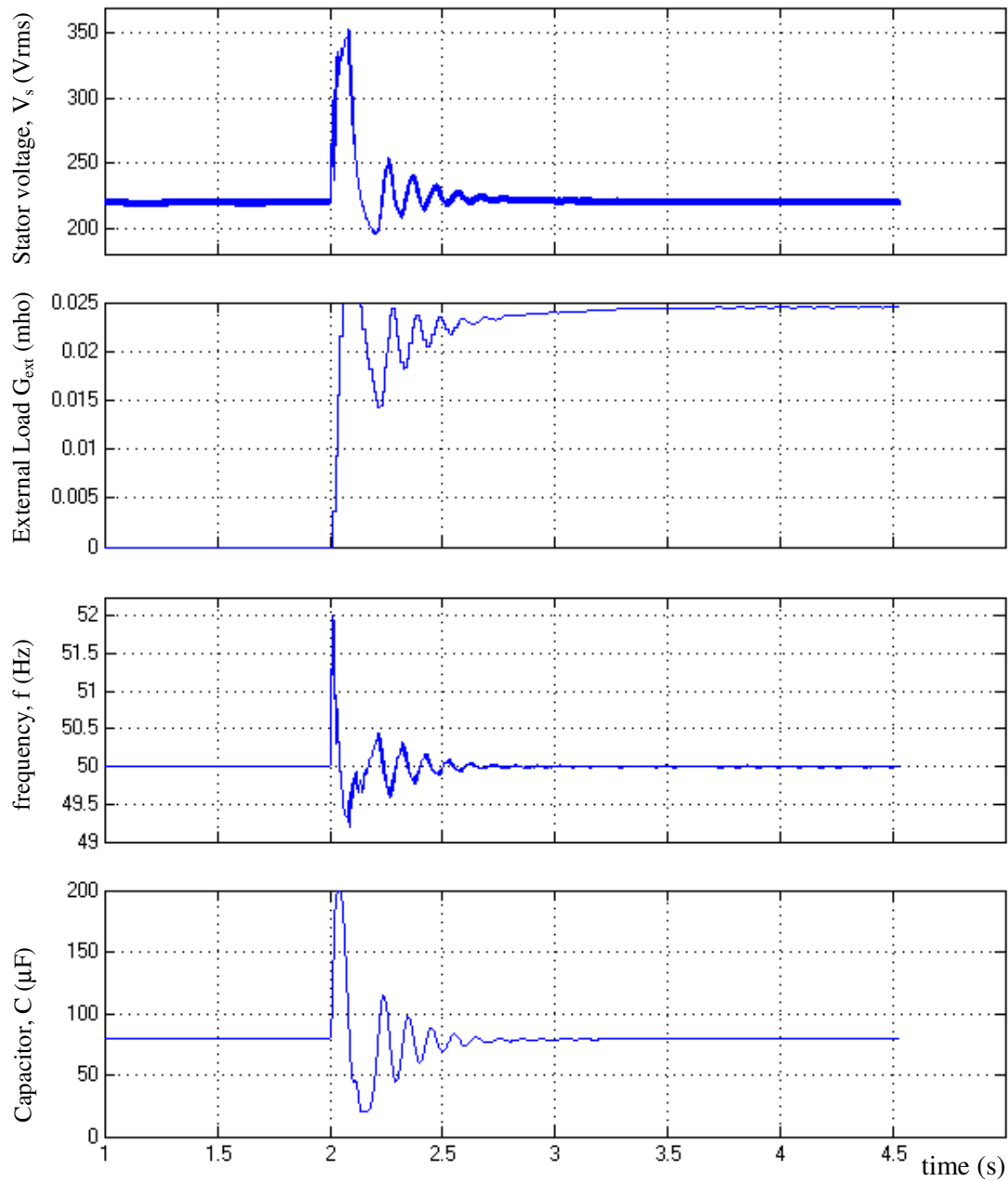
Figure 3.53 Stator line-to-neutral Voltage (V_s), External Load (G_{ext}), Frequency (f) and Required Excitation Capacitor (C) responses in case of the PD control of the external load G_{ext} and PI control of the Excitation Capacitor
(G=0.0247mho → 0 mho, no load at t=2s)

The performance of the controllers for the double disturbance in the wind speed and in the load at the same time is shown in Figure 3.52. It is seen that there is a relatively big fluctuation in the Stator Voltage, while the frequency does not show big changes. However, double step disturbances can not occur at the same time in the practical life.

No load condition, on the other hand is shown in Figure 3.53. In this case, the main load is switched off completely at time t=2s. 50 % overshoot in the stator voltage is shown in the figure. This overshoot does not affect the main load since it is removed completely. Induction machine and the resistive external loads of course can withstand to this overshoot. The thyristor switches in the TCR should be selected with higher than the rated voltage in the design phase.

CHAPTER 4

CONCLUSIONS

In this study, a variable speed self-excited induction generator is modeled with Matlab/Simulink with variable self-excitation capacitance and a variable resistive load. For this purpose, a general mathematical model of the system in a synchronously rotating reference frame has been derived. Based on this model, steady-state and transient characteristics of the SEIG are studied.

Different control schemes are developed both to the squirrel-cage induction generator and to the wound-rotor type induction generator. Control schemes aim to ensure a constant voltage-constant frequency operation. It is shown that, a cage type induction machine can be used with controlled external loads and with a static VAR compensator as a constant voltage-constant frequency supply.

Static VAR Compensator is modeled with a Thyristor Controlled Reactor (TCR) and a fixed capacitor. It is shown that by controlling the conduction angle of the TCR, variable excitation capacitance value is supplied for the constant frequency operation. It has been known that TCR generates harmonic currents is the system. Triplen harmonics are removed with delta-connected TCR, and the other harmonics can be removed with filters. Harmonic analysis and harmonic elimination methods of TCR need further study.

Also the capacity of the TCR can be made smaller (bigger inductor in the TCR) by using Thyristor Switched Capacitors whose operation principles are given in [17].

Voltage regulation, on the other hand is modeled with controlled loads connected to the stator terminals in parallel to absorb the excessive active power from the system. Controlled Loads are simulated with eight three-phase resistances having eight switches for each phase. The switches are controlled with a PD type controller.

Reactive power source can be modeled with a shunt inverter which is connected to stator terminals having a big dc capacitor in dc side [4]. In this case reactive power value is adjusted by successfully controlling the inverter switches.

Another attractive solution for CVCF operation appears as the use of two converters connected in series to the generator terminals [18]. In this configuration, the generated voltage first converted to dc voltage with a rectifier and then inverted to 50 Hz ac voltage with a PWM inverter.

The practical realization of the proposed control methods can be considered as a further study.

As a conclusion, constant voltage-constant frequency operation of the self excited induction generator for stand alone applications is simulated with matlab's standard blocks.

REFERENCES

[1]   BASSETT E. D., POTTER E. M., "Capacitive Excitation for Induction Generators" Elect. Eng., vol. 54, pp. 540-545, May 1935.

[2]   WAGNER C. E., "Self Excitation of Induction Motors" Trans. AIEE, vol. 58, pp. 47-51, Feb. 1939.

[3]   ERMİŞ M., "Modelling and Analysis of a Wind Turbine Driven Self-Excited Induction Generator", Ph.D. Thesis, METU, 1982.

[4]   LIAO Y. W., LEVI E., "Modelling and simulation of a stand-alone induction generator with rotor flux oriented control" Electric Power Syst. Res. 46 pp. 141-152, 1998.

[5]   ERMİŞ M., ERTAN H.B., et al., "Various Induction Generator Schemes for wind-electricity generation" Electric Power Syst. Res. 23 pp. 71-83, 1992.

[6]   LEIDHOLD R., GARCIA G., VALLA M. I., "Field Oriented Controlled Induction Generator with Loss Minimization" IEEE Tran. Ind. Electron., vol. 49, pp. 147-156, Feb. 2002.

[7]   ÜÇTUĞ M. Y., "Modelling, Analysis and Control of a Wind Turbine Driven Self-Excited Induction Generator", Ph.D. Thesis, METU, 1986.

[8]   Danish Wind Industry Association, www.windpower.org

[9]   SAULNIER B., BARRY A. O., DUBE B., REID R., "Design and development of a Regulation and Control System for the High-Penetration No-Storage Wind/Diesel Scheme" European Community Wind Energy Conference 88, 6-10 June 1998, Henning, Denmark.

[10]   ÇADIRCI I., "Steady-state and transient performance analyses of a double output induction generator operating at subsynchronous and super-synchronous speeds", Ph.D. Thesis, METU, 1994.

[11]   European Wind Energy Association (EWEA) and Greenpeace, WIND FORCE 12 Report, 2004.

[12]   American Wind Energy Association (AWEA) www.awea.org

[13]   BOSE B. K., Modern Power Electronics and AC Drives. Prentice Hall, 2002.

[14]   KRISHNAN R., Electric Motor Drives. Prentice Hall, 2001.

[15]   ONG C. M., Dynamic Simulation of Electric Machinery. Prentice Hall, 1998.

[16]   YÜKSEL A., "Simulation of an Arc Furnace System and Examination of the Effects of Current Transformer Saturation" M.Sc. Thesis, METU, 2000.

[17]   MILLER T. J. E., Reactive Power Control in Electric Systems. John Wiley & Sons, 1982.

[18]   SIMOES M. G., BOSE B. K., SPIEGEL R. J.,   "Design and Performance Evaluation of a Fuzzy-Logic-Based Variable-Speed Wind Generation System" IEEE Tran. Ind. Electron., vol. 33, pp. 956-965, July/Aug. 1998.

APPENDIX A

SIMULATION PARAMETERS

A.1 EQUILIBRIUM STATES

%Obtaining Equilibrium States for Syteady-State operation

```
Rs=0.9;                    % Stator resistance
ls=0.011;                  % Stator leakage inductance
lr=0.0017;                 % Rotor leakage inductance
M=0.15783165;              % Mutual inductance
N1/N2=2.5;                 % Stator turn / rotor turn ratio
pp=2;                      % pole pair
J=1;                       % inertia
Ls=ls+M;                   % Stator self inductance
Lr=2.5*2.5*lr+M;           % Rotor self inductance

G=0.0246897                % rated load
v=10;                      % rated wind speed

Rr=1.25;                   % Rotor resistance referred to stator side
C=0.000078518;             % Excitation Capacitor

k1=-3.2281;                % wind turbine constants
k2=12.9094;
k3=-8.80384;
nt=7.2;                    % gear transmission ratio

Gm=-M/(Ls*Lr-M*M);         % reciprocal inductances
Gr=Ls/(Ls*Lr-M*M);
Gs=Lr/(Ls*Lr-M*M);

A=[-G/C -Gs/C; 1 -Rs*Gs];
B=[1/C; Rs];
AA=A*A;
```

```
e1=[1 0];              % canonical basis vector
e2=[0 1];              % canonical basis vector


gamma=-Gr/Gm^2;

pol=[C*gamma 0 AA(1,1)*C*gamma+AA(2,2)*C*gamma-A(2,1)-C*Rs*A(2,2) 0
C*gamma*(AA(1,1)*AA(2,2)-AA(2,1)*AA(1,2))-
A(2,1)*AA(2,2)+A(2,2)*AA(2,1)-C*Rs*(A(2,2)*AA(1,1)-A(2,1)*AA(1,2))];
root=roots(pol);
root                   %Appropriate Root should be selected from the list
w=root(3)              %Resonance Frequency

gamma=e2*A*inv(A*A+w^2*eye(2))*B;
delta=e2*inv(A*A+w^2*eye(2))*B;
xsi=e1*A*inv(A*A+w^2*eye(2))*B;
eta=e1*inv(A*A+w^2*eye(2))*B;


f=w/2/pi;              %Resonance frequency in Hz

s0=-Rr*Gm^2*delta;         %slip

Tm=k1*v*w*(1-s0)/(pp*nt^2)+k2*v^2/nt+k3*pp*v^3/(w*(1-s0));

lamdar=Tm/(pp*w*Gm^2*delta);    %rotor flux
lamdas=Gm^2*(gamma^2+w^2*delta^2)*lamdar;        %stator flux
Vs0=Gm^2*(xsi^2+w^2*eta^2)*lamdar;     %Stator Voltage

Result=[G v f s0 sqrt(lamdar) sqrt(lamdas) sqrt(Vs0/3)]    %Equilibrium values
```

A.2 REPRESENTATION OF THE MAGNETIZING CURVE

```
%This file represents double-exponential magnetizing curve

function denklemler
global M;
global Gm;
global Gs;
global Gr;

ls=0.011;
lr=0.0017;
M=0.15786626;
```

```
Ls=ls+M;
Lr=2.5*2.5*lr+M;

Gm=-M/(Ls*Lr-M*M);
Gr=Ls/(Ls*Lr-M*M);
Gs=Lr/(Ls*Lr-M*M);

tspan = [0 4];

y0 = [-361.3; 121.07; 0.3717; 1.1769; 0.1852; 1.1383; -0.1432]; %(i) M=0. 1579

[t,y] = ode45(@f,tspan,y0);

plot(t,(y(:,5).*y(:,5)+y(:,6).*y(:,6)));        %plot rotor flux

function dydt = f(t,y)
global M;
global Gm;
global Gs;
global Gr;

Rs=0.9;
ls=0.011;
lr=0.0017;
Nt=2.5;
pp=2;
J=1;

 G=0.02;  %change G and v values to find Msaturated i
 v=10;      % for dictıurbances
 Rr=1.25;  %it can be changed
 C=0.000078518; %it can be changed

k1=-3.2281;
k2=12.9094;
k3=-8.80384;
nt=7.2;

h1=1.528544;
h2=0.164617;
h3=0.291987;
h4=21.888520;
h5=0.005858;

ws=100*pi;

Ls=ls+M;
```

```
Lr=2.5*2.5*lr+M;

Gm=-M/(Ls*Lr-M*M);
Gr=Ls/(Ls*Lr-M*M);
Gs=Lr/(Ls*Lr-M*M);

A=[-G/C -Gs/C; 1 -Rs*Gs];
B=[1/C; Rs];
AA=A*A;

e1=[1 0];
e2=[0 1];

gamma=e2*A*inv(A*A+ws^2*eye(2))*B
delta=e2*inv(A*A+ws^2*eye(2))*B;
xsi=e1*A*inv(A*A+ws^2*eye(2))*B;
eta=e1*inv(A*A+ws^2*eye(2))*B;

dydt = [(-G/C*y(1)+ws*y(2)-Gs/C*y(3)-Gm/C*y(5))
   (-ws*y(1)-G/C*y(2)-Gs/C*y(4)-Gm/C*y(6))
   (y(1)-Rs*Gs*y(3)+ws*y(4)-Rs*Gm*y(5))
   (y(2)-ws*y(3)-Rs*Gs*y(4)-Rs*Gm*y(6))
   (-Rr*Gm*y(3)-Rr*Gr*y(5)+ws*y(7)*y(6))
   (-Rr*Gm*y(4)-ws*y(7)*y(5)-Rr*Gr*y(6))
   pp/(J*ws)*(pp*Gm*(-y(3)*y(6)+y(4)*y(5))-k1*v*ws*(1-y(7))/(pp*nt^2)-
k2*v^2/nt-k3*pp*v^3/(ws*(1-y(7))))  ];

FrNs=sqrt(3/2)*((Gs+Gm)^2*(y(3)*y(3)+y(4)*y(4))+(Gr+Gm)^2*(y(5)*y(5)+y(6)*
y(6))+2*(Gm+Gs)*(Gm+Gr)*(y(3)*y(5)+y(4)*y(6)))^0.5;
Msat=(1.5/FrNs)*(h1*(1-exp(-h2*FrNs))-h3*(1-exp(-h4*FrNs))+h5*FrNs);
M=Msat
```

A.3 MACHINE PARAMETERS USED IN SIMULINK

```
%***THIS IS THE PAREMETERS OF THE SIMULINK SIMULATIONS

%**********Parameters of the SEIG
ls=0.011;
lr=0.0017;
M=0.15783165;
Lr=2.5*2.5*lr+M;
Ls=ls+M;
```

VDo=-380.512; VQo=-20.2495; LDo=-0.0928; LQo=1.2367; Ldo=-0.298;
Lqo=1.0988; so=-0.036583;
%Initial conditions of Voltages, fluxes and slip

Rr=1.25; C=0.000078518;   %for v=10, G=0.0247

Rs=0.9; pp=2; J=1; nt=7.2;

k1=-3.2281; k2=12.9094; k3=-8.80384;

ws=100*pi;

G=0.0246897;
v=10;

h1=1.528544; %***Parameters of the saturation curve
h2=0.164617;
h3=0.291987;
h4=21.888520;
h5=0.005858;

A.4 PARAMETERS FOR THE FINAL SIMULATION

% Parametrization file for the SVC files

ls=0.011;
lr=0.0017;
M=0.15783165;   %initial value for M mutual inductance
Lr=2.5*2.5*lr+M;
Ls=ls+M;

LDo=-0.728262; LQo=0.70628; so=-0.036583; %i

Rr=1.25

C=0.000078518; %initial value for capacitor C

ki=0.001; %integral control coefficient

Rs=0.9; pp=2; J=1; nt=7.2;

k1=-3.2281; k2=12.9094; k3=-8.80384;

ws=100*pi;   % synchronous frequency

```
G=0.0246897;          %rated load
v=10;  %rated wind speed

h1=1.528544;
h2=0.164617;
h3=0.291987;
h4=21.888520;
h5=0.005858;


BC=130e-6*(100*pi) % C=130 micro F capacitor susceptance
XL=0.125*(100*pi)   % L=125 milli H inductor reactance
```

APPENDIX B

MATLAB

B.1 MATLAB

MATLAB is a high-performance language for technical computing. It integrates computation, visualization, and programming in an easy-to-use environment where problems and solutions are expressed in familiar mathematical notation.

The name MATLAB stands for matrix laboratory. It is an interactive system whose basic data element is an array that does not require dimensioning. This allows solving many technical computing problems, especially those with matrix and vector formulations. Typical uses include:

- Math and computation
- Algorithm development
- Modeling, simulation, and prototyping
- Data analysis, exploration, and visualization
- Scientific and engineering graphics
- Application development, including Graphical User Interface building

MATLAB has evolved over a period of years with input from many users. In university environments, it is the standard instructional tool for introductory and advanced courses in mathematics, engineering, and science. In industry, MATLAB is the tool of choice for high-productivity research, development, and analysis.

MATLAB features a family of application-specific solutions called toolboxes. Toolboxes are comprehensive collections of MATLAB functions (M-files) that extend the MA TLAB environment to solve particular classes of problems. Areas in which toolboxes are available include signal processing, control systems, neural networks, fuzzy logic, wavelets, simulation, and many others.

B.2 Simulink

Simulink is an interactive system for simulating non-linear dynamic systems. It is a graphical mouse-driven program that allows somebody to model a system by drawing a black diagram on the screen and manipulating it dynamically. It can work with linear, non-linear, continuous-time, discrete-time, multivariable, and multirate systems. Blocksets of Simulink provide additional libraries of blocks for specialized applications like communications, signal processing, and power systems.

Simulink is a software package for modeling, simulating, and analyzing dynamical systems. It supports linear and non-linear systems, modeled in continuous time, sampled time, or a hybrid of the two. For modeling, Simulink provides a graphical user interface (GUI) for building models as block diagrams, using click-and-drag mouse operations. With this interface, one can draw the models just as he/she would with pencil and paper.

Simulink includes a comprehensive black library of sinks, sources, linear and non-linear components, and connectors. One can also customize and create his/her own blocks. Models are hierarchical, so they can be built both top-down and bottom-up approaches. One can view the system at a high level, then double-click on blocks to go down through the levels to see increasing levels of model detail. This approach provides insight into how a model is organized and how its parts interact.

After deriving a model, it can be simulated, using a choice of integration methods, either from the Simulink menus or by entering commands in MATLAB's command window. The menus are particularly convenient for interactive work, while the

command-line approach is very useful for running a batch of simulations. Using scopes and other display blocks, the simulation results can be seen while the simulation is running. In addition, one can change parameters and immediately see what happens, for "what if" exploration. The simulation results can be put in the MATLAB workspace for post processing and visualization.

Model analysis tools include linearization and trimming tools, which can be accessed from the MATLAB command line, plus the many tools in MATLAB and its application toolboxes. And because MATLAB and Simulink are integrated, one can simulate, analyze, and revise his/her models in either environment at any point.

In the last few years, Simulink has become the most widely used software package in academia and industry for modeling and simulating dynamical systems. One can easily build model s from scratch, or take an existing model and add to it. Simulations are interactive, so one can change parameters "on the fly" and immediately see what happens. Also one have instant access to all of the analysis tools in MATLAB, so he/she can take the results and analyze and visualize them.

With Simulink, one can move beyond idealized linear model s to explore more realistic nonlinear models, factoring in friction, air resistance, gear slippage, hard stops, and the other things that describe real-world phenomena. It turns a computer into a lab for modeling and analyzing systems that simply wouldn't be possible or practical otherwise, whether the behavior of an automotive clutch system, the flutter of an airplane wing, the dynamics of a predator-prey model, or the effect of the monetary supply on the economy. Similar to MATLAB and its application toolboxes, the MathWorks offers blocksets for use with Simulink. Blocksets are collections of Simulink blocks that are grouped in a separate library from the main Simulink library.

B.3 Power System Blockset

The Power System Blockset allows scientists and engineers to build models that simulate power systems. The blockset uses the Simulink environment, allowing a model to be built using click and drag procedures. Not only can the circuit topology be drawn rapidly, but also the analysis of the circuit can include its interactions with mechanical, thermal, control, and other disciplines. This is possible because all the electrical parts of the simulation interact with Simulink's extensive modeling library. Because Simulink uses MATLAB as the computational engine, MATLAB's toolboxes can also be used by the designer.

The blockset libraries contain model s of typical power equipment such as transformers, lines, machines, and power electronics. These models are proven ones coming from textbooks, and their validity is based on the experience of the Power Systems Testing and Simulation Laboratory of Hydro-Quebec, a large North American utility located in Canada. The capabilities of the blockset for modeling a typical electrical grid are illustrated in demonstration files. For users who want to refresh their knowledge of power system theory, there are also case studies available.

APPENDIX C

PRINCIPLE OF THE TCR OPERATION

Thyristor Controlled Reactor (TCR) with shunt capacitors (shown in Fig. 3.40) are used as static compensator in the power system [17]. Static means it has no moving part. Static compensators have many practical applications in electric power system; maintaining constant voltage, improving system stability, improving power factor and correcting phase unbalances. In this study TCR with shunt capacitor compensator is used as the variable reactive power generator for the SEIG. The compensator is controlled to meet the exact reactive power demand of the SEIG. A reactive power balance is maintained and constant frequency operation is granted with the compensator.

Two oppositely poled thyristors in Figure 3.39 conduct on alternate half-cycles. If the thyristors are gated into conduction at the peaks of the voltage, full conduction results in the reactor. If the gating is delayed in the thyristors partial conduction is obtained in the reactor. The waveforms in Figure C.1 show the current in the inductor for different gating angles α.

The instantaneous current i is given by

$$i = \begin{cases} \dfrac{\sqrt{2}V}{X_L}(\cos\alpha - \cos\omega t), & \alpha < \omega t < \alpha + \sigma \\ 0, & \alpha + \sigma < \omega t < \alpha + \pi \end{cases} \qquad \text{(C.1)}$$

where V is the rms voltage; $X_L = \omega L$ is the fundamental-frequency reactance of the reactor (in Ohms); $\omega = 2\pi f$; and α is the gating angle. The time origin is chosen to coincide with a positive going zero crossing of the voltage. The fundamental component is found by Fourier analysis and is given by.

$$I_1 = \frac{\sigma - \sin\sigma}{\pi X_L} V \qquad \text{A rms} \qquad\qquad\qquad (C.2)$$

σ is the conduction angle, related by α by the equation

$$\alpha + \sigma/2 = \pi \qquad\qquad\qquad (C.3)$$

then the equation (C.2) can be written as

$$I_1 = B_L(\sigma)\ V \qquad\qquad\qquad (C.4)$$

Where $B_L(\sigma)$ is an adjustable fundamental frequency susceptance controlled by the conduction angle by the equation,

$$B_L(\sigma) = \frac{\sigma - \sin\sigma}{\pi X_L} \qquad\qquad\qquad (C.5)$$

With the required capacitance command the conduction angle σ for the inductor is calculated. The relationship between the σ and α is given in Figure C.2, which is the control law of the TCR. According to Figure C.2 a look-up table is constructed between the $B_L(\sigma)$ and firing angle α. In this study the required excitation capacitor value is generated by the controller. The required capacitor value is extracted from the total capacitor value. The remaining is the excess capacitor that should be compensated by the TCR. Therefore the adjustable susceptance of the TCR $B_L(\sigma)$ is equated to the susceptance of the excess capacitor value. The operation of the TCR is shown in Thyristor Firing Block in Appendix D.
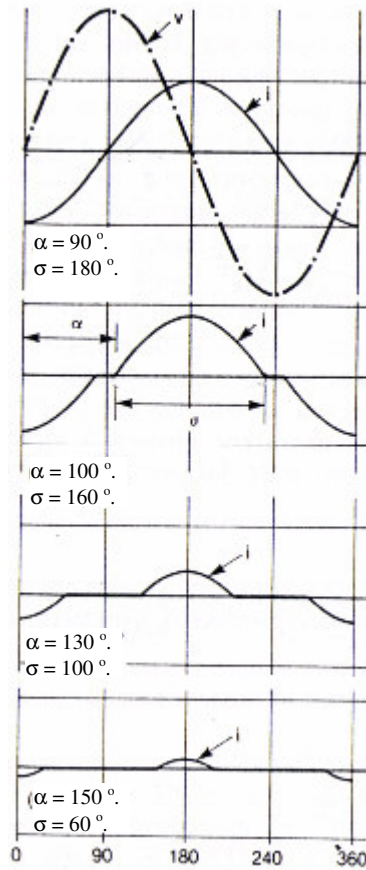
Figure C.1 Phase current waveforms in the TCR.
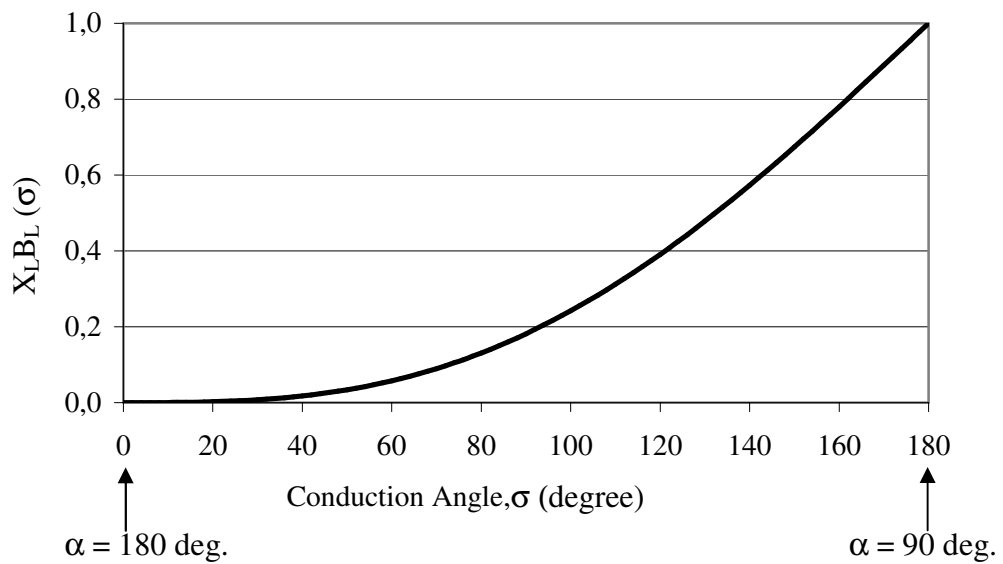
Figure C.2 Control law of the TCR

122

APPENDIX D

BLOCKS USED IN THE FINAL SIMULATION

D.1. VOLTAGE REGULATION BLOCKS
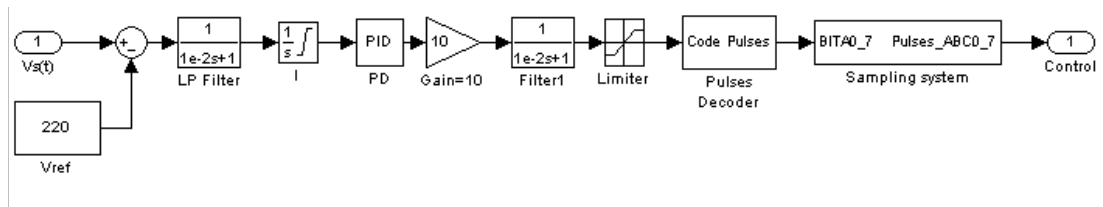
Figure D.1 Voltage Controller Block
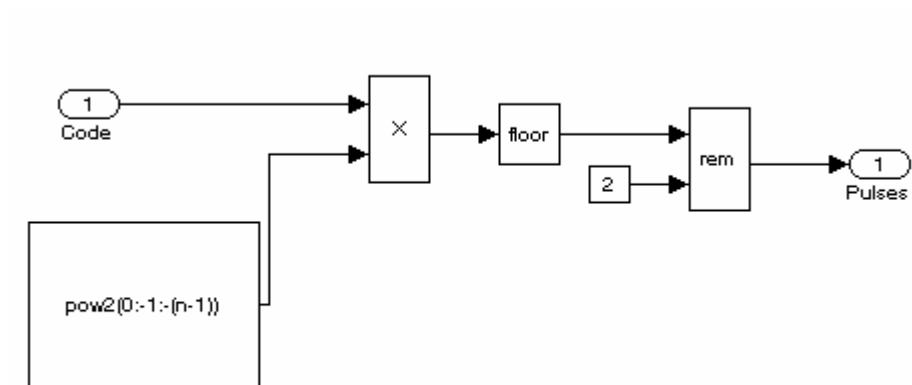
Figure D.2 Pulses Decoder Block
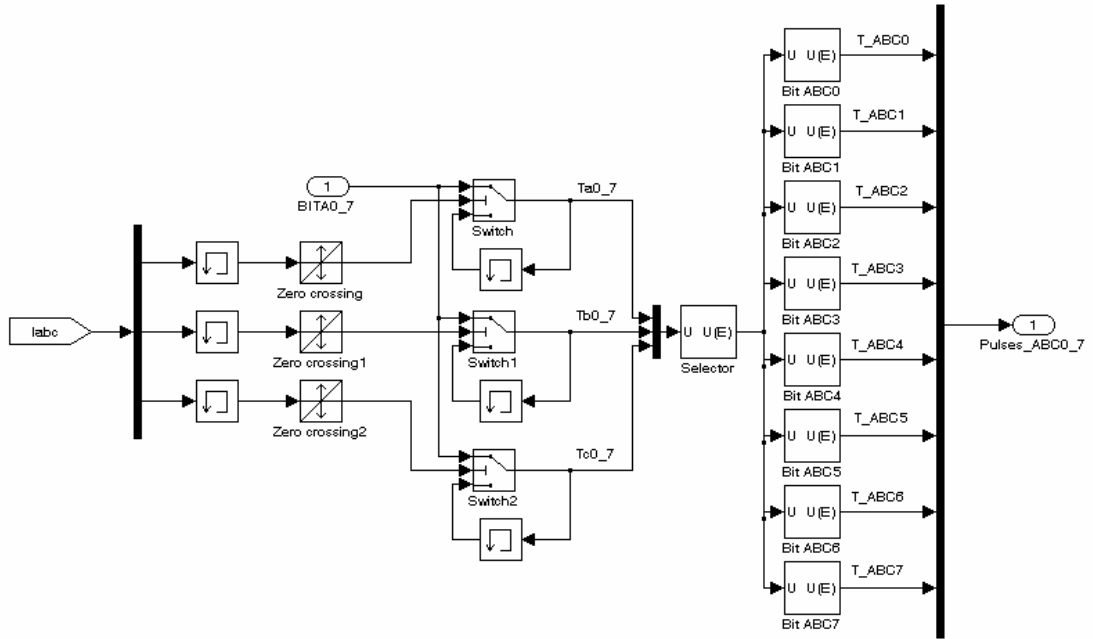
Figure D.3 Sampling System Block
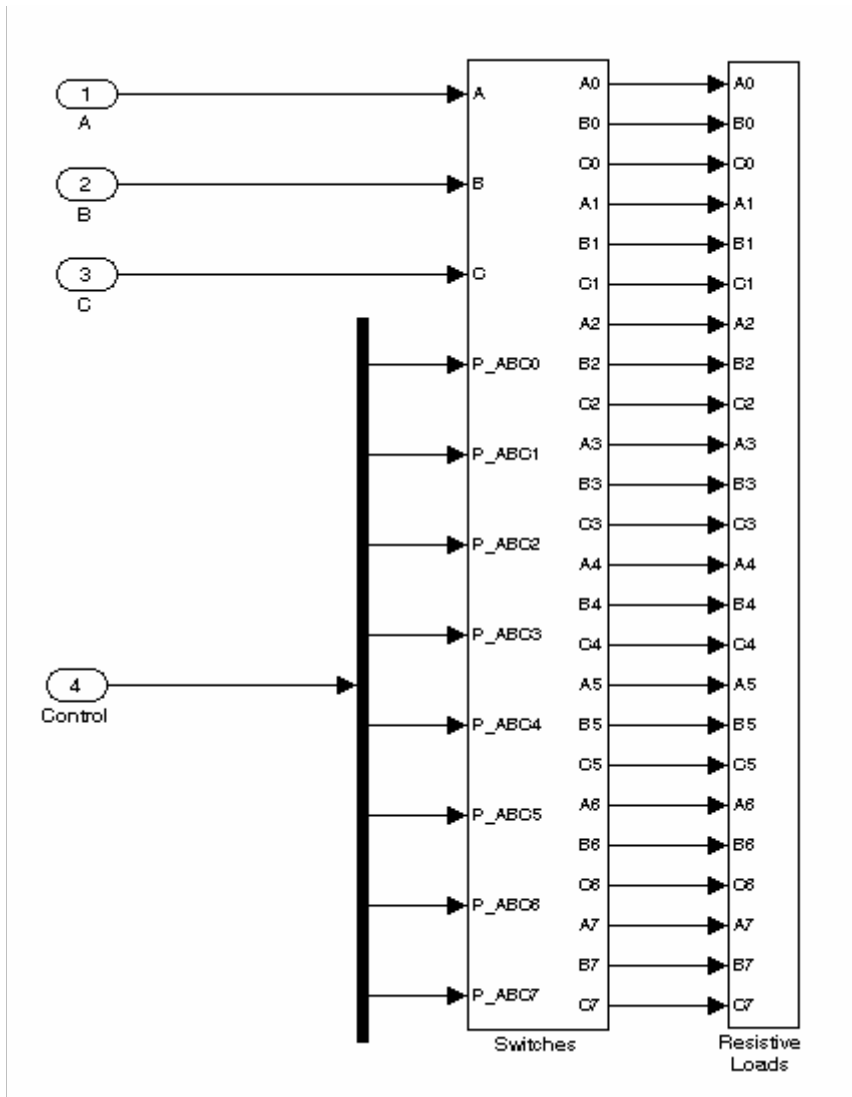
Figure D.4 External Load Block
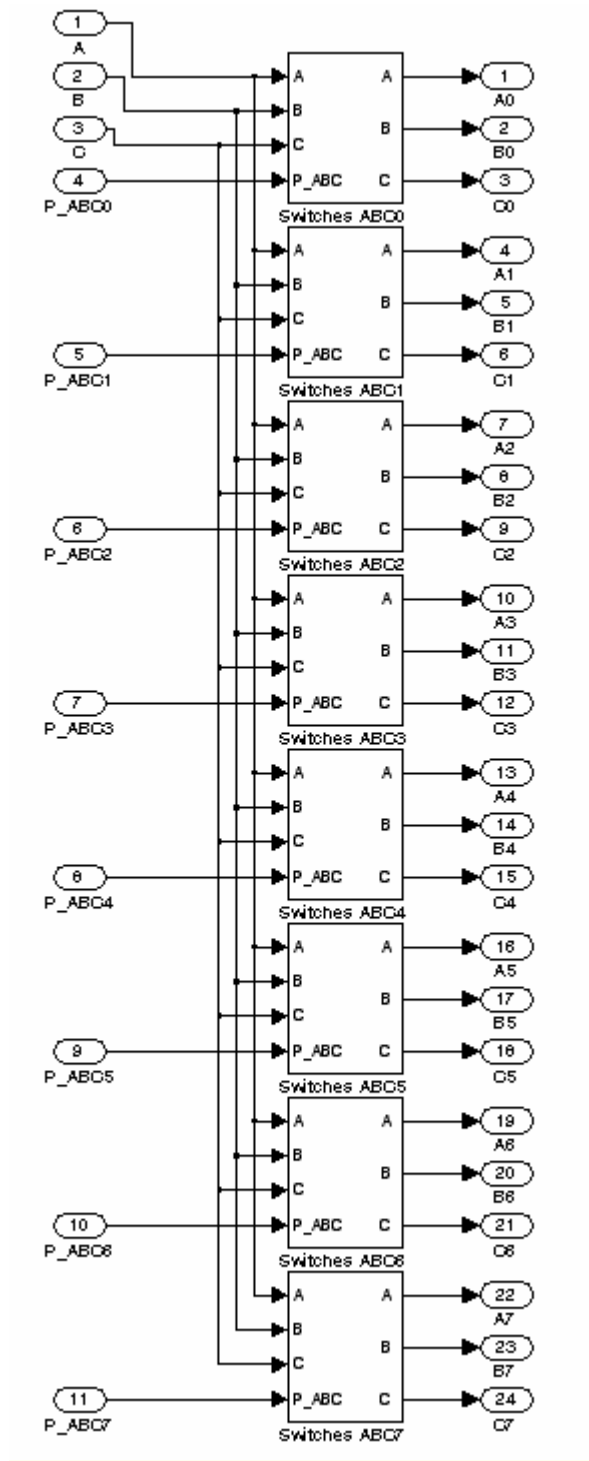
Figure D.5 Switches Block
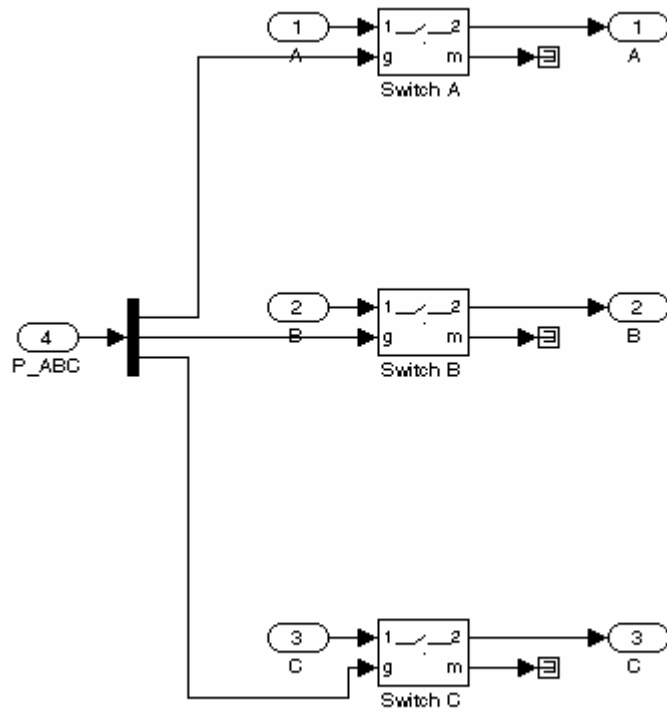
Figure D.6 Switches ABC Block (Three switches for a three phase resistor)
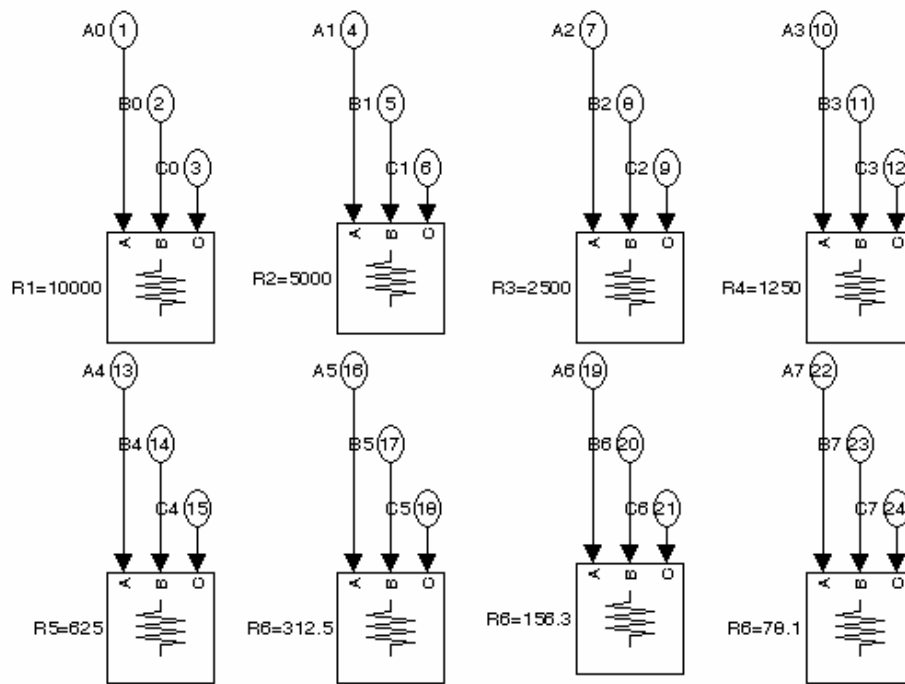
Figure D.7 Resistive Loads Block

D.2 FREQUENCY REGULATION BLOCKS
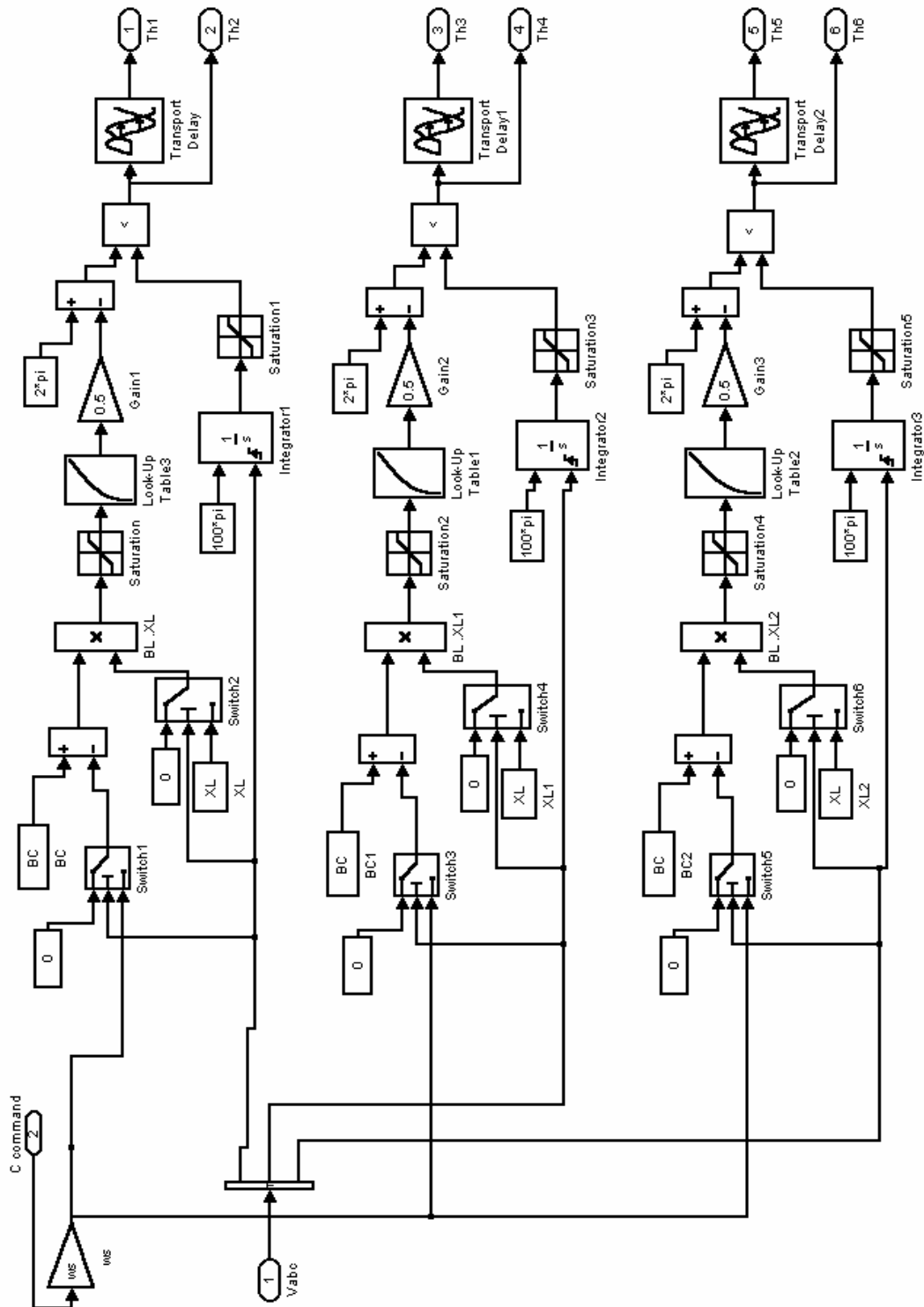
Figure D.8 Thyristor Firing Block

Figure D.9 TCR Block